UNIVERSITÀ DEGLI STUDI DI PADOVA

Department of Information Engineering

Ph.D. COURSE IN: INFORMATION ENGINEERING

CURRICULUM: INFORMATION and COMMUNICATION TECHNOLOGY

Series: XXXII

Sustainable Management of Energy-Harvesting Communication Systems

Supervisor: Prof. Leonardo Badia

Coordinator: Prof. Andrea Neviani

Ph.D. student: Elvina Gindullina

Academic Year 2018/2019

Abstract

Internet of Things (IoT) systems have been massively infiltrating our everyday's life for various applications. One of the main constraints inhibiting the further development of these applications is the limited autonomy of present day batteries. Moreover, energy sustainability is a crucial requirement for systems employed in critical mission applications. A widely used approach to increase the autonomy of IoT systems is the use of renewable sources of energy such as solar, wind, heat, and others to power the devices. For instance, one of the most widespread solutions for wireless sensor nodes is the use of solar panels, which can provide reasonable power input. Their efficiency is determined by the panel's material that defines the conversion efficiency [1].

Renewable sources of energy are too erratic to provide complete system reliability unless over-dimensioned. In reality, energy supply is often limited, which causes the need for adaption of the node operational strategy to ensure the functional reliability of the system. However, the unreliable nature of renewable energy causes several challenges, which we address in this work. In particular, this thesis investigates the effect of battery imperfections caused by inner diffusion processes in the battery on the energy harvesting wireless device operation and effective energy-balancing strategies for different scenarios and system types.

We propose 1) the transmission strategy, that takes into account the battery properties (leakage, charge recovery, deep discharge, etc.), and reduces the data losses and discharge events; 2) adaptive sampling algorithms, that balances the erratic energy arrivals, validated on the industrial data-logger powered by a solar panel; and 3) energy cooperation in Wireless Sensor Network (WSN) and Smart City (SC) contexts. We also focus on critical-mission IoT systems, where the freshness of delivered packets to the monitoring node by the information sources (communication nodes) is the important parameter to be tracked. In this context, we set the objective of age of information minimization taking into account the battery constraints, asymmetry in reliability of information sources, and stability of energy arrivals, that is, the Energy

Harvesting (EH) rate.

This array of strategies covers a wide range of applications, scenarios, and requirements. For instance, they can be applied to a smart city represented as a large system of interconnected smart services, or a WSN employed for critical mission applications. We demonstrated that the knowledge of battery and environmental characteristics, and the asymmetric properties of a system is beneficial for designing transmission/sensing strategies.

Contents

List of Tables **v**

List of Figures **vi**

List of Acronyms **ix**

1 Introduction **1**

1.1 Motivation and research objectives 1

1.2 Thesis Contributions 4

1.3 Manuscript Outline 7

2 Energy sustainability of a single EH-device **9**

2.1 Introduction 10

2.2 Battery non-ideal effects 11

2.2.1 A Markov model accounting for charge recovery in EH-devices . 11

2.2.2 Self-control of service rate for battery management 21

2.3 Energy modeling and adaptive sampling algorithms for energy harvesting powered nodes 29

2.3.1 Background in adaptive sampling for sensing devices 30

2.3.2 Adaptive sampling algorithms with sampling rate limitations . . 33

2.3.3 Energy model 36

2.3.4 Numerical results 43

2.4 Conclusions 49

3 Energy sustainability of systems with multiple EH-devices **51**

3.1 Introduction 51

3.2 Study of asymmetry in EH-WSN 53

3.2.1 Background in game theory approach for WSNs 53

3.2.2 System model 55

3.2.3 Simulation and numerical results 58
3.3 Energy cooperation 59
3.3.1 Background on energy cooperation 60
3.3.2 Energy topologies in SCs 61
3.3.3 Energy cooperation for sustainable IoT services within SCs . . . 69
3.4 Conclusions 77

4 Energy management for EH IoT-systems deployed for critical operations 80
4.1 Introduction 80
4.2 Background in age-of-information 81
4.3 Average age-of-information with a backup information source 82
4.3.1 System overview 83
4.3.2 Numerical results 86
4.4 Average age-of-information with multiple heterogeneous information sources 93
4.4.1 System model and problem formulation 94
4.4.2 Numerical results 99
4.5 Conclusions 106

5 Summary and Future Directions 108

List of Publications 111

Acknowledgements 113

References 114

List of Tables

2.1 Transitions of the Markov chain from (q, e, a), with $a>0$ 17
2.2 Simulation parameters and results 25
2.3 Error values 40
2.4 Simulation parameters 46
2.5 Comparison of algorithms 48

3.1 Simulation parameters 58
3.2 Simulation parameters 66
3.3 Simulation parameters 75

4.1 Default parameters. 87
4.2 Default parameters 101

List of Figures

1.1 Data collecting systems 2
1.2 Thesis outline 8

2.1 Scheme of energy harvesting sensing node 10
2.2 Apparent outage probability for our scenario. 20
2.3 Real outage probability for our scenario. 20
2.4 Comparison between apparent and real outages. 21
2.5 Probability of packet drop for our scenario. 21
2.6 Probability of correct discharge notice. 22
2.7 Apparent discharge and data loss event for μ=0.4 26
2.8 Apparent discharge and data loss event for μ=0.7 26
2.9 Changes of data loss and apparent discharge frequency for $\mu = 0.1 - 1.0$. 26
2.10 Comparison of condition (2.2) with apparent discharge events, for $n =$ 25, in the High stress scenario ($\mu = 0.7$). 26
2.11 Data loss parameter values ($\mu = 0.4$) 28
2.12 Apparent discharge event ($\mu = 0.7$) 28
2.13 Revised sigmoid function [2] 34
2.14 Comparison of average daily irradiation. 39
2.15 SoC estimation model 41
2.16 Example of tiltmeter installation for Courtesy of Sixense Oceania [1] . . 43
2.17 Radio consumption profile of LS device [2] 44
2.18 Theoretical power output of solar panel SOLEM 10/150/100 (south, 37°) located in Barcelona, Spain 45
2.19 Hourly air temperature profile of Barcelona, Spain for 2017 year 45
2.20 Comparison of energy arrival profiles. 46

2.21 Comparison of initial dataset obtained under constant sampling rate of 1 hour with a dataset obtained under DDASA (here initial tiltmeter data and sampled data respectively) 47
2.22 Comparison of DDASA, ideal conditions strategy and EA-DDASA. . . 49

3.1 System model 55
3.2 Numerical Results 59
3.3 Topology scheme 62
3.4 Distance distribution vs. optimal amount energy links 66
3.5 Optimal amount energy links vs. energy level distribution 66
3.6 Optimal amount energy links vs. energy arrival profile 67
3.7 Optimal amount energy links vs. energy threshold 67
3.8 Optimal amount energy links vs. amount of communication nodes in WSN 68
3.9 Amount of depleted communication nodes with/without optimization . 68
3.10 Energy framework for interconnected smart services. 71
3.11 Sustainability ratio across an entire day. 76
3.12 Average GW battery level across an entire day. 76
3.13 Sustainability ratio performance varying the number of GWs N. 76
3.14 Sustainability ratio evaluation increasing the number of ongrid GWs. . 76
3.15 Sustainability ratio varying sensor nodes throughput. 77

4.1 System model 83
4.2 Illustration of the optimal policy for different energy cost ratios c_2/c_1. . 89
4.3 Dependency of average AoI and energy cost ratio for $\gamma_2 = 0.2$. 90
4.4 Dependency of average AoI and energy cost ratio for $\gamma_2 = 0.8$. 90
4.5 Dependency of average AoI and energy cost ratio for $\gamma_1 = 0.4$. 90
4.6 Illustration of the optimal policy for different EH rates λ. 91
4.7 Average AoI as a function of the EH rate, λ. 93
4.8 Average AoI as a function of the backup source reliability, γ_2. 93
4.9 Average AoI vs. time for the aggressive and optimal policies. 94
4.10 System model 95
4.11 Geometric distribution of status updates' ages, with $p = \gamma_i$ 97
4.12 Dependency of a source's cost and reliability 98
4.13 Illustration of the optimal policy for different energy cost/ reliability combinations for $\lambda = 0.2$. 101

4.14 Illustration of the optimal policy for different energy cost/ reliability combinations for $\lambda = 0.6$. 103
4.15 Illustration of the optimal policy for different energy cost/ reliability combinations for $\lambda = 0.8$. 104
4.16 Dependency of average AoI and EH rate for different devices/cost dependencies 105
4.17 Number of information sources vs. optimal average AoI for different values of EH rates, λ. 106
4.18 Number of information sources vs. average AoI if destination node adopts aggressive strategy for different values of EH rates, λ. 106
4.19 Number of information sources vs. optimal average AoI for different values of energy arrival units, $\bar{e}$. 106
4.20 Number of information sources vs. average AoI if destination node adopts aggressive strategy for different values of energy arrival units, $\bar{e}$. 106

List of Acronyms

AC	Alternating Current
ADC	Analog to Digital Converter
AoI	Age of Information
ANN	Artificial Neural Networks
ASA	Adaptive Sampling Algorithm
BS	Base Station
CASA	Compensation Adaptive Sampling Algorithm
DDASA	Data-Driven Adaptive Sampling Algorithm
EH	Energy Harvesting
EASA	Energy Aware Adaptive Sampling Algorithm
EA-DDASA	Energy Aware DDASA
GW	Gateway
ICT	Information and Communication Technology
IoT	Internet of Things
L-ASA	Limits-Based Adaptive Sampling Algorithm
L-DDASA	Limits- and Thresholds-Based DDASA
MDP	Markov Decision Process
PV	Photovoltaic
PPDR	Public Protection and Disaster Relief

RVI	Relative Value Iteration
RASA	Resuscitation Adaptive Sampling Algorithm
STC	Self-turning Control Systems
SoC	State of Charge
STC	Standard Test Conditions
SC	Smart City
T-ASA	Threshold-Based Adaptive Sampling Algorithm
TCP	Transmission Control Protocol
TDMA	Time Division Multiple Access
VI	Value Iteration
WSN	Wireless Sensor Network

Chapter 1
Introduction

1.1 Motivation and research objectives

Future communication technologies are deemed to reach a pervasive penetration in many technological scenarios of everyday's life. One major downside of this achievement is an unprecedented increase in worldwide energy consumption: it is estimated that power demands of the Information and Communication Technology (ICT) ecosystem are approaching one tenth of the electricity generation on the planet [3].

In spite of their limited energy requirements for individual tasks, their intensive usage makes tablets and smartphones more energy-hungry on a long time scale than domestic electric appliances like the refrigerator; furthermore, the latter is generally shared in each household, while the formers are individually owned. These estimates can become even more worrisome if embodied energy is also included [4].

Nowadays, technologies related to the IoT are extremely successful and ubiquitous; their advantages are observed in the areas of: logistics, agriculture, marketing, transportation, healthcare, manufacturing [5].

In this thesis, we mainly focus on power management in WSNs of communicating sensors with the ability to collect, buffer, and transmit information. In such a system, interconnected nodes transmit useful measurement information and control instructions via distributed processes [6], in other words, use wireless communication to perform *distributed* sensing tasks (Fig. 1.1). Distributed data sensing enables data collection in a more efficient way, improving delivery even if one of the nodes fails to deliver a data packet. Scalability, fault-tolerance and energy efficiency are three main requirements for designing efficient WSN [7].

One of the main limitations putting the brakes on further developments of applications for wireless networks is the limited autonomy of present-day batteries [8]. In

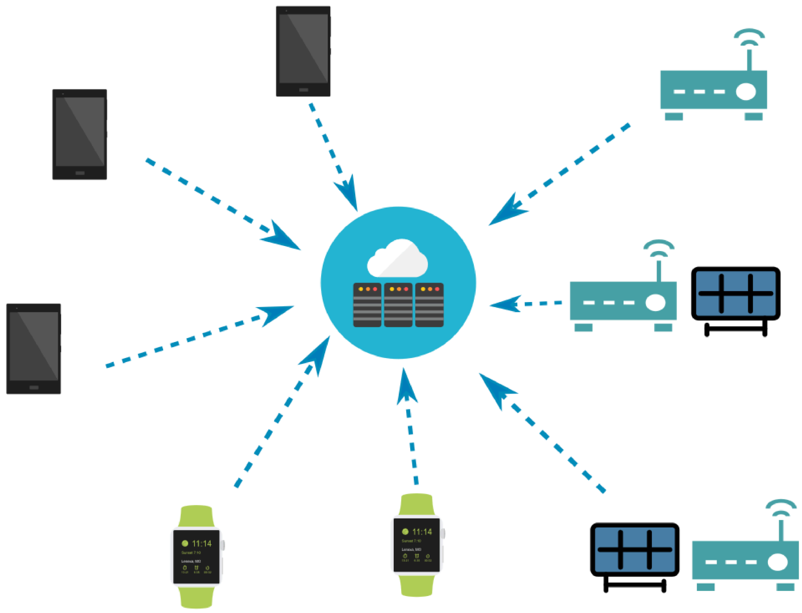

Figure 1.1: Data collecting systems

principle, wireless nodes should be able to exploit both wireless connectivity and sufficiently long autonomy. However, the energy reserve that can be stored in a battery is limited, and even more so for tiny devices. In light of this, the use of renewable sources (solar, wind, vibration, etc.) integrated in communication systems through some energy harvesting techniques is gaining appeal as a way to reduce global energy consumption, with the benefits of controlling pollution and greenhouse emissions, enabling longer operation for wireless communications, as well as significantly enhance the field of applicability of WSN [8–10]. State of the art harvesting technologies provide sustainable and green energy, and can be inserted in many types of WSN. However, renewable sources are too erratic (energy arrivals are randomly distributed over time) to guarantee reliable functioning, thus batteries are still needed to provide backup energy supply when the devices are not powered by the harvesting process. For example, objects powered by solar energy are dependent from daytime and the position of the solar panel. Therefore, it is important to take into account the differences in energy arrivals of the nodes. Energetic sustainability requires the combination of the harvesting process with a smart management of the battery seen as an *energy buffer* [11], or some form of intelligent control to avoid outages at critical instances [12]. Such an energy buffer is needed to both store the energy harvested from the environment for a later use, and also guarantee quality objectives, while still dealing with the limited energy supply. In many existing contributions [8, 13], mathematical models for energy harvesting devices are proposed, often with a focus on designing power management policies that balance energy consumption and provide extensive sustainability for WSN systems.

If the battery gets depleted, the wireless device will stop operating and will not be able to transmit data anymore. This situation often occurs when adopting an aggressive strategy of battery usage, i.e., when data packets are transmitted with extremely high service rate [8]. Another situation is observed if packets arrive faster than the device can transmit them (such as in a burst transmission), so the device inserts them into the queue [14]. This could lead to an event where the device data buffer is full and due to the finite maximum queue size, no more data packets could be buffered and there is no other choice rather than to reject excess packets; opposite to the previous event, this happens when the service rate is relatively low. Such situation could be observed in transport layer operations, e.g., due to a badly managed Transmission Control Protocol (TCP) queue. In addition, the more congested the data queue, or in other words, the longer the line of waiting packets to be dispatched, the higher the queueing delay [15]. Based on the aforementioned reasons, the development of an efficient operation strategy should take into account both reduction of data losses and also reduction of the battery inactivity time.

The overall objective of this thesis is to develop efficient power managements, that increase the energy sustainability of various EH communication systems. We highlighted the following aspects to be taken into account for designing energy strategies:

- Battery is not an ideal source of energy. Charge/discharge processes depend on factors such as the environment temperature and/or depth of charge-and-discharge cycles. Therefore, the battery management should take into account the battery non-idealities.

- The transmitting nodes in the network may have different energy characteristics (size of energy buffer, energy harvesting capabilities) that affect the overall system performance. To develop an efficient energy management, we should take into consideration the system asymmetries.

- Energy cooperation may be one of the techniques capable to handle the differences in energy arrivals of different nodes. In this case, objects that are not advantageously located will be powered by a node with better energy capabilities.

- The efficient adaptive sampling strategy adopted in an energy harvesting sensor node is required to provide a failsafe operation under unstable environmental conditions, and be implementable in the existing hardware. For the sustainable management, the sampling strategies should be adapted for the unstable energy arrivals.

- Apart from energy outages prevention, another objective for sustainable management of some IoT systems is minimization of the Age of Information (AoI). Status updates must be acquired sparingly depending on the level of energy available in the battery.

The outlined aspects are taken into consideration for developing sustainable management and define the thesis contribution.

1.2 Thesis Contributions

The contributions of this thesis are as follows. Chapter 2 is dedicated to the energy sustainability of a single EH-device.

- Section 2.2 studies the effect of battery non-idealities on the performance of an EH wireless device, representing the single device as a double queue system. In particular, Subsection 2.2.1 highlights some battery non-ideal effects, especially the so-called "charge recovery," can have a dramatic impact on the operation policy of autonomous devices. To do so, we construct a Markov model, where we introduce a bi-dimensional battery value, including the apparent energy level, which is what available at the electrodes to power the device, and the actual energy level stored in the battery. We show that this non-ideality leads to considerably different estimates of undesirable events such as battery outages, and may cause a general underutilization of the devices if not properly accounted for. In Subsection 2.2.2 we propose a simplified self-control management of a non-ideal battery expressed by restrictions, which could be used for an efficient operational strategy of the EH-device. We performed some simulation and observed that we can diminish the number of variables in the model to predict possible unwanted events such as apparent discharge events and data losses. The results of this section are the subject of the following published papers:
  Badia L., Feltre E., **Gindullina E.**, "A Markov model accounting for charge recovery in energy harvesting devices", in *Proceedings of the 2017 IEEE Wireless*

Communications and Networking Conference Workshops (WCNCW), San Francisco, USA, 2017.

Gindullina E., Badia L., "Towards self-control of service rate for battery management in energy harvesting devices", in *Proceedings of the 2017 IEEE International Conference on Communications Workshops (ICC Workshops)*, Paris, France, 2017.

- In Section 2.3 we propose the Adaptive Sampling Algorithm (ASA) that takes the advantages of data-driven approach and balances the erratic energy arrivals. The proposed algorithm is simple enough to be implemented in low complexity hardware. To validate the performance of the proposed schemes, we simulated the operation of the industrial data-logger powered with a solar panel located in Barcelona, Spain. We observed that with prior knowledge of the environmental characteristics it is reasonable to set threshold based rules and sampling rate limits that significantly increase the performance of the existing data-driven approach without increasing the complexity of the algorithm. The results of this section are the subject of the following published paper:

  Gindullina E., Badia L., Vilajosana X., "Energy Modeling and Adaptive Sampling Algorithms for Energy Harvesting Powered Nodes with Sampling Rate Limitations", in *Wiley Transactions on Emerging Telecommunications Technologies*, 2019.

Chapter 3 is dedicated to energy sustainability of communication systems consisting of multiple devices. To investigate these scenarios, firstly, we studied the effect of the system energy asymmetry on the overall performance (Section 3.2), and considered the energy cooperation as a mean to handle the asymmetry properties (Section 3.3).

- Section 3.2 considers the system consisting of two asymmetric sensors. We investigate the asymmetry by means of game theory. In particular, we focused on the asymmetry in energy capabilities of both sensors. It was observed that the system performs significantly better and in a more balanced way if the asymmetric properties of the system are taken into account. The results of this Section are the subject of the following published paper:

  E. Gindullina, L. Badia, "Asymmetry in Energy-Harvesting Wireless Sensor

Network Operation Modeled via Bayesian Games", *IEEE 18th International Symposium on A World of Wireless, Mobile and Multimedia Networks (WoWMoM), 2017.*

- Section 3.3 focuses on the energy cooperation among SC objects. In particular, we consider the design of energy typologies among wireless communication nodes (Subsection 3.3.2) and the effect of the energy cooperation on the performance in the SC scenario (Subsection 3.3.3). In Subsection 3.3.2, we adopt a global optimization perspective. More specifically, we consider an SC scenario where the IoT network is represented by a set of wireless nodes, with some information sinks collecting data from the other nodes. These sink nodes are supposed to handle all incoming information [16]. In Subsection 3.3.3, we consider energy cooperation in an IoT scenario, which is a possible solution to provide the key issue of energy sustainability. We assume the presence of interconnecting EH-IoT Gateways (GW), collecting and aggregating data from field sensing devices. The proposed solution transfers energy from energy rich GWs to energy scarce ones, i.e., those which are not connected to the power grid. To identify the optimal energy transfer/allocation scheme, we formulate a convex optimization problem that finds the optimal solution for heterogeneous smart systems. With this energy allocation technique, the GWs are unlikely to run out of energy during operation and the gap between energy offer and demand among interconnected GWs is kept to a minimum. The results of this section are the subject of the following published papers:
  E. Gindullina, L. Badia, "An optimization framework for energy topologies in smart cities", *IEEE Wireless Communications and Networking Conference (WCNC), 2018.*
  A. Gambin, **E. Gindullina**, L. Badia, and M. Rossi "Energy Cooperation for Sustainable IoT Services within Smart Cities", *IEEE Wireless Communications and Networking Conference (WCNC), 2018.*

Chapter 4 investigates the systems, where the AoI is a crucial parameter, for instance, for critical-mission systems (automation, intelligent transportation and smart cities).

- Section 4.3 investigates the optimal policy of an EH-IoT monitoring system, that with the given energy budget minimizes the average AoI of a system with a

backup information source. For this problem, we formulate the scheduling of status updates from the two sources (primary and backup) as a Markov decision process and obtain a policy that decides which source to query or update from. We compared the performance of the optimal policy with the so-called aggressive policy, which tries to query the most expensive source it can afford, and demonstrated that the gain from the optimal policy increases as the backup source characteristics become worse (i.e., decreasing reliability or increasing cost) or the energy harvesting rate decreases. We have also shown that employing a backup source of information is justified when the reliability of the backup source is relatively high and the cost of the information requesting is relatively low. The results of this chapter are the subject of the following published paper:
E.Gindullina, L. Badia and D. Gündüz, "Average Age-of-Information with a Backup Information Source", in *Proceedings of the IEEE International Symposium on Personal, Indoor and Mobile Radio Communications (PIMRC)*, Istanbul, Turkey, 2019.

- Section 4.4 extends the Section 4.3, and considers an EH-IoT monitoring system, that with the given energy budget minimizes the average AoI of a system with multiple information sources. We investigate AoI-optimal policies, and what is the sufficient amount of monitoring devices in the system for an up-to-date information.

Chapter 5 draws the conclusions and possible future research directions in designing the sustainable management systems for energy harvesting communication systems.

1.3 Manuscript Outline

The outline of this thesis is demonstrated in Fig. 1.2. The aspects of the sustainable management for a single EH-device case is considered in Chapter 2. As part of this chapter, Section 2.2 explores battery imperfections that affect the device performance. While Section 2.3.2 studies the adaptive sampling techniques in order to balance the energy consumption and energy arrivals of an EH-device.

Chapter 3 consider the sustainable management in SC scenarios. Under this chapter, we study the energy asymmetry in WSN (Section 3.2), and investigate the benefits of energy cooperation as a way to handle asymmetry in energy harvesting capabili-

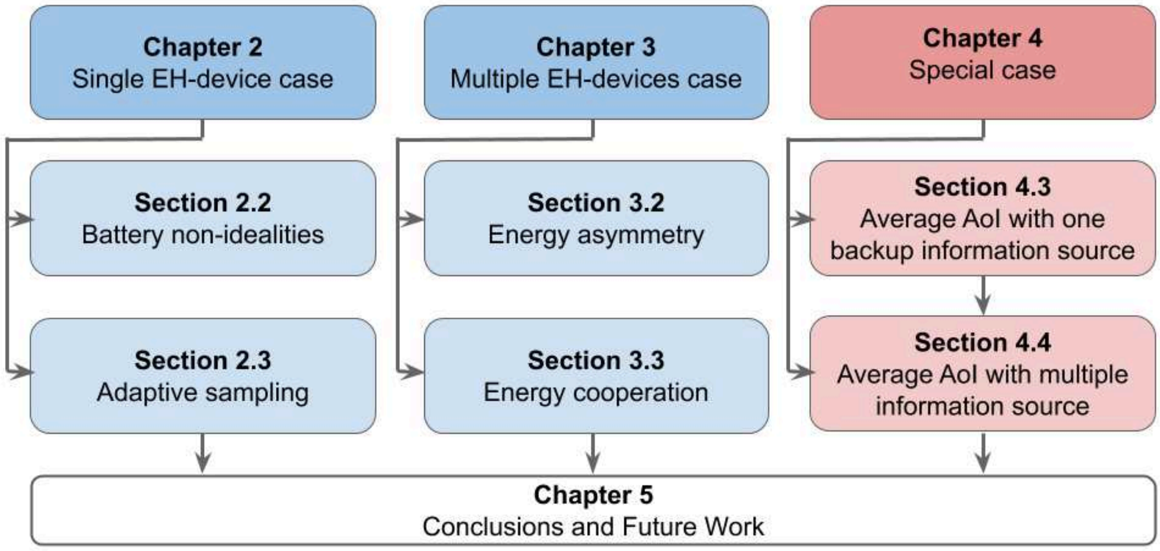

Figure 1.2: Thesis outline

ties and energy consumption (Section 3.3). In Chapters 2 and 3 the energy balancing is the main objective, while the objective outlined in Chapter 4 is the minimization of average AoI in a system with two and more information sources (Sections 4.3 and 4.4, respectively). Finally, Chapter 5 draws the conclusions and outlines the possible research directions.

Chapter 2
Energy sustainability of a single EH-device

Energy harvesting is an important feature that can be implemented in mobile devices to provide them with extended autonomy, yet it poses several challenges in terms of optimal battery usage. Energy is harvested and stored in a device battery. The battery performance is defined by the battery properties as well as by its operation policy.

First, we dedicate the Section 2.2 to the effect of battery imperfections to the operation of EH-device. In the Subsection 2.2.1, we consider the operation of an EH-device powered by a rechargeable battery, taking non-idealities into account. We analyse the effect of battery non-idealities to the EH-device performance, in particular, the effect of *charge recovery* to the battery outage.

In the Subsection 2.2.2, for a single device case, we proposed the simplified self-control transmission management of a battery expressed by restrictions. We rely on the double-queue model which includes the battery imperfections and bi-dimensional battery value. We demonstrated, that just tracking a few parameters, such as real and apparent energy levels, and the status of the data buffer can improve the performance of an energy-harvesting device in terms of energy sustainability.

Another perspective of battery management of an energy-harvesting device is adaptive sampling algorithms. In the Section 2.3, we consider the different sampling strategies implemented in a practical wireless EH-device powered by a rechargeable battery, as a way to adapt and balance an energy consumption to the EH-pattern.

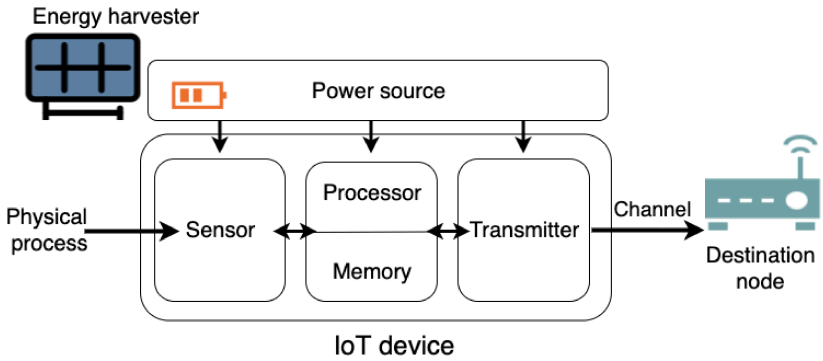

Figure 2.1: Scheme of energy harvesting sensing node

2.1 Introduction

A single device can be treated as performing specific energy-consuming tasks (e.g., sending data and/or sensing the environment), while being powered by a renewable source. Without loss of generality, we will see the tasks as the transmission of *packets*, generated by a sensor according to a known arrival process to the *data queue* (or memory) of the device, located in its transmission buffer, and regulated by a transmission policy. Instead, energy is harvested and stored in the device battery (or power source), seen as an *energy queue*. The sensor unit convert the physical signal with Analog to Digital Converter (ADC), and the sensing frequency is regulated by sampling algorithms. The scheme of such a device is demonstrated in Fig. 2.1.

Design of the efficient power management for such a device includes the following challenges:

- Batteries are not ideal sources of energy. It is required to analyse the effect of battery imperfections on the operation of EH-device. Transmission policies should take into account battery imperfections.

- Sensing plan can be violated due to the unstable energy arrivals. Sampling algorithms should be adapted to the EH case.

To analyse the first challenge, we adopt the double queue system with joint service, meaning that a packet can be transmitted if and only if the battery has got enough energy. Data packets and energy are *simultaneously* taken from the transmission buffer and the battery, respectively; if either queue (data or energy) is empty, packet transmission has to wait for replenishment.

The basic model outlined above dictates that the energy level of the battery only changes when a transmission occurs. This contrasts with the practical observation that batteries are subject to non-idealities. An example is leakage [17], causing the battery level to decrease even in the absence of transmissions. An even more complicated phenomenon is the so-called *charge recovery* effect [18, 19], according to which the battery level apparently raises when no energy is drained. It is important to develop the smart battery management, taking into account the battery non-idealities, and adapting the transmissions based on the battery behaviour, energy arrivals and consumption. Therefore, in this thesis, we investigate the more realistic battery model, and effect of battery non-idealities on the EH performance.

Within the second challenge, we developed a policy that adapts the energy consumption of a wireless sensor device to a harvesting pattern and build an energy-sustainable system is to adjust its sampling rate. The sampling frequency or sampling rate is the average number of samples collected in one second. Sampling rate significantly affects the energy consumption of a sensing device. If a device goes out of charge, then it fails to deliver a data packet. This might be even more significant if data-driven sampling approaches are adopted. This happens, for example, when a sample is gathered if the difference in data values are high enough, and/or a packet failed delivery, so that a gap is present in the collected data.

However, the erratic nature of the ambient energy requires to adopt a sampling strategy that, on one hand, tailors the sampling rate to the underlying energy arrival process, while on the other hand being implementable on simple hardware. Therefore, we seek a strategy that takes advantage of data-driven approaches, is readily implementable to the state-of-the-art devices, and balances volatile energy arrivals. The study is based on the more generic model, where the device has an unit data-queue, and transmissions occur followed by sensing event. The model also takes into account the battery non-idealities.

2.2 Battery non-ideal effects

2.2.1 A Markov model accounting for charge recovery in EH-devices

The contribution of this Section is to explore a more realistic battery model, where these non-idealities are included. We implement a discrete-time finite-state Markov chain, and investigate the battery behaviour as a function of the characterizing parameters, especially the probabilities of deep discharge and battery recovery. To do so, we extend the standard representation considering the lengths of the data and the energy queue into a *triple* of values, in which the energy level is split into the *real* and the *apparent* one. This duality is key for charge recovery, which is actually just an increase of the apparent battery level. The model is solved and results are discussed, in particular for the probability of *energy outage*, i.e., that the battery cannot power the device anymore. Actually, we need distinguish between the *real* and *apparent* outage; such a difference implies that the occurrence of the outage event can be severely overestimated, and we quantitatively show how the parameters of charge recovery effect impact on this.

The rest of this section is organized as follows. In Subsection 2.2.1.1 we discuss analytical models proposed in the literature for mobile batteries and their non-ideal effects. In Subsection 2.2.1.2 we outline our contribution of a Markov model where the battery recovery effect is taken into account by expanding the state of the double queue into a triple of values. The model solution is discussed in Subsection 2.2.1.3, while Subsection 2.2.1.4 presents numerical results, showing that neglecting battery recovery effects can lead to overestimating of the apparent outage probability (and conversely, the battery is almost never depleted for real).

2.2.1.1 Background on battery non-idealities

Batteries employed for mobile devices usually include multiple cells, each containing two electrodes separated by an electrolyte, referred to as the *active materials*. The electrolyte participates in the electrochemical reaction leading to charging and discharging of the battery [20]. The cell is discharged when it is connected to an external circuit and an oxide-reduction reaction transfers charge bearers among the electrodes, thus converting chemical into electrical energy. This process goes on until the battery reaches a cutoff voltage, i.e., the one at which it can be considered as disconnected. Alternatively, the discharge can be reversed by supplying the battery with electrical energy that is converted back into chemical energy stored by the active materials.

Yet, this entire process is far from ideal, depending on factors such as the environment temperature and/or the depth of charge-and-discharge cycles. For these reason, a battery can hardly be treated as an ideal source if certain conditions are not met. For example, [21] describes several non-idealities, such as the variation of the internal resistance depending on the external temperature. Also, capacity fading effects may take place, causing a degradation of the maximum amount of energy that can be stored in the battery, primarily depending on how many charge/discharge cycles have been performed, as well as their depth [22]. Even when the battery is inactive, inner electrochemical processes still take place, which can cause a constant leakage [23]. All these aspects are heavily influenced by the kind of battery, its weariness, and environmental conditions (such as the external temperature); a detailed analysis of the impact that these limitations is available in [24].

Here, we focus instead on a previously overlooked aspect, the *charge recovery effect* [25,26], which corresponds to the rise in the apparent energy level of a battery that is not discharged for a while. The reason is as follows. When the cells are fully charged, active materials have maximum concentration in the entire cell; when a discharging current is generated, those close to the cathode are consumed by electrochemical reactions, and replaced by other active materials moving towards the electrode according to a diffusion mechanism. If the current intensity is above a limiting value, this mechanism is not able to compensate the consumption of active materials around the electrode, which lowers the voltage. Especially, if the cutoff voltage is reached, electrochemical reactions halt and the battery is seen as discharged, even though some charge is still present in the cell. Now that the active materials are no longer drained, though, they diffuse across the cell and their concentration around the electrode increases. A *charge recovery* effect can be observed as causing a slow gradual rise of the apparent energy level. The extent of the recovery depends on the duration and the depth of the previous discharge, even though, according to [19], a long and intense discharge impulse increases the inner temperature of the battery, which in turn decreases the recovery effect. This means that if the battery is being constantly discharged, no recovery is possible and the device is no longer powered quite early, so that only a fraction of the battery charge is actually used, in some cases even less than 30% [25].

A better idea is to cyclically alternate discharge intervals with inactive periods, during which charge recovery is exploited. Setting a duty cycle involves a tradeoff between intense battery usage for a limited period of time, and extended operation time by exploitation of the recovery effect, at the price of not always using the battery, even when needed [18]. Also, note that the recovery effect cannot be exploited indefinitely, since when a new equilibrium of the active materials is reached, the recovery ceases to bring any benefit.

2.2.1.2 Markov model setup

We formulate a Markov model for energy harvesting devices including the non-idealities such as leakage and charge recovery effects. We refer to a system consisting of a generic wireless transceiver, e.g., a sensor node, transmitting data packets, and the battery powering it, which in turn can be recharged by some energy harvesting mechanism.

As per existing analytical studies [22], the entire system is framed as a double queue with simultaneous service. The general idea is to consider a *data queue*, describing arrival, buffering, and transmission of traffic, and an *energy queue* that includes energy generation, storage, and consumption. For the ease of modelling, both data and energy are discretized into identical atomic units, so that the queues can be seen as having customers arriving and being served one at a time. The clients of the data queue are *data packets*, all assumed to be of identical size, while we label the one of the energy queue as *energy quanta*, as discussed in [8]. A quantum is taken as the precise amount of energy that the transceiver requires to transmit one data packet. This in turn means that both queues have joint service of clients, i.e., a data packet can be transmitted only if an energy quantum is spent.

For the sake of simplicity, in line with existing contributions, we consider a discrete time, and packet and energy quantum generations according to independent homogeneous Bernoulli processes of rate λ and η, respectively. This means that, at every time slot, each queue can receive either one new client with probability λ (or η), or nothing with probability $1-\lambda$ (or $1-\eta$). We remark that these assumptions are not critical for the realism of the model, since the time discretization can be made arbitrarily small. Including correlation in client arrivals at both queues may deserve further investigations, since it is reasonable to assume that in reality data and energy generation processes have memory (in some cases even considerably so). However, we already studied correlation of arrivals in similar scenarios [22, 27] and therefore we expect the same conclusions to apply here. To keep this analysis simpler, we leave these considerations for future investigations.

This system can be studied with stochastic analysis, characterizing its state as a pair of integers (i.e., the lengths of the both queues). The novelty of the present section is to consider the system state as a *triple* of values, so as to keep into account charge recovery effects. Our system state (q, e, a) consists of:

- the number of packets in the data queue, q
- the true number of quanta in the energy queue, e
- and finally, the *apparent energy level*, denoted as a.

We set values Q and E as the maximum ranges for these non-negative variables. Specifically, Q is the maximum queue length, which relates to the data buffer size, so that $0 \leq q \leq Q$. Instead, E is the maximum value for *both* the true and the apparent energy levels, e and a. We also set the additional constraint that the apparent energy level cannot exceed the true level, so that $0 \leq a \leq e \leq E$. These state variables evolve over a discrete time (for notational simplicity, we omit the temporal reference). We assume that data and energy arrivals, as well as transmissions, take place simultaneously within the time slot. This means that a packet or a quantum of energy arriving at time instant t cannot be immediately exploited but are available for transmission or use from time $t + 1$ onwards.

In some contributions [8], the service rate μ of these queues follows from an *operation policy* keeping into account the state of the device; in principle, we could denote it as $\mu(q, a)$.[1] This policy can be optimized to pursue an objective, such as maximizing battery lifetime [22]. For the sake of simplicity, we consider instead a constant value of μ, where the only limitations to service are given by not having either packets to transmit or energy quanta to spend, or both. The higher μ, the more intense the battery usage; thus, $\mu \to 1$ corresponds to what in [8] is referred to as an "aggressive" operation policy.

Importantly, the choice of a fixed μ, instead of an optimized one, is not restrictive for what concerns the conclusion that we will draw later. Indeed, as will be clear from the results, our main message is that most of the outages are apparent, and there is still energy in the battery that is not exploited when the device stops operating. We expect that this conclusion is even more relevant when the discharge rate μ is optimized, since in that case the optimization is in reality based on the apparent value, and not the real one, as assumed by [8]. The main implication of our analysis will therefore still be true; this could be an interesting subject to explore as a future work.

Another deviation from classic queueing models, which are generally framing the energy queue as a birth-and-death process, is that our battery non-ideality implies that the discharge can sometimes seem to be stronger than one energy quantum. Indeed, an uneven distribution of the active materials leads to an *apparent* discharge that is heavier than normal. A packet transmission corresponds to the consumption of one energy quantum, therefore we should decrease both e and a by one unit. However, similar to [25], we consider that, whenever a packet is transmitted, a *deep discharge* event may happen, corresponding to decreasing the true energy level by 1, same as the normal case, whereas the apparent level decreases by 2. This way, a can be at times lower than e; we model it by defining a deep discharge probability α, i.e., whenever a

[1] We can adapt to the observable values q and a, but not to e that is hidden.

packet is transmitted, a deep discharge happens with conditional probability α, whereas a normal discharge (both e and a decrease by 1) takes place otherwise.

Some limitations are introduced for the sake of realism. First, discharges (either normal or deep) can only happen when $a > 0$. Moreover, the gap between a and e cannot be too high; to discard situations where the distributions of active materials in the cell would be unrealistically uneven, e.g., a very high e and a very low a, we set a maximum gap Δ, such that $[e - \Delta]^+ \leq a \leq e$, where $[x]^+ = \max(x, 0)$. Thus, deep discharge can only happen if $e - a < \Delta$.

We also consider leakage and especially charge recovery. The former is represented through parameter γ, i.e., the probability of decreasing the energy levels (both apparent and true) by 1 during a time slot, due to internal chemical degradation of the active materials. Conversely, we describe recovery effects through the probability β that, if $a{<}e$, the apparent energy level is increased by 1. Similarly to what assumed for the deep discharge, we have to account for the physical nature of the battery, as discussed in Section 2.2.1.1; especially, if $e{=}E$, which means that the battery is fully charged, the distribution of active material will reach a steady state quite soon. This comes from the fact that the intensity of charge recovery depends on a number of internal reactions [28], and bigger amount of active materials causes its faster distribution. For the same reason, in the literature the diffusion coefficient is considered as a function of the state of charge of a battery [29]. Therefore, to accelerate the recovery process if $a{<}e{=}E$ we assume that charge recovery of one energy quantum happens with probability $1{-}\gamma$ (instead of β). This forces a fully charged battery to recover quickly to the apparent level of maximum charge $a{=}E$ with probability $1{-}\gamma$ (i.e., if no leakage happens in the meantime with probability γ). In other words, we exclude the situation of non transition from one energy state to another if no transmission happens.

Finally, for physical coherency, we assume that leakage and recovery cannot happen in the same time slot, thus $\beta + \gamma \leq 1$. For the sake of simplicity, we consider that all these events (deep discharge, charge recovery, leakage) as well as arrivals and services, are independent of each other and identically distributed over time. The investigation of more complex scenarios involving some correlation (e.g., a dependence on an external parameter) is left for future work.

Taking all the constraints into account, we see that the model must include the combination of all choices for q (that has $Q + 1$ possible values from 0 to Q), and the pair (a, e) that instead has $[(E + 1)(E + 2) - \Delta(\Delta + 1)]/2$ values. Thus, the total

Table 2.1: Transitions of the Markov chain from (q, e, a), with $a>0$

No Packet Arrival, No Service		
→ new state	**probability**	**explanation**
(q, e, a)	$(1-\lambda)(1-\eta)(1-\mu)(1-\beta-\gamma)$	no energy variation
$(q, e, \max(e, a+1))$	$\beta(1-\lambda)(1-\eta)(1-\mu)$	charge recovery
$(q, [e-1]^+, [a-1]^+)$	$\gamma(1-\lambda)(1-\eta)(1-\mu)$	leakage
$(q, \max(e+1, E), \max(a+1, E))$	$\eta(1-\lambda)(1-\mu)$	energy arrival
Packet Arrival, No Service		
→ new state	**probability**	**explanation**
$(\min(q+1, Q), e, a)$	$\lambda(1-\eta)(1-\mu)(1-\beta-\gamma)$	no energy variation
$(\min(q+1, Q), e, \min(a+1, e))$	$\lambda\beta(1-\eta)(1-\mu)$	charge recovery
$(\min(q+1, Q), [e-1]^+, [a-1]^+)$	$\lambda\gamma(1-\eta)(1-\mu)$	leakage
$(\min(q+1, Q), \min(e+1, E), \min(a+1, E))$	$\lambda\eta(1-\mu)$	energy arrival
No Packet Arrival, Service		
→ new state	**probability**	**explanation**
$([q-1]^+, [e-1]^+, [a-1]^+)$	$\mu(1-\lambda)(1-\eta)(1-\alpha)$	normal discharge
$([q-1]^+, [e-1]^+, [\max(a-2, e-\Delta-1)]^+)$	$\mu(1-\lambda)(1-\eta)\alpha$	deep discharge
$([q-1]^+, e, a)$	$\mu(1-\lambda)\eta$	energy arrival
Packet Arrival, Service		
→ new state	**probability**	**explanation**
$(q, [e-1]^+, [a-1]^+)$	$\mu\lambda(1-\eta)(1-\alpha)$	normal discharge
$(q, [e-1]^+, [\max(a-2, e-\Delta-1)]^+)$	$\mu\lambda(1-\eta)\alpha$	deep discharge
(q, e, a)	$\mu\lambda\eta$	energy arrival

number N of states in the Markov chain is

$$N = (Q+1)\frac{E^2 + 3E - \Delta^2 - \Delta + 2}{2} \,. \tag{2.1}$$

The Markov chain evolves through changes of its state variables q, e, and a. This can be represented via balance equations that ultimately lead to a steady-state solution of the system. It is straightforward to prove that the resulting chain is positive recurrent.[1] For the sake of readability, instead of just giving the balance equations, we detail a step-wise derivation of the individual transitions. The next section presents such a constructive derivation of the transition matrix $\mathbf{T}$.

[1] Data stability $\lambda < \mu$ and energy stability $\eta < \mu$ can be imposed. However, $Geo/G/1/K$ queues are blocking systems and admit a steady-state even if those conditions are not met. Yet, in that case the stochastic analysis will have little utility (e.g., energy outages never happen).

2.2.1.3 Markov model solution

Some preliminary remarks help writing down the chain. Observe that the data queue has three options about what can happen in a time slot: (i) a data packet arrives, and none is served, then q increases by one, if $q < Q$ (otherwise, the packet is discarded and q is still equal to Q); (ii) a data packet is served (if $q > 0$), and none arrives, then q decreases by 1; (iii) or q is left unchanged, since either nothing arrives to the queue nor packets are served, or a simultaneous service an arrival take place. Note that we do not exclude the case of simultaneous arrival and departure from the queue, even though this event has smaller probability to happen.

Analogously, we can derive the same transitions for the true energy level, only replacing data arrivals with the generation of an energy quantum from the harvesting mechanism. In addition, e is also subject to the consequences of leakage, so we assume that when there is no transmission in a specific slot, still e can decrease by 1 with probability γ.

Finally, the apparent energy level a can instead increase by one because of two events: either an energy quantum is harvested from the environment (and none is consumed in the same time slot) or, if $a<e$, a charge recovery event can happen. The probability of this event is β, unless $e=E$, in which case we assumed that charge is recovered with probability $1-\gamma$. Conversely, a can also decrease because of a packet transmission that is not combined with an energy arrival in the battery. When this happens, the discharge is deep with probability α, meaning that the apparent energy level is decremented by 2. Otherwise, with probability $1-\alpha$, the discharge is normal and a just decreases by 1. Incidentally, this kind of transition breaks the quasi-birth-and-death model of similar investigations [27], but it is still manageable. Note that leakage affects a in the same way as it does for e. The cases where either an energy quantum arrives but at the same time another one is spent, or nothing arrives and no quantum is spent, still lead to a transition where a is unchanged.

Thus, we can consider the transitions reported by Table 2.1 and collect them to derive matrix $\mathbf{T}$. However, the table must be properly read in that, whenever to destination states are the same (as happens on border cases, e.g., $q=0$ or $a=e$, the corresponding transition probabilities must be summed. The table has to be adapted for the case $a = 0$; in this case, no service is allowed, therefore one should look only at the first two parts ("no service") and also remove any term $(1-\mu)$ from the probability, since the event of no service happens with probability 1. As a final remark, note that leakage is still possible when $a = 0$ but it only affects the true energy level.

The transitions reported by the table can be collected into an $N \times N$ transition matrix $\mathbf{T}$, with the generic element t_{ij} of $\mathbf{T}$ being the transition probability from the ith state to the jth, according to a given exhaustive labelling of the triples (q, e, a). We are actually interested in finding the steady-state probabilities of the Markov chain, which represent the probabilities of finding the system in a given state in stationary conditions. These values can be represented by the $1 \times N$ row vector $\boldsymbol{\pi}$, which is the solution of the fixed point condition $\boldsymbol{\pi} = \boldsymbol{\pi}\mathbf{T}$, combined with a normalization condition $\boldsymbol{\pi}\mathbf{1}^{\mathrm{T}} = 1$, where $\mathbf{1}$ is an all-one row vector. The last condition is required because the columns of $\mathbf{T}$ are not linearly independent, yet we can exploit the fact that $\boldsymbol{\pi}$ is a vector of state probabilities.

Vector $\boldsymbol{\pi}$ can be used to derive several metrics of interest. The steady-state probabilities of certain events (thereafter simply referred to as their "probabilities") can be computed by considering the π-terms of the corresponding states. It may be useful to focus on the *energy outage* events [8], describing that the device is no longer powered. Energy outage is a generally undesirable event that can be partly avoided by means of clever transmission policy design. However, two aspects of our expanded model are in special relationship with that event.

Outage is of special interest for our analysis, as opposed to other undesirable events such as energy overflow (i.e., the true level of the battery exceeding E, which means that energy is wasted). This is because our model involves leakage effects and deep discharges that can drain the battery even more. Also importantly, we considered two separate energy levels, therefore we expect that multiple definitions of outage coexist. In the next section, we will consider a practical evaluation case and discuss this point even further.

2.2.1.4 Numerical results

We show quantitative evaluations resulting from the application of the model previously outlined. The device parameters are set as follows. The maximum data queue and energy queue lengths are $Q = 20$, $E = 20$, with a maximum gap $\Delta = 6$ between the apparent and the true energy levels. This results in 4368 states, as per (2.1). The leakage rate is $\gamma = 0.1$, while α and β are kept variable to evaluate their impacts. Arrival rates to the queue are set as $\lambda = 0.5$ for the data packets and $\eta = 0.6$ for the energy quanta, while the service rate of both queues is set to $\mu = 0.7$. Notice that our choices imply stability of all the involved queues; however, μ is still sufficiently far from an aggressive battery usage that would drain the harvested energy quite soon, thereby

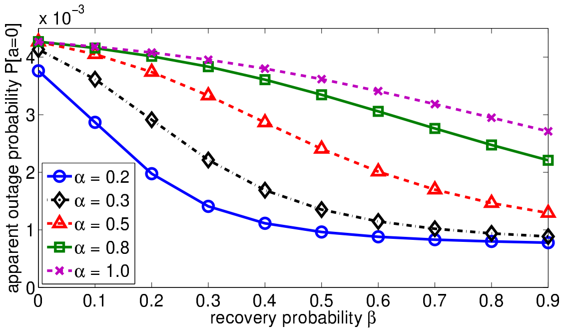

Figure 2.2: Apparent outage probability for our scenario.

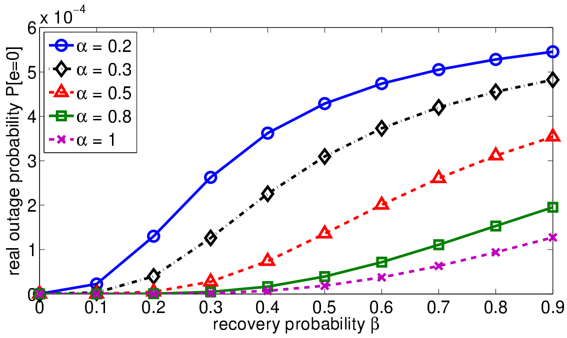

Figure 2.3: Real outage probability for our scenario.

causing frequent outages. We tried other scenarios and the result were always found to be in agreement with those shown here.

We evaluate the probabilities of the following events. The *real outage* event is defined as $[e = 0]$ and happens when the device is truly out of charge. If the apparent level a reaches 0, we are just in *apparent outage*; note that this does not necessarily implies that the battery is without charge; actually, if $a = 0$ but $e > 0$, it is possible to "recover" some charge thanks to the recovery effect, even in the absence of energy arrivals. Thus, we finally evaluate the *correct discharge notice* as $[e = 0|a = 0]$. All of the metrics are plotted versus the charge recovery parameter β (which must be between 0 and $1 - \gamma = 0.9$) and for various choices of the deep discharge probability α. This means that for low values of α and/or high values of β the charge recovery effect more frequently keeps e and a around the same value. Conversely, the larger α and the lower β, the higher the average gap between the two levels.

Fig. 2.2 shows the probability of apparent outage. For high values of β, the curves have a floor to a lower bound. This value is not zero: for our specific numerical choices, it is equal to $7.8 \cdot 10^{-4}$. However, low values of β can lead to a much higher apparent outage probability as high as $4.3 \cdot 10^{-3}$, more than five times higher. Moreover, the bound is actually loose if α is high, which means that even a high recovery probability cannot catch up the frequent deep discharges and therefore the apparent outage probability does not decrease significantly.

Fig. 2.3 shows the real outage probability. It may surprise that the curves increase in β and are actually very close to 0 for $\beta \to 0$. This counterintuitive behaviour can be explained by observing that the device stops operating at the *apparent* outage, and not at the real outage event. As previously shown, this occurs more frequently when α is high and β is low, in which cases the real outage event is very rare. However, the

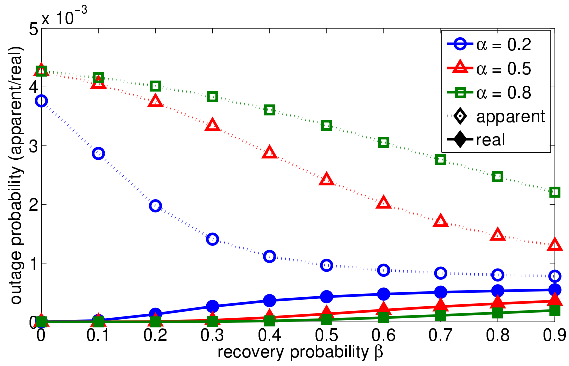

Figure 2.4: Comparison between apparent and real outages.

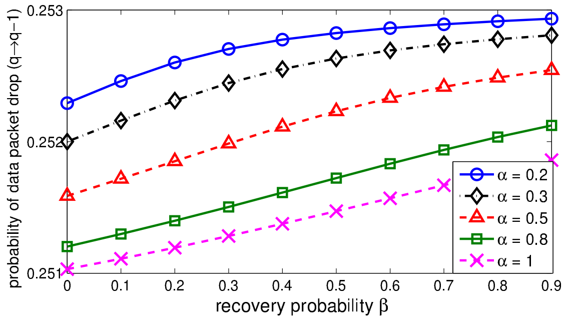

Figure 2.5: Probability of packet drop for our scenario.

results also show that, among the considered cases, the highest real outage probability is equal to $5.5 \cdot 10^{-4}$ for $\alpha = 0.2$ and $\beta = 0.9$. Thus, even when they are most frequent, real outages do not occur nearly as often as the apparent ones.

Such a comparison between apparent and real outage is summarized by Fig. 2.4. It is highlighted that the curves approach only for low α and high β. At the right-most end of the curve, $\alpha = 0.2$ still leads to more than 25% of difference. This gap can grow up to one order of magnitude, as if the case, for example, when $\alpha = 0.8$ and $\beta = 0.3$.

Fig. 2.5 shows the probability of the packet drop when no packet arrival is observed (transition from q to $q-1$ state). It seems logical, that higher probability of charge recovery leads to lower meaning of apparent outage which increases the probability of data packet drop, because a data packet cannot be transmitted if the battery is depleted (a=0).

Finally, Fig. 2.6 shows the probability of correct discharge notice. This is the conditional probability that the battery is truly without any charge when the apparent level is 0. Yet, the figure shows that this is not very likely. Even in the best considered case, there is a 30% of false alarm when the battery is recognized as apparently discharged. Also, if $\alpha > 0.5$ the probability of correct discharge notice is less than 30% even in the best case of a very high recovery probability β.

2.2.2 Self-control of service rate for battery management

In this subsection, we introduce the following contributions. First, we perform simulations of a Markov model introduced in the subsection 2.2.1, and designed to keep into account energy harvesting, but also some non-idealities of the battery management. This is done to analyse the evolution of system parameters, and to identify the key

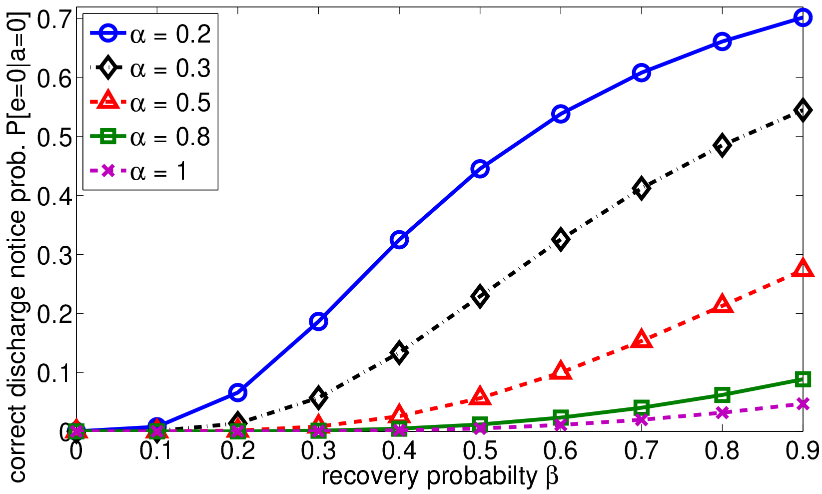

Figure 2.6: Probability of correct discharge notice.

variables required to predict possible undesirable events, such as apparent discharges and data losses.

Based on these observations, as a second contribution, we formulate some possible criteria, where tracking just a limited number of parameters, we are able to obtain a sufficiently effective self-control management, where the number of undesirable events is significantly reduced. We believe that this can be a first step in direction of developing policies for self-tuning control of energy harvesting WSN. Indeed, as a further evolution of the present work, we conjecture that autonomic policies can be thought and derived so as to allow efficient management without any prior knowledge on the device itself and/or the energy harvesting and the data arrival processes.

The rest of this Section is organized as following. In Subsection 2.2.2.1, we discuss models of battery and device operation proposed in the literature, and battery imperfections considered in previous papers and possible objectives of an efficient operational strategy. The numerical results of simulations are described in Subsection 2.2.2.2. Here is proposed the simplified self-management of a battery expressed by restrictions, which are integrated into the model; moreover, we evaluate the efficiency of the proposed management strategy.

2.2.2.1 Background on battery-efficient operation policies

Many recent papers challenged the task of identifying battery-efficient operation policies for energy harvesting devices in the IoT.

In [30], authors considered a network of nodes exchanging information over a shared channel. In order to optimize the battery work duration (i.e., to reduce battery degradation state), a random channel access scheme is proposed based on an aging-aware Binary Exponential Backoff algorithm, whose objective is to avoid excessive charges and discharges of the battery. A similar idea is used in [23], in which a double-threshold policy is considered as an optimal strategy; storage and retrieval of energy happens in connection with these thresholds. In particular, the authors developed a water-filling algorithm, which is based on the double-threshold structure. In [31], it is proved that the threshold structure of the policy while using the Markov decision process approach is optimal. In addition, the optimal strategy is formulated with maximization of channel gain as the objective function. A dynamic approach is considered, where energy storage losses are included in the model. The effect of different management policies on battery degradation using a Markov degradation model are also analysed in [22].

The aforementioned works describe the offline models of battery operation, meaning that model parameters are known, such as energy arrival records, past history, system status. In [32], [33], and [34] the situation of the online optimization of the policy is considered, whenever information about the device is unknown or partially unknown (statistical knowledge of the environment is required).The idea of incomplete available information regarding system parameters for development of the self-control battery management system is something that can be studied and discussed further.

The operational policies can follow different purposes, so the objective function can take different forms:

- minimization of transmitting completion time for a given number of data packets (in offline settings) [14]
- minimization of battery health degradation [30]
- maximization of channel usage [31]
- minimization of energy overflow [23]
- maximization of the battery lifetime [22]
- maximization of the network sum rate [34]

For the development of the optimal policy, different operating battery models are considered. State of the art articles usually focus on battery operation considering different kinds of imperfections and their combinations. As the model gets more realistic, a better operation strategy can be developed. We considered the operation policies, which are based on the battery models with imperfections. For example, in [35] authors presented the policy optimization problem, which optimizes the quality of the service and battery lifetime taking into account the degradation of the battery. The linear programming optimization algorithm can be applied for this formulation. In [36] similar optimization problem is formulated for hybrid electric vehicles, based on dynamic programming theory. Authors of [37] showed the effect of real battery constraints on the throughput optimization problem and a comparison between the ideal and real model. It was shown that ignoring real battery effects could even lead to zero throughput. The effect of leakage was considered in [24] and the optimization framework was proposed in order to optimize the amount of data transmitted within a given transmission deadline. In [38], it is highlighted that the leakage can lead to 10-20% of energy loss, thus, throughput optimization was proposed, subject to energy stochastic constraints, and a dynamic-programming type algorithm was offered as well. In this work, we want to avoid similar optimization formulations, which requires lots of computational effort to be solved, instead we devise a simple policy with limited number of required parameters. We will take into consideration such imperfections as the battery leakage, deep discharge, and charge recovery. This means that our energy queuing model for the battery involves events where the battery is discharged even when data is not sent (leakage), or it gets discharged more than it should (deep discharge). This leads to an *apparent* energy level which is lower than the actual one [39], but on the other hand a charge recovery effect may be present, leading the apparent energy level to raise towards the actual one when the battery is not used.

Within this setup, we focus on undesired events such as battery outage, corresponding to depletion of the energy queue, and data overflow, i.e., an excess in the data queue implies that some packets to be discarded. This happens when the service rate is too high or too low, respectively. However, the exact definition of “high” or “low” strongly depends on the entire system parameters of data and energy queues, also including non-idealities such as the leakage rate, that are impervious to estimate. Our goal will be to identify which essential parameters can be employed to set rules to regulate the service rate, so as to avoid the aforementioned undesirable events, still keeping the management simple.

2.2.2.2 Simulation and numerical results

We manage the simulations to analyse the behaviour of model parameters and possibility to reduce the number of variables needed to predict possible negative events. We consider a model for an energy harvesting device (wireless transmitter, sensor node),

Table 2.2: Simulation parameters and results

Parameters	**Low stress**	**High stress**
Packet arrival rate λ	0.5	0.5
Energy arrival rate η	0.6	0.6
Max queue size Q	10	10
Max battery size E	10	10
Deep discharge rate α	0.4	0.5
Charge recovery rate β	0.1	0.1
Max gap of apparent/true energy level Δ	6	6
Leakage rate γ	0.1	0.1
Service rate μ	0.4	0.7
Results		
Apparent discharge freq.	0.5%	3.1%
Data loss event	2.5%	0.0%

which transmits data packets and is powered by a battery, recharged by a harvesting mechanism. In this work, we use the model proposed and discussed in detail in [39]. To evaluate the effectiveness of the proposed conditions, we will consider the battery outage frequency (apparent and full) and data loss event frequency, which happens when at time t we observe $q = Q$ and a new packet is to arrive to the data queue in the next time slot.

We consider different values of the service rate μ, specifically leading to: a **Low stress** situation for the battery, where $\mu < \eta$, and a **High stress** case, where $\mu > \eta$, which we expect may cause several apparent discharges in the battery. This serves to see how the service rate influences the frequency of the apparent discharge event. Specifically, the parameters are chosen as $\eta = 0.5$ and thus $\mu = 0.4$ (for Low stress) and $\mu = 0.7$ (for High stress). Table I reports the simulation parameters and also summarizes the most relevant results. For the following instance, data was generated randomly with the respect to the parameters in Table I and time horizon $t = 1000$.

Most notably, Table 2.2 reports that for the battery under low stress ($\mu = 0.4$), the event of data loss is more frequent than the apparent discharge. We observe the opposite situation if the battery is highly stressed, i.e, for $\mu = 0.7$, in which the data loss event does not happen at all.

We better analyse the results by showing the full evolutions of two sample simulations in Figs. 2.7 - 2.8, showing the cases of low and high battery stress, respectively. In the former case, it is visible from Fig. 2.7 that a lower service rate leads to a higher

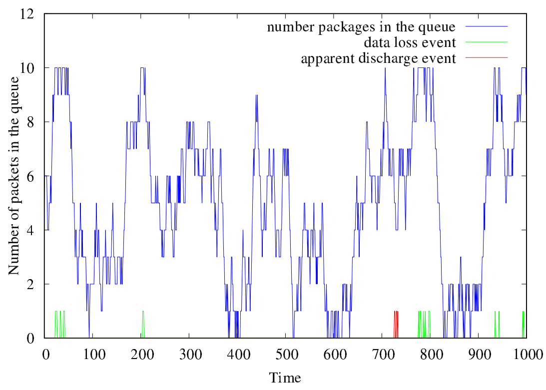

Figure 2.7: Apparent discharge and data loss event for μ=0.4

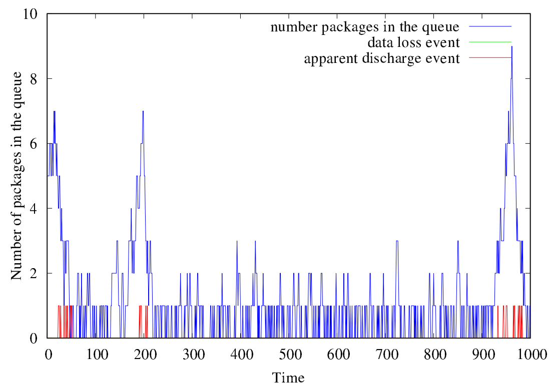

Figure 2.8: Apparent discharge and data loss event for μ=0.7

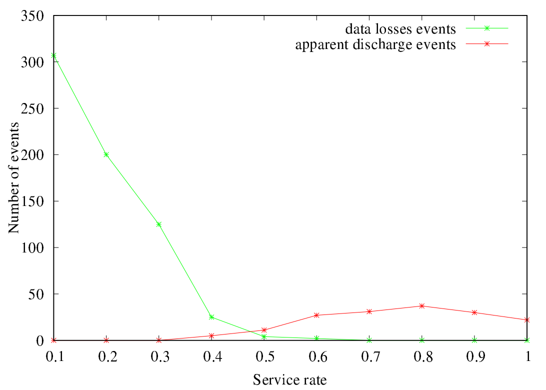

Figure 2.9: Changes of data loss and apparent discharge frequency for $\mu = 0.1 - 1.0$.

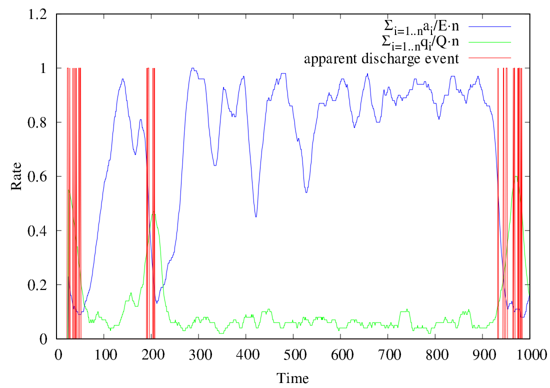

Figure 2.10: Comparison of condition (2.2) with apparent discharge events, for $n = 25$, in the High stress scenario ($\mu = 0.7$).

probability of data loss event. Conversely, Fig. 2.8 shows how higher service rate leads to apparent outages and minimization of the data loss events. Furthermore, we can plot the occurrences of these two events in a more generalized setup, where μ is varied from 0.1 to 1; the result is reported in Fig. 2.9, which confirms what observed before. Thus, we can identify that there is a connection between the data buffer occupancy (i.e., the q/Q ratio) and the apparent discharge and data loss events.

Now, considering a scenario where μ can be regulated by the device, and recalling that $q = Q$ is the condition triggering a data loss event, it is clear that keeping q/Q as relatively close to 1 may increase the frequency of data losses. However, increasing the rate so as to keep q/Q low also incurs a likely situation where apparent battery outages appear. More in general, the relationship between μ and q/Q may be descriptive of this tradeoff. On one hand, the value of q/Q has to be minimized, which is possible by increasing the value of service rate μ. On the other hand, high values for μ is responsible for a fast battery discharging and increasing of apparent/full discharge probability. So the aim is to find optimal relationship between q/Q and μ.

However, we remark that q/Q can change in a time slot when packets leave the data queue, which would imply an energy consumption, but also when packets arrive, that has nothing to do with the energy level. Conversely, the energy level changes also because of deep discharges, leakage, or charge recovery effects, and none of these phenomenons is reflected by a change of q. Thus, the current value of q/Q cannot exactly predict that the apparent/full discharge event is about to happen, also the previous states of the battery needs to be taken into account. For this reason, instead of just the local value of q and a, we propose to consider a moving average value of q/Q and a/E for n steps. Therefore, we seek to establish a condition that takes form:

$$\sum_{i=1}^{n} \frac{q}{nQ} - \sum_{i=1}^{n} \frac{a}{nE} < 0 \tag{2.2}$$

This condition can be better observed in Fig. 2.10, where we plot, for an instance of the system under the High stress case ($\mu = 0.7$) the time evolution of the two terms involved in (2.2) and we also highlight, in red, the occurrence of the apparent discharge event. For this specific evaluation, we chose $n = 25$. As we can see from Fig. 2.10, apparent discharge events occur only when (2.2) is violated.

To describe the data loss, we obviously involve again the value of q/Q, but we want to derive a connection to the battery level as well. We denote with ϵ the data loss probability. From empirical observations, we found out that the following relationship is often closely achieved, which establishes an exponential behavior of the data loss probability versus the ratio q/Q but also linear in the apparent energy level:

$$\epsilon = \frac{a}{E \cdot e^{1-\frac{q}{Q}}} \tag{2.3}$$

The initial assumption is that the probability of data packet transmitting is equal to the relative energy level of the battery. But while our goal is not to let the buffer to get full ($q = Q$), we adjust ϵ by $1/e^{1-\frac{q}{Q}}$. Higher value of q/Q, performs less correction (decrease) of ϵ.

Let us consider changing of the ϵ value for the case of Low Stress of the battery

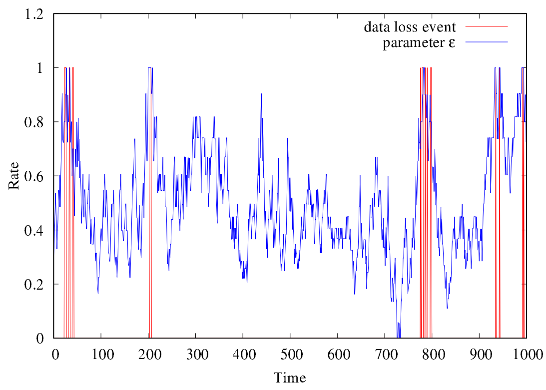

Figure 2.11: Data loss parameter values ($\mu = 0.4$)

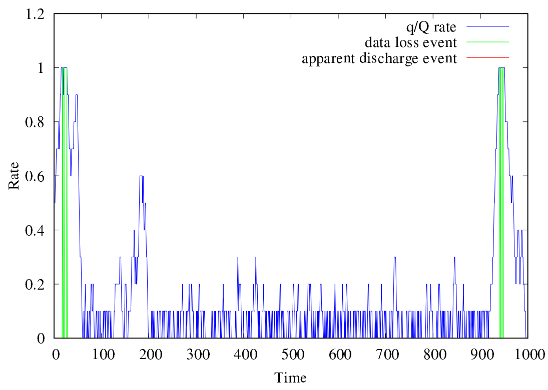

Figure 2.12: Apparent discharge event ($\mu = 0.7$)

($\mu = 0.4$). In this case, ϵ takes the maximum value of 1 exactly wherever there are data loss events. This is plotted in Fig. 2.11, where data loss events are highlighted in red.

Now, we extend these conditions to an *active* control of the data packet transmissions. In particular, we employ these remarks about the aforementioned connections to establish some preliminary checks in the decisions to be made by the wireless device on whether to transmit a packet or not. We add two more conditions to the model, reflecting (2.2) and (2.3), that is, a packet can be transmitted only if $(q/Q)-(a/E) < 0$ (condition 1) and $a(E \cdot e^{1-\frac{q}{Q}})^{-1} < 1$ (condition 2). If both conditions are met, then we allow data packets to be sent (the actual decision on whether to transmit a packet is made depending on the service rate and the state of the system). If condition 1 is violated (that is, the energy level is estimated to be low) and condition 2 is not, then the data packet is held and cannot be transmitted. If the opposite happens, i.e., the energy level is sufficient but conversely there is an abundance of data in the queue and the buffer risks an overflow, we *force* packet transmission, i.e., we transmit with service rate 1. Note that this heuristic rule is anyway not almighty, since if both conditions are violated, it means that we estimate that both energy outage and data overflow are about to occur, but there is nothing that can be done, since any data sent to avoid overflow will probably be lost because of low battery.

To examine conditions 2.2 and 2.3 we integrate these inequalities into the simulation models for the example considered above. The results of the simulations are presented on Fig. 2.12, where we consider a case of High stress for the battery ($\mu = 0.7$). The figure shows that integrating restrictions 2.2 and 2.3 reduces the number of apparent discharge events. For the previous example, when $\mu = 0.7$, integrating these conditions reduces the number of apparent discharge events by 77.4%. Also, we verified that, similarly to this case, when $\mu = 0.8$ we have a reduction of 75.6% of the apparent outage events, when $\mu = 0.9$ this reduction is of 73.1%, which means that this result is pretty consistent also for other values of μ.

2.3 Energy modeling and adaptive sampling algorithms for energy harvesting powered nodes

This section explores the implementation of different sampling strategies for a practical energy harvesting wireless device (sensor node) powered by a rechargeable battery. We look for a realistic yet effective sampling strategy that prevents packet delivery failures, which is simple enough to be implemented in low complexity hardware. Finally, the proposed methods are compared based on energy consumption over a year and amount of packet delivery failures, thus showing how some modifications of available strategies achieve satisfactory performance in this sense.

This work investigates possible extensions to improve the performance of the Data-Driven Adaptive Sampling Algorithm (DDASA) [2] in terms of energy awareness, taking advantage of other ideas presented in the literature. We complement the algorithm with sampling rate limitations, regarded as constraints to the adaptive sampling policy, which are realistically present in industrial applications.

The proposed algorithms aim at balancing the performance of the sensor device considering energy harvesting capabilities as well as its current battery status. We compared based on energy consumption over a year and amount of packet delivery failures the proposed solutions with DDASA and a strategy with constant sampling rate and energy arrivals.

To perform a realistic assessment of the resulting performance, we tried to realistically simulate all operational aspects, including an accurate model of the environment, energy harvesting, and battery behaviour, so as to derive a correct quantification of the State of Charge (SoC) as well as the energy consumption of the device. As we found out, most of the evaluations in the literature do not take all these aspects into account. For instance, most of the SoC models do not consider battery deterioration due to continuous usage or environmental factors.

Therefore, we considered an extension of those models to a practical setup to derive a realistic SoC estimation. For our validation, we used a LoadSensing commercial data-logger (further - LS) [40] powered by the commercial solar panel SOLEM 10/150/100 TD. We forecast the operation of the industrial data-logger for a period of one year and compared the performance under different sampling rate strategies.

The Section is organized as follows. The state of the art and background information in adaptive sampling for wireless sensing devices is given in Section 2.3.1. In Subsection 2.3.2, we introduce our sampling policies dealing with sampling rate limitations. In the following section, we present the simulator system model (Subsection 2.3.3). In particular, the solar irradiation model is discussed in subsection 2.3.3.1, the Photovoltaic (PV) power output model is presented in Subsection 2.3.3.2, the improvements of SoC estimation is demonstrated in Subsection 2.3.3.3. Numerical results are discussed in Subsection 2.3.4.

2.3.1 Background in adaptive sampling for sensing devices

According to [41], energy management in WSN is defined as a set of instructions to efficiently handle power consumption and energy provision in a constrained sensor node. In the literature, papers dealing with energy management try to either enhance their provisioning, or minimize the energy consumption.

For the latter goal, i.e., to reduce (or adapt) the energy consumption, duty-cycling, data-driven and mobility based approaches are considered. Duty cycles is one of the most effective way to improve the network energy sustainability. In [42], the authors propose to adjust the nodes duty cycles, or, in other words, the wake/sleep phases. The volatility of the energy arrivals is accounted by energy prediction. The authors of [43] proposed a method to reduce the energy consumption by adjusting the sensing duty cycles according to the available energy levels. Mobility based approaches consider the mobile nodes in the network [41, 44].

Finally, data-driven approaches are based on spatial correlation of data, and aim to reduce the amount of the sampled data keeping the sensing accuracy within an acceptable range. These approaches are subdivided on data prediction schemes and data acquisition approaches. Data acquisition schemes try to reduce the energy consumption in the node sensing subsystems, and can be implemented using three different approaches [41]: hierarchical sensing, adaptive sampling, and model-based active sensing. In hierarchical sensing, multiple sensors are installed on the sensor nodes and observe the same event with a different resolution and power consumption. Hierarchical sensing can be divided into two types:

- triggered sensing - when more accurate and power-consuming sensors are activated after the low-resolution sensors to detect some activity within the sensed area;

- multi-scale sensing - identifies areas within a region that require more accurate monitoring.

Adaptive sampling techniques provide online sampling frequencies for sensing nodes and change the sampling rate by evaluating correlations between the sensed data and the available energy [45]. If the subsequent samples do not differ very much, then it is possible to reduce the sampling rate based on this temporal correlation. Another possibility to decrease the overall energy consumption by adapting the sampling rate frequency is to apply harvesting aware optimization of the power consumption using the known remaining battery level and forecast harvested energy.

Model-based active sensing is a forecasting model of the sensing phenomena based on an initial set of sampled data. As underlined in [46], some sensors may even consume significantly more energy than the transmission component. The authors propose a general approach that leverages two complementary mechanisms at the sensor level: 1) duty cycling (i.e., the sensor board is switched off between two consecutive samples) and 2) adaptive sampling (i.e., the optimal sampling frequency is estimated on-line). The proposed ASA in [46] is tested on a snow-monitoring applications sensor. It is demonstrated that ASA performs 79% more efficiently in terms of energy consumption in comparison with the constant sampling rate. Nevertheless, the algorithm has room for enhancement regarding the residual energy level.

Srbinovski et al. [47] introduce the Energy Aware Adaptive Sampling Algorithm (EASA), that modifies the ASA algorithm by taking into account the current energy level of a sensor. That is, ASA is combined with an energy aware function, assuming that each node in the network is able to monitor its own energy level. The sampling rate of EASA is consecutively decreased under certain energy level without limitation since the sampling rate of EASA is proportional to the remaining energy of nodes. EASA is evaluated on two testbeds powered by two sources of energy - wind and solar, and is demonstrated that EASA outperforms ASA.

Other energy-aware adaptive sampling algorithms are proposed in [48]: Resuscitation Adaptive Sampling Algorithm (RASA) and Compensation Adaptive Sampling Algorithm (CASA). The purpose of RASA is to set low sampling rate and guarantee self-sustainability when energy state of sensors is extremely low. Sensor nodes in CASA can be recharged by saving the consumption energy when the harvesting quality is good. The algorithms are compared with ASA and demonstrated a better performance in terms of energy consumption.

An optimal scheduling sensing policy for an energy harvesting system equipped with a finite battery is considered in [49]. The objective is to select the sensing epochs such that the long-term average sensing performance is optimized. Finding the optimal solution can be a computationally intensive task and requires a device to have sufficient computational capabilities.

The data-driven approach is adopted to develop ASA for power management in automated monitoring of the quality of water. Data-driven adaptive sampling algorithm (DDASA) is proposed in [2]. DDASA can save 30.66% of energy for three months in comparison with the fixed rate strategy. DDASA changes the sampling frequency based on the nature of the sampled ratio compared with ASA. A sigmoid function is proposed to dynamically set the sampling frequency. DDASA is tested on a device, powered by a non-rechargeable battery, thus, it does not take into account the harvesting capabilities as well as battery level.

From the described algorithms only CASA takes into account energy harvesting potential of a sensing device, even though the benefits of using a data-driven approach such as including the data accuracy in the optimization are not incorporated. Therefore, one of the objective of this work is to adjust the data driven approach to calculate the sampling rate of a battery and harvester equipped device. Yet, we integrate sampling rate limitations as a mechanism to adapt to the industrial requirements.

In the literature, further adaptive sampling algorithms for more specific applications in WSN are proposed. In particular, in [50] optimality criteria for mobile robotic WSN is suggested to the most informative location of interest. The adaptive sampling strategy for mobile sensors in the environment monitoring context was proposed in [51], where the sequential Bayesian prediction algorithm minimizes the prediction error variance. An adaptive sampling system for sensor network is considered in [52], that is, the analog method for signal dependent ADC clocking. Another adaptive sampling algorithm was proposed in [53] for target tracking in underwater WSNs, that simultaneously balance the energy consumption and maximizes the energy efficiency. All of these proposals are specific to their applications and leverage some further aspects of their scenarios. Even though we considered a definite use case related to the geotechnical industry, our proposal is instead more general and we believe that we can extend our same rationale to all these contributions to improve their results.

2.3.2 Adaptive sampling algorithms with sampling rate limitations

Adaptive sampling algorithms estimate at runtime the expedient sampling frequencies for sensor devices.

Sampling algorithms can be extended by including sensing frequency limitations. This is motivated by the industrial requirement of guaranteeing a certain amount of data per unit of time. In particular, it might be desirable to limit the minimum sensing frequency, while maximum sampling rate can be as high as possible. In this case, the maximum frequency can be only bound by a duration of a cycle, in which a sensor performs warming up, measurement and transmissions:

$$F_{max}[Hz] = \frac{1}{t_{warm} + t_{meas} + t_{trans}}, \tag{2.4}$$

where t_{warm}, t_{meas} and t_{trans} are the time required for warming up of the sensor, taking a measurement and transmitting the measurement, respectively.

In this section, we propose 4 methods taking into account energy harvesting capabilities and battery level information, in order to improve the DDASA performance. Differently from DDASA, the proposed methods include sampling rate limitations, energy capabilities as well as the capability to sectorize the battery level and apply different rules to the different sectors.

Sampling rate limits F_{max} and F_{min} serve as boundaries for the proposed adaptive sampling algorithms.

The original DDASA changes the sampling frequency based on the nature of sampled data (Algorithm 1). Specifically, DDASA updates the sampling frequency based on the sigmoid function $y(D)$ $(0 < y(D) < 2)$, where D is calculated as a difference between two measurements x_i and x_{i+1} over the average value of the N recent data. D rises if the environment suddenly changes (Fig. 2.13).

The sigmoid function represents a deterministic growth pattern. The simple way to represent the sigmoid function is [54]:

$$w = \frac{w_{max}}{1 + e^{-k(t-t_m)}}, \tag{2.5}$$

where w is the weight to be calculated, w_{max} is the maximum value of w, t_m is the period of time when the maximum value of w was observed, and k defines the curvature of the pattern.

Our first proposal is Threshold-Based Adaptive Sampling Algorithm (T-ASA), which is based on the energy level and harvesting rate thresholds, and corrects the

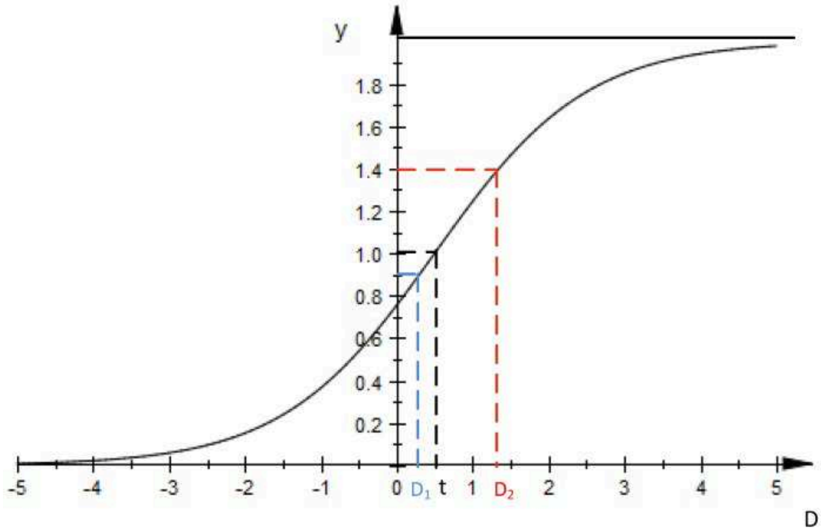

Figure 2.13: Revised sigmoid function [2]

sampling rate when the energy level or energy arrival rate go beyond a threshold. T-ASA utilizes the mechanisms proposed in [47] and [48]. Based on their approach, we propose the mapping between different battery and energy arrival levels (thresholds) and equations that adjust the sampling rate. This method considers four states:

1. High energy arrivals ($H/H_{max} > k$) and high battery level ($E_{batt} > E_{th}$): $f_{new} = f_{curr}$;

2. High energy arrivals ($H/H_{max} > k$) and low battery level ($E_{batt} < E_{th}$): $f_{new} = f_{curr} \cdot (\frac{E_{th}-E_{batt}}{100})^m$;

3. Low energy arrivals ($H/H_{max} < k$) and high battery level ($E_{batt} > E_{th}$): $f_{new} = f_{curr} \cdot (1 + \frac{H}{H_{max}}) \cdot N$;

4. Low energy arrivals ($H/H_{max} < k$) and low battery level (($E_{batt} < E_{th}$): $f_{new} = f_{curr} \cdot (\frac{E_{th}-E_{batt}}{100})^m \cdot (1 + \frac{H}{H_{max}}) \cdot N$,

Parameter k is an energy arrivals threshold, m and N denote the parameters of the algorithm, H and H_{max} are current solar radiation and maximum possible solar energy arrival, correspondingly, E_{batt} and E_{th} are the current battery level (%) and battery threshold (%). Coefficient $(E_{th} - E_{batt})/100 \in [0, 1]$ represents the deviation of the energy level from its threshold. The parameter m adjusts the granularity of the algorithm. Higher values of m decrease the value of the sampling frequency more significant. In other words, m is adjusted depending on the strength of the required intervention. Coefficient $(1 + H/H_{max}) \in [1, 2]$ increases the value of the sampling

Algorithm 1 DDASA

Initialize a constant sampling rate denoted as f_{const}, sample a number of N for later use;
Predetermine a threshold according to the characteristics of the monitored parameters;
Define $D = |X_{i+1} - X_i| / \frac{1}{N} \sum_{i-N+1}^{i} X_i$;
Define $f_{curr} = f_{const}$, where f_{curr} is the current sampling frequency;
for $i = N; i++$ **do**
    Sample X_{i+1} based on f_{curr} (or f'_{curr});
    $D = |X_{i+1} - X_i| / \frac{1}{N} \sum_{i-N+1}^{i} X_i$;
    $y(D) = \frac{2}{1+e^{-(D-t)}}$;
    $f_{new} = f_{curr} \cdot y(D)$, where f_{new} denotes the new (updated) sampling frequency.;
    $f'_{curr} = f_{new}$;
    $S(i+1) = X_{i+1}$;
end for
return S;

frequency in the case of more frequent energy arrivals. Parameter $N \in (0, 1]$ similarly with m defines the granularity of the method.

The second method, analogously to T-ASA, uses f_{max} and thresholds. However, instead of correcting the current sampling rate as done in the previous method, the calculation is based on the sampling rate limit f_{max} and current energy capabilities. The method is defined as Limits-Based Adaptive Sampling Algorithm (L-ASA):

1. High energy arrivals ($H/H_{max} > k$) and high battery level ($E_{batt} > E_{th}$): $f_{new} = f_{max}$;

2. High energy arrivals ($H/H_{max} > k$) and low battery level ($E_{batt} < E_{th}$): $f_{new} = f_{max} \cdot (\frac{E_{th}-E_{batt}}{100})^m$;

3. Low energy arrivals ($H/H_{max} < k$) and high battery level ($E_{batt} > E_{th}$): $f_{new} = f_{max} \cdot (1 + \frac{H}{H_{max}}) \cdot N$;

4. Low energy arrivals ($H/H_{max} < k$) and low battery level (($E_{batt} < E_{th}$): $f_{new} = f_{max} \cdot (\frac{E_{th}-E_{batt}}{100})^m \cdot (1 + \frac{H}{H_{max}}) \cdot N$,

In the third method called Limits- and Thresholds-Based DDASA (L-DDASA), we propose to adjust the sampling rate to its limits if the following conditions are satisfied:

1. High battery level ($E_{batt} > E_{th}^{up}$): $f_{new} = f_{max}$;

2. Low battery level ($E_{batt} > E_{th}^{low}$): $f_{new} = f_{min}$

If $E_{th}^{low} < E_{batt} < E_{th}^{up}$ then sampling rate is determined by DDASA. To take into account the harvesting capabilities of a sensor node, we introduce the calculation of derivatives, that determines the period of time when the energy arrivals have a tendency to grow or decrease over time.

3. if $\frac{df}{dt} > 0$: $f_{new} = f_{curr} * \alpha$, where α ($0 < \alpha \leq 1$) is a coefficient increasing the sampling frequency;

4. if $\frac{df}{dt} < 0$: $f_{new} = f_{curr} * \beta$, where β ($0 < \beta \leq 1$) is a coefficient decreasing the sampling frequency.

Finally, Energy Aware DDASA (EA-DDASA) is based on the calculation of the sigmoid function presented in DDASA. In contrast with DDASA, we include the calculation of the sigmoid function not only for collected data, but also for energy arrivals and battery level:

$$\begin{aligned} y(D) &= \frac{2}{1 + e^{-(D-t)}} \\ x(SoC) &= \frac{2}{1 + e^{-(SoC-k)}} \\ z(H) &= \frac{2}{1 + e^{-(k-\frac{H}{H_{max}})}} \\ f_{new} = f_{curr} &\cdot y(D) \cdot x(SoC) \cdot z(H) \end{aligned} \tag{2.6}$$

All three components in (2.6) are combined to define the value of sampling rate, so that, for instance, low values of battery level can be compensated by high energy arrivals.

In order to validate the proposed methods, we simulate the operation of an industrial sensor node powered by a solar panel. Simulations are based on the system model presented in the following section.

2.3.3 Energy model

To test the proposed adaptive sampling algorithms we introduce the energy model for the energy-harvesting wireless sensor, specifically, for a tiltmeter powered by a solar panel.

To analyze the sustainability of the solar-powered sensor device with integrated adaptive sampling algorithm, we first describe our model for the node SoC. This can be divided into four stages:

1. Model of the solar irradiation taking into account meteorological conditions, location, reflection, solar panel inclination, soiling effects, etc.
2. Model of the power output based on the inner characteristics of the solar panel, such as cell temperature, area, losses, solar radiation on the tilted surface etc.
3. The actual load model based on the battery effects, such as battery degradation and duty cycling
4. The energy consumption model based on the expenditure for one sensing cycle and the adopted adaptive sampling algorithm

2.3.3.1 Solar irradiation modelling

Solar irradiation represents the amount of solar power (or instantaneous energy) per unit area $[W/m^2]$. Few parameters that determine the solar irradiation on the surface of Earth are discussed in [55]: the Earth's geometry and location (declination, latitude, solar hour angle); terrain (elevation, surface inclination and orientation, shadows); atmospheric attenuation (scattering, absorption) by gases, solid and liquid particles and clouds.

Different combinations of these parameters are included in the solar irradiation models. Global solar energy models are considered in [56], divided into two components: extraterrestrial and global solar energy, i.e. above or below the atmosphere, respectively. Global energy models may be further categorized into computation of direct beams and diffuse solar energy. These parameters are usually measured, but the installation of measurement devices is costly. Therefore, prediction models are widely used to measure the global solar radiation [56].

The following groups of solar irradiation models can be outlined: linear and non-linear. Linear models give the correlation between solar energy on a horizontal surface and some meteorological variables, such as shining hours, ambient temperature and relative humidity. Due to the model simplicity, linear models are more commonly used. Diffuse solar energy models describe the relationship between the average daily diffuse and global solar radiations incident on a horizontal surface and the sky clearness index.

Other more sophisticated types of models are based on the Artificial Neural Networks (ANN). The commonly used input variables in ANN-based models are the sunshine ratio, ambient temperature, and relative humidity to predict global solar energy at different locations, but also following inputs can be used: latitude, longitude, altitude, month, time, wind speed, relative humidity, and rainfall. The results of the study showed that the ANN-based models are more accurate in predicting the diffuse radiation compared to the linear regression models, but are much more demanding in terms of data and complexity.

In [57], the astronomical solar model is presented, which is used to translate the instantaneous solar radiation (I_{sun}) into effective radiation. The effective (or available) solar radiation ($I_{eff} = I_{sun} \cdot \cos\Theta$) is dependent on factors such as: location, inclination of a solar module, time of the year and hour of the day, where Θ is the angle between the sunlight and the normal to the solar module surface.

In [58], a clear-sky radiation model is introduced. The total radiation G_T is divided on 3 components: beam (G_{bT}),diffuse (G_{dT}), and reflection (G_{rT}), which can be calculated as:

$$G_{bT} = G_{on}\tau_b cos\theta_s \tag{2.7}$$

$$G_{dT} = G_{on}cos\theta_z\tau_d\left(\frac{1+cos\beta}{2}\right) \tag{2.8}$$

$$G_{rT} = \rho G_{on}cos\theta_z\tau_r\left(\frac{1+cos\beta}{2}\right) \tag{2.9}$$

where G_{on} is the solar radiation outside of the atmosphere, τ_b, τ_d and τ_r are the atmospheric transmittance for a beam, diffuse and reflected solar radiation, respectively. θ_z, θ_s, β and ρ are the solar zenith angle (rad), the incident angle on the surface, the inclination angle of the surface (deg) and the average reflection on the ground.

The clear-sky model is suitable for meteorological conditions without clouds, mist or haze, but in comparison with the astronomical model, it includes the diffusion and reflection components.

Astronomical and clear-sky models do not include atmospheric attenuation and are not as accurate as ANN models. However, these models do not require meteorological data and solar radiation measurements, therefore the model is easily applicable and can be adapted to any location. Clear-sky solar radiation model is a wider model that includes parameters such as diffusion and reflection solar energy. Therefore, this model can be used as a foundation to compute the solar radiation in a particular location for a solar panel with known inclination angle and direction.

We test and compare astronomical and clear-sky models to obtain an input solar

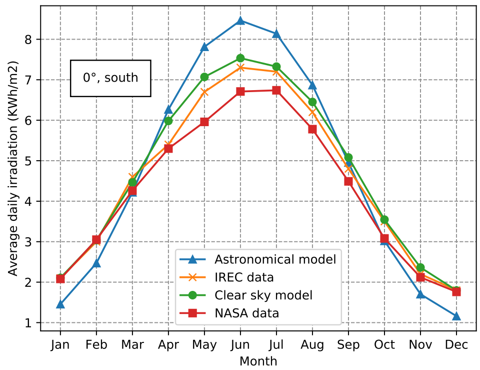

(a) 0°

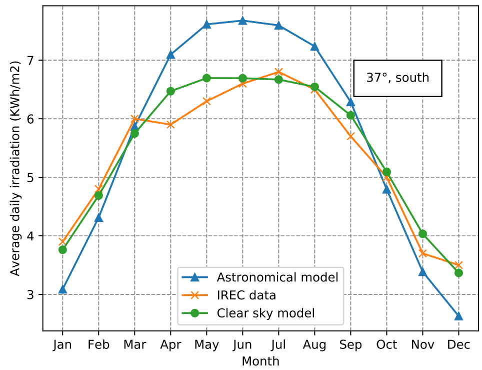

(b) 37°

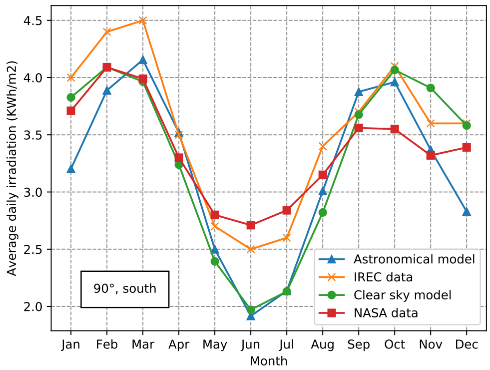

(c) 90°

Figure 2.14: Comparison of average daily irradiation.

radiation. These models do not demand the real data sheets, although the knowledge of the reflection characteristics of the location and ground are needed. We set the reflection parameters that correspond to the concrete surroundings since we consider the urban scenario.

The models were implemented and compared with real data, provided by IREC (Institut de Recerca en Energia de Catalunya) for Barcelona, Spain, and with the database of NASA for a tilted solar panel: 0° (Fig.2.14(a)) , 37° (Fig.2.14(b)) and 90° (Fig.2.14(c)). For this purpose we aggregate hourly data over one year, obtained as an output of these two models. The incident solar power data for the input of an astronomical model was derived from [59].

For the performance evaluation of the models, we consider the mean square error E of the average daily irradiation y. That is, if y_i is a data point and $\hat{y}_i$ is its estimate,

Table 2.3: Error values

	Astronomical model			Clear sky model		
Data source	**0°**	**37°**	**90°**	**0°**	**37°**	**90°**
IREC	6.421	7.654	2.462	0.738	0.871	1.507
NASA	12.064	-	2.196	3.839	-	2.005

we compute E as:

$$E = \sum_{i=1}^{N} (y_i - \hat{y})^2, \tag{2.10}$$

A comparison of the results for two models is presented in Table 2.3. Clear-sky model showed higher accuracy in comparison with the astronomical model.

2.3.3.2 PV power output modelling

In general, the power output depends on the active area of the solar panel and the technology [60]:

$$E = A_{pv} \cdot r \cdot G_T \cdot PR, \tag{2.11}$$

where A is the total solar panel area (m^2), r is a solar panel yield of efficiency (%), G_T is an annual average solar radiation on a tilted panel (shading is not included) that depends to solar position, cloud cover, atmospheric transmittance, and power orientation; moreover, PR is a performance ratio, i.e. a corrective coefficient for losses (in the range between 0.5 and 0.9, with a default value of 0.75), and finally r is the effective power, derived from Standard Test Conditions (STC), that corresponds to 1000 W/m^2, at a cell temperature of 25 °C, wind speed 1 m/s, $AM = 1.5$.

Alternatively, solar power output depends to global solar irradiation, area of the solar panel, efficiency of the solar panel, average losses, and temperature, as per [61]:

$$P_{pv} = \eta \cdot A_{pv} \cdot G_T \cdot [1 - 0.005(T_c - 25)], \tag{2.12}$$

where η is the photoelectric conversion efficiency (%), T_c is the panel operation temperature ($^{\circ}C$). Temperature of the cell can be obtained from the following equation: $T_{\text{air}}[i] + 0.035 * G_T[i]$, where T_{air} is an hourly temperature [62].

In practice, a correct definition of G_T is required to obtain a proper estimate of the AC power output. Alternative power output formula does not take into account the temperature, which leads to ignoring the effect of the temperature raising on the effectiveness of the solar panel.

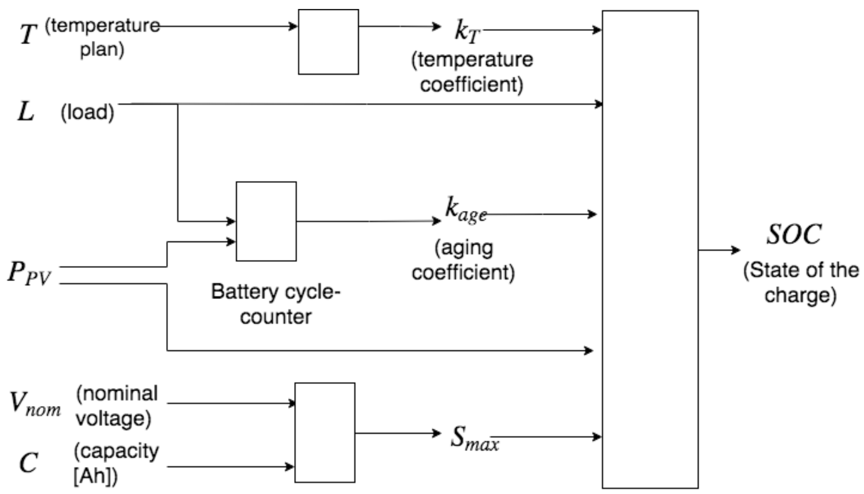

Figure 2.15: SoC estimation model

One of the main correction factors for the solar panel output model is power losses. In particular, the main parameter derived from the clear-sky model is a global solar radiation $[W/m^2]$. The value of this parameter significantly changes according to the meteorological factors, shading etc., and moreover, other losses occur in the solar panel itself. In general, other loss parameters can be included, for example: annual losses due to the soil, inverter losses, Direct Current (DC) cable losses, Alternating Current (AC) cable losses, shading, losses at weak radiation, losses due to the dust, snow, and so on [63].

2.3.3.3 SoC modelling

SoC can be defined as a rate of available capacity (in Ah) against its nominal capacity [64]. In the literature, we can find common methods to estimate SoC, however these methods are just general representation and lack many details, as they usually do not consider a realistic battery behavior, but rather define SoC based on energy consumption, arrivals of energy, and battery capacity.

In addition, complex calculations and high computational cost are other concerns that make the estimation process very difficult. Exhaustive classification of SoC estimation methods are presented in [65] and [66]. Few general SoC definitions are presented below.

SoC can be defined as a relation between current capacity $(Q(t))$ and nominal capacity(Q_n): $SoC(t) = \frac{Q(t)}{Q_n}$ [66].

The most common way to estimate SoC is current integration: $SoC = 1 - \dfrac{\int idt}{C_n}$, where i is a battery current and C_n is a nominal capacity.

Another common way to define SoC is through Coulomb efficiency: $SoC = 1 - \frac{\int \eta i dt}{C_n}$, where i is a positive/negative current, η is Coulomb efficiency, i.e. the ratio of the energy required for charging to the discharging energy needed to regain the original capacity. This method requires the knowledge of initial SoC and precise measurements of the battery current. Coulomb method is not precise and does not include duty cycle and temperature. Apart from it, additional equipment is necessary for SoC calculation.

Another general model for defining SoC of a battery was presented in [67]:

$$SoC_t = \frac{S_{t-1} + \Delta S_t}{S_{max}} \tag{2.13}$$

$$\Delta S_t = \Delta C_t - \Delta D_t - \Delta L_t, \tag{2.14}$$

where ΔC_t is the charging energy, ΔD_t is a demand parameter and ΔL_t is energy losses.

Demand ΔD_t is defined as:

$$\Delta D_t = \Delta t P_{e,t} = \Delta t \cdot I_t \cdot U_{dc,t}, \tag{2.15}$$

where $P_{e,t}$ is the electric power consumption, I_t is the discharging current, $U_{dc,t}$ is a voltage output of the battery.

$S_{\max}$ is defined as follows:

$$S_{\max} = C \cdot U_n = \Delta P_{c,t} \cdot t, \tag{2.16}$$

where U_n is the nominal voltage, $P_{c,t}$ is the charging power at time t.

Due to the non-linear time-varying characteristics and electrochemical reactions, battery SoC cannot be defined directly. Furthermore, the performance of the battery is highly affected by aging, temperature variation, charge-discharge cycle, which make the task of accurately estimating the SoC very challenging. We consider an SoC model based on the reasoning above, but we should also include additional parameters such as battery age and temperature coefficient. The general scheme of the model is reported in Fig. 2.15.

The current SoC depends on the SoC on the previous time interval, capacity, and nominal voltage of the energy storage, degradation of the battery, and energy charges and consumption of the device.

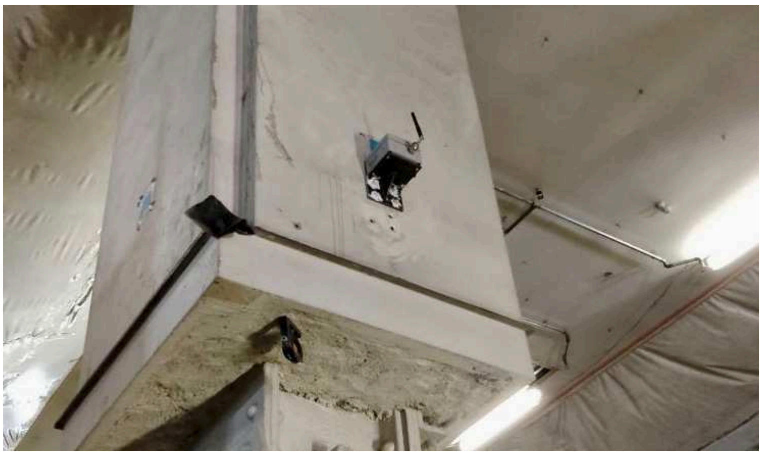

Figure 2.16: Example of tiltmeter installation for Courtesy of Sixense Oceania [1]

2.3.4 Numerical results

In this section, we report the numerical experiments we conducted to compare different sampling strategies: constant sampling rate, DDASA with and without limits and methods, presented in Subsection 2.3.2.

All algorithms were tested on the tiltmeter data extracted from LS, that is a part of the *Auckland City Rail Link Extension project* [68]. Tiltmeters can be used to measure the surfaces' inclination of construction objects. An example of LS tiltmeter installation is presented in Fig. 2.16. Replacing the batteries in such objects is problematic and not economically profitable. Powering of tiltmeters by solar panels can be considered as a valid solution for the outdoor construction objects (bridges, buildings etc.).

2.3.4.1 LS description and energy consumption

LS is a wireless data logger powered by batteries. It performs periodic sensing and sends the measures via radio transmission to a gateway or concentrator. It has multiple possible configurations, which affect the battery life drastically. LS can be configured to employ different duty cycles of measurements, from one measure every 30 seconds to one measure per day. The product is designed for the geotechnical industry and usually installed at locations that are difficult to reach, therefore where battery replacement to be avoided. In order to create an accurate estimation model of the battery discharge, it is necessary to outline the application scenario. We consider worst case energy consumption scenario, determined by:

1. warming up - 3 seconds (60 mA, 12 V)

[1]This figure is provided by Worldsensing SL

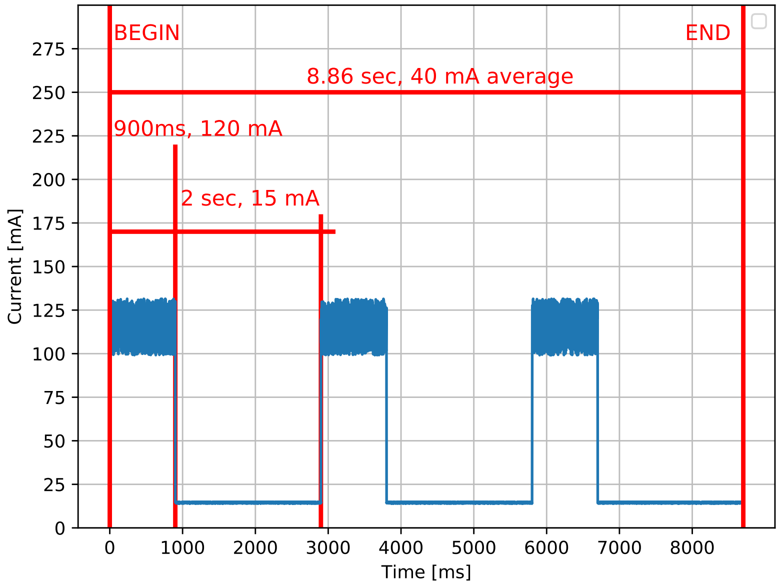

Figure 2.17: Radio consumption profile of LS device [1]

2. measurement - 3 seconds (60 mA, 12 V)
3. transmission - 3 pulses (900 ms, 120 mA, 3.6 V each) and time between pulses (2s, 15 mA, 3.6 V)
4. background consumption between cycles is 30 µAh, 3.6 V.

After a measure is taken, it is sent by radio. The system has about 5 minutes to send the radio message. The message transmission has also multiple variables but for the sake of simplification we consider the worst case.

When LS performs a complete cycle once per hour, then the hourly consumption is about 2.844 W. The radio transmission consumption is presented in Fig. 2.17.

2.3.4.2 Solar panel characteristics

We obtain the power output for the solar panel SOLEM 10/150/100 TD with size 138.8 mm × 90 mm oriented on the south with inclination 37°. The theoretical efficiency of the amorphous silicon PV module is 12.7%, plus average losses due to the shading, dust, wiring etc. are included with a loss coefficient of 0.75, see Fig. 2.18.

The temperature dataset for solar panel power output estimation (Fig. 2.19) is extracted for Barcelona, Spain for 01.01.2017 - 31.12.2017 from [59].

[1] This figure is provided by Worldsensing SL

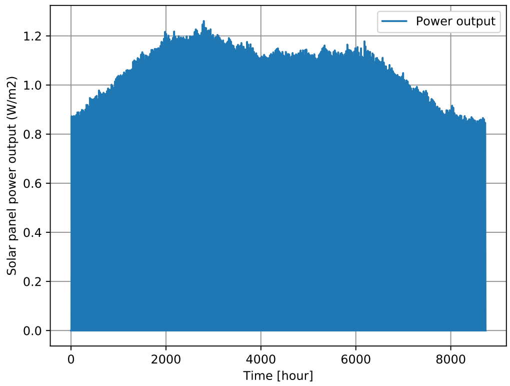

Figure 2.18: Theoretical power output of solar panel SOLEM 10/150/100 (south, 37°) located in Barcelona, Spain

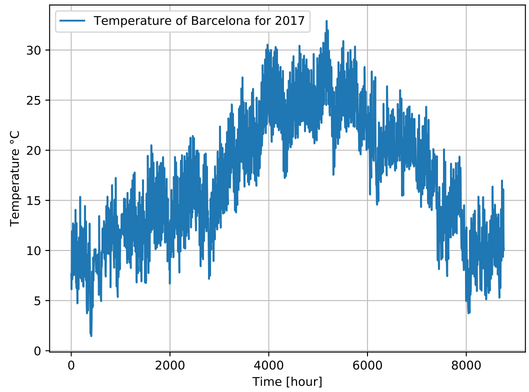

Figure 2.19: Hourly air temperature profile of Barcelona, Spain for 2017 year

2.3.4.3 Battery characteristics

The battery present in the simulator is an LG18650B4 with nominal capacity of 2600 mAh and nominal voltage of 3.6 V.

The coefficient of aging was obtained from data, provided by IREC. The capacity of the battery depends on the number of cycles performed: after 300 cycles the battery loses capacity from 2600 to about 2500 mAh. In addition, battery capacity depends on the air temperature and varies from 59% of total capacity if the air temperature is below −20 °C to 104 % if the temperature exceeds 40 °C.

2.3.4.4 Evaluation of simulation results

The proposed algorithms are aimed to balance irregular energy arrivals. In line with this, we set the benchmark case, that corresponds to the ideal scenario of regular energy arrivals. To do so, we average the energy arrival profile presented in Fig. 2.20(a) over time.

We compare the performance of DDASA and all other proposed algorithms with the sensor performance under ideal conditions. Simulation settings are presented in Table 2.4. The duration of a time slot is one hour.

The failure rate is chosen as a comparison performance metric. A device fails when the battery does not have enough energy to transmit a data packet. If the significant gain in decreasing of failure rate by adapting the algorithm is achieved, then we will have simple and effective lightweight solution, which can be implemented on the real sensor devices.

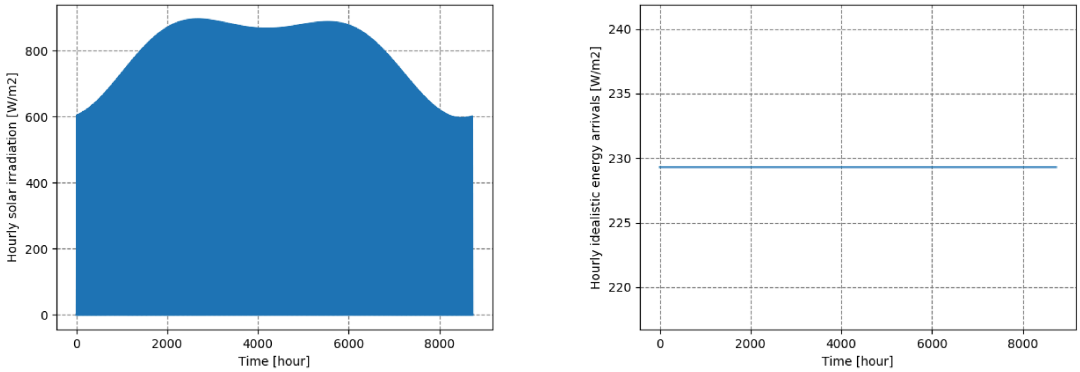

(a) Realistic solar irradiation profile for Barcelona, 2017

(b) Idealistic energy arrivals

Figure 2.20: Comparison of energy arrival profiles.

Table 2.4: Simulation parameters

Parameter	**Value**
Minimal sampling rate, F_{min}	$1.157 \cdot 10^{-5} Hz$ (24h)
Maximum sampling rate, F_{max}	$4.639 \cdot 10^{-5} Hz$ (6h)
Algorithm parameter, m	1
Algorithm parameter, N	0.5
Initial number of samples, N_{DDASA}	50
Inclination data threshold, t	0.001
Harvested energy threshold, k	0.1
Battery level threshold, E_{th}	$0.2SoC$
Upper battery level threshold	$0.4SoC$
Lower battery level threshold	$0.1SoC$
Coefficient, α	1.2
Coefficient, β	0.8

The implementation of DDASA algorithm in LS demonstrated that the algorithm needs to be improved in terms of energy awareness and robustness, that have to be more balanced and adapted to the available energy level and harvesting capabilities.

DDASA leads LS device to frequent failures to transmit a data packet (Table 2.5). Sampling rate obtained with DDASA depends to the data variation only. And it can lead to the situation when the energy arrivals are poor, but data variation is high. It causes more aggressive battery drain and termination of LS operation. Therefore, the original version of DDASA is not able to ensure the robust operation of LS that is

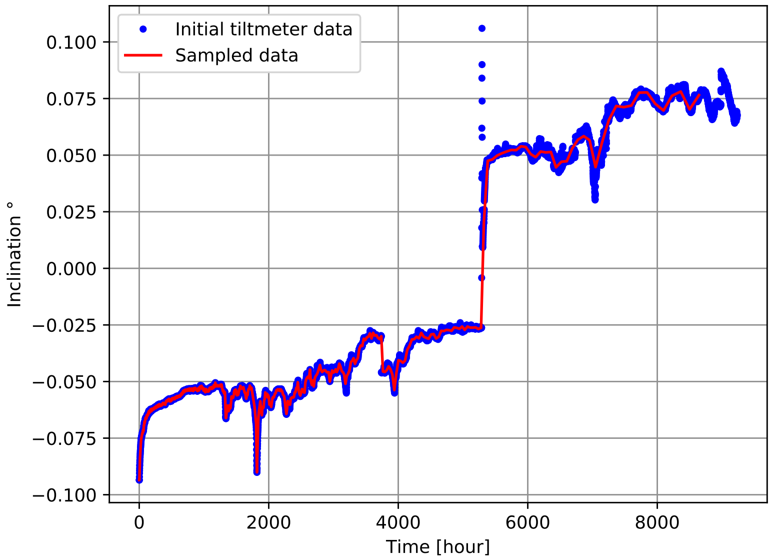

Figure 2.21: Comparison of initial dataset obtained under constant sampling rate of 1 hour with a dataset obtained under DDASA (here initial tiltmeter data and sampled data respectively)

powered by a solar panel over a whole year.

The sampling rate during data collection phase (or transition phase) is adjusted to 1 hour, which is the duration of a time slot. All device failures of the proposed strategies (T-ASA, L-ASA, L-DDASA, EA-DDASA) are accounted for this transition period. If we compare the similar throughput results presented in Table 2.4, then EA-DDASA provides the closest performance results to the ideal conditions case. The failure rate is 0 during all months except January, that includes the transition phase 2.22(a).

EA-DDASA demonstrates balanced energy consumption 2.22(b): during winter it consumes less energy, while during summer months it consumes more energy, except July, that can be explained by the power output pattern, shown in Fig. 2.18. DDASA energy consumption is guided by data variations and therefore the energy consumption is unbalanced, and during some winter months we observe much higher energy consumption, than during summer months, which causes the device to operate on the edge of its capabilities.

In general, the choice of the algorithm can be dictated by different circumstances. In particular, if the environmental conditions have a stable pattern over the span of the year (i.e., energy provision has little volatility), then L-ASA can be adopted, since it provides a higher throughput, but the average SoC is lower, comparing to other proposed algorithms. If the environmental characteristics are highly unstable, then

Table 2.5: Comparison of algorithms

Algorithm	**Throughput, [packets]**	**Failure rate (with/ without transition phase)**	**Total energy consumption, [W]**	**Average SoC, %**
Constant energy arrivals, sampling rate (24h)	364	0.00	1036	99.5
Constant energy arrivals, sampling rate (9h)	970	0.00	2759	98.1
Constant energy arrivals, sampling rate (6h)	1028	0.05	2919	5.8
Realistic energy arrivals, sampling rate (24h)	364	0.00	1036	98.5
Realistic energy arrivals, sampling rate (6h)	938	0.06	2668	5.3
DDASA	1336	0.58/0.56	7603	3.0
DDASA with limits	951	0.04/0.02	5414	5.6
T-ASA	407	0.02/0.00	2319	92.8
L-ASA	945	0.02/0.00	5379	19.9
LT-DDASA	709	0.02/0.00	4037	75.7
EA-DDASA	915	0.02/0.00	5209	68.9

T-ASA can be implemented, that provides the highest average SoC. The most balanced methods are L-DDASA and EA-DDASA. In addition, if the Li-ion battery is attached to the device, then the recommended energy level holds. For some batteries chemistry, it is preferable to keep the average battery level low to preserve the battery life [69]. As the battery level stays around 100 % SoC, the battery degrades faster, since Keeping charging the battery leads to micro-charges and discharges, thus negatively affecting the battery's life. Therefore, the average SoC may be also worth considering.

In order to improve robustness of the proposed schemes, the energy arrivals learning models can be implemented, that will exclude the usage of the predefined environmental characteristic evaluations. This method is more effective, but at the same time computationally heavy and requires to install additional hardware, that measures the solar radiation information (pyranometers). This will lead to the overall cost increase of a sampling device.

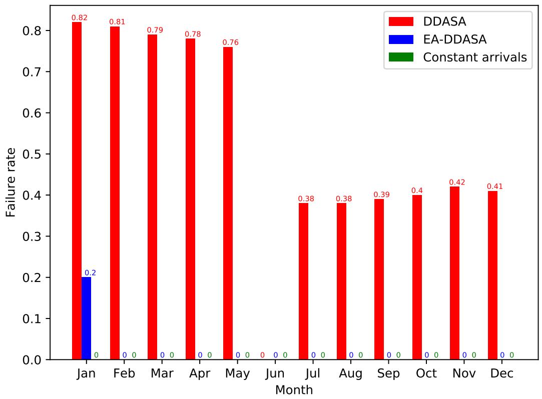

(a) Monthly failure rate

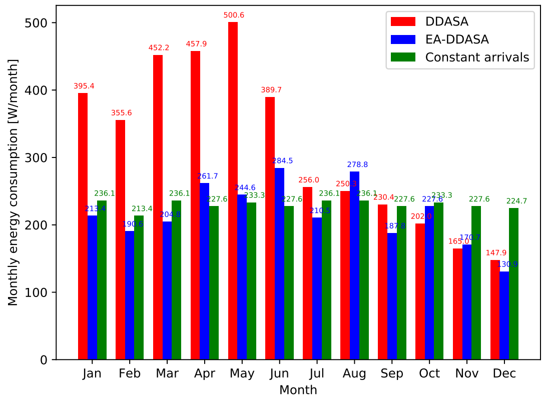

(b) Monthly energy consumption

Figure 2.22: Comparison of DDASA, ideal conditions strategy and EA-DDASA.

2.4 Conclusions

Firstly, we developed a stochastic model for battery-powered energy harvesting mobile devices, based on a discrete-time finite-state Markov chain. We keep into account the data queue and the energy level of the device; the latter is mapped through variables a and e, representing the apparent and true state of the battery, respectively. This way, we can represent non-idealities such as leakage and more importantly charge recovery, which is generally overlooked in most investigations.

We apply the model to sample evaluations, capturing energy outage under two definitions, i.e., depending on whether a is zero, or e is. The main conclusion is that charge recovery severely affects the performance, as the apparent outage probability can be significantly larger than that of real outage. Conversely, the probability that e actually reaches 0 is lowered by the early operational stop caused by reaching an apparent level a equal to 0, which can lead to heavy underutilization of the device. The key parameters in determining the extent of this phenomenon are the probabilities of deep discharge and recovery, which should be kept low and high, respectively.

For simplicity, we considered constant parameters in the Markov chain. The main point of our contribution is proven in spite of this simplifying assumptions, although future work may relax this assumption and investigate exponential or multi-step [25] discharging. We can also include a dependence on the energy level in the leakage probability. Finally, we can merge the present contribution with the investigations of [22] about correlation in data and energy arrivals, or those of [8] where the service rate depends on the energy level, to optimize the battery usage under an overall more realistic model.

We demonstrate the effect of battery operation policy and evaluate the occurrence of undesired events which could cause negative consequences, for example, battery inactivity. We based on a model which deals with the data queue and the energy queue of the device as well as battery imperfections such as leakage, charge recovery and deep discharge. By inspecting the simulation results we found that certain parameters are significant for prediction of such events as apparent discharge and data loss. Based on these parameters, we propose a simplified self-control management for a battery, which is to verify the conditions in the model decision making process for battery-powered energy harvesting mobile devices. The purpose of the self-control management is to reduce both the data losses that happen when the data buffer is full, and the apparent outage of the device. The restrictions integrated in the strategy can be easily rewritten to take into account full outage of the device. The effectiveness of the proposed scheme was numerically proved.

Finally, we propose energy aware strategies applied to the data driven adaptive sampling approach, that balance the energy consumption and decrease the number of packet delivery failures. To validate the performance of the proposed schemes, we simulated the operation of the industrial data-logger powered with a solar panel located in Barcelona, Spain.

We observed that with prior knowledge of the environmental characteristics it is reasonable to set threshold based rules and sampling rate limits that significantly increase the performance of the existing data-driven approach without increasing the complexity of the algorithm.

Improving sensor operation strategies is needed to provide the full autonomy of a device with energy harvesting capabilities, which is a key to design successful and self-sustainable IoT systems.

Chapter 3

Energy sustainability of systems with multiple EH-devices

To investigate the multi-device case, we study the asymmetry in energy-harvesting WSNs (Section 3.2), and proposed energy cooperation as a mean of overcoming systems heterogeneity (Section 3.3). We introduce the concept of energy topology with integrated energy cooperation, and analysed the efficiency of energy cooperation (Section 3.3.2). The application of energy cooperation in SC is considered in Section 3.3.3.

3.1 Introduction

IoT systems play a significant role in forming SC, that are expected to be home to most of the future society and can be defined as [70]: "well defined geographical areas, where technologies such as ICT, logistics, energy production, and so on, interact to create benefits to the citizens in terms of well being, easier and faster access to services, inclusion/participation, environmental quality, and intelligent development". The integration of ICT within SCs, in particular, IoT technologies, makes it possible to build smart decision making systems based on real-time awareness, bringing together people, processes and knowledge. All the smart system components have to be intelligently interconnected [71].

IoT technologies are becoming a major driver for the industry and affect our everyday life through a number of services. For example, a 2009 survey conducted in Republic of Korea has counted 228 types of smart services, classified in many categories including, among others: administration, transportation, medical care, environment, crime and disaster prevention, education, tourism, sport, and work production [72]. Public Protection and Disaster Relief (PPDR) is key service encompassing critical applications handling direct threats to life, individual or public health and safety, property, and environment [73]. Often, these applications are highly dependable: service outages have severe effects and should be avoided. This means that energy provisioning is key for the design of smart services. Yet, at the same time it is predicted that 50 billion IoT devices will be interconnected by 2020 [74]; thus, the reduction of their energy footprint is also important.

Interconnected objects such household or office equipments [75], vehicles [76, 77], human wearable sensors [78], and any other devices belonging to the IoT, in a SC can be powered by external energy sources, i.e., either the power grid or renewable sources; energy consumption represents a dynamic process that requires real-time energy management.

At the same time, paradigm for network intelligence dictates that smart management also involves optimal cooperation schemes among nodes [79, 80]. While this has been mostly applied to data communications, the emergence of converging network schemes likely suggest that ICT will interlink independent systems at many levels. As a result, "system-to-system" topology creates the possibilities for new Smart Cities' scenarios. Cooperation capabilities in these contexts will help building new business models, as linking smart cities objects in an optimal way will result in the increase of individual and collective profit as well as sustainability.

IoT technologies enable network optimization by introducing a holistic perspective where the network is considered as a multi-agent cooperative system. As a consequence, we can seek to optimize the energy flows between smart city objects or, generally speaking, energy management in a smart city, which can be considered as including both wireless connected nodes and the power grid as an integral part of it, all included in a common distribution space of information and energy. The outlined distributed system can be considered as a system-of-system topology in which both information and energy flows exist, and they mutually aid each other, so that the power connections supports data communication links, and conversely data communication also carries out the task of optimizing the energy topology.

However, energy management in large complex networks such as a SC requires high computational capabilities for real-time optimization of energy flows, storage, distribution, and consumption [81]. To manage energy flows and cooperation between IoT nodes, an algorithm defining the optimal nodes to cooperate is needed. Usually, this is handled by considering energy-aware clustering algorithms that try optimizing the energy topology or decrease the number of links in the network [82]. This is because one of the issues limiting the overall network performance is the power limitation of a communication node. To avoid a node failure, energy efficient clustering algorithms were expansively studied in the literature, mainly focusing on the energy awareness rather than energy cooperation. As an initial step for designing a clustering algorithm with energy cooperation capabilities or with embedded energy topology, the study of a scenario with a single cluster (one sink node) is needed.

3.2 Study of asymmetry in EH-WSN

We consider the management of an EH-WSN, inspired by game theory so as to obtain a distributed multi-agent operation. In particular, we focus on asymmetries in the nodes energetic capabilities, and how do they impact on the resulting performance. We frame the problem as a repeated Bayesian game with asymmetric players and incomplete information, where also the private information available at each node is asymmetric. We find out that instead of a proportionally fair resource utilization, such a situation ends up in an even more unbalanced situation, which leads to an inefficient management where certain nodes are utilized beyond their fair share. Future research directions are identified so as to recover information about asymmetries from the strategic gameplay of the sensors and thus enable a better management.

The Section is organized as follows. The background in game theory approach for WSN is provided in the Subsection 3.2.1. The system model is introduced in the Subsection 3.2.2. Finally, the numerical results are demonstrated in the Subsection 3.2.3.

3.2.1 Background in game theory approach for WSNs

Nowadays, this still presents several challenges related to the design of efficient policies for WSN [83], [84], since nodes are usually programmed to carry out tasks without coordination. Depending on the rules set and making a decision on which sensor is associable to a certain task, there may still be inefficiencies. No node can be active to provide service, or multiple nodes are simultaneously active, which represents an energetic wastage. This is further complicated by the lack of information about the energy levels of the nodes. If a node is delegated to a task, but due to high battery stress it gets depleted, that task will be unsolved even though another sensor could have carried it out.

One possible solution is to approach the problem from the standpoint of game theory, so as to model multi-agent interactions with different objectives [85]. Relevant to this paper, [86] applies a game theoretical approach for battery-powered WSN in which the battery state of a sensor is private information; it computes a Bayesian Nash equilibrium that is found and compared with the perfect-information game. In [87] game-theoretic approach is applied to analyse multi-channel and multi-access schemes. Authors prove the Pareto-optimality of the Nash equilibrium of the system and offer an online-learning algorithm for the multi-channel and multi access system.

Authors of [88] consider the WSN as Bayesian for warning notifications to avoid energy overuse in bottleneck nodes in a clustered solar-powered network. All these papers consider a symmetric case, e.g., with identical battery storage.

In general, game theory is used for distributed optimization under the assumption that nodes are all rational but they are also assumed to be identical and perfectly coordinated, so that the functioning conditions are equivalent for all of them. In reality, there may be several differences in environmental conditions for EH of each sensor; for example, sensors can be equipped by solar panels with different orientations, or they can significantly differ in their circuitry or battery type. Past activity history of each sensor, and private information about the surrounding environment, also affect the ability of the sensor to operate. Each sensor performs differently in managing and transmitting data, and battery stress can change considerably. Another cause of asymmetry can be that a sensor may or may not have complete information about the energy level performance of other players.

Specifically, we study a case of non-identical EH sensors that perform some tasks (transmissions of packets with variable size) assigned to a common service available to all of them, but distributively managed as a participatory activity. We formulate the analysis as a repeated Bayesian game with asymmetric players. We consider the operation of the WSN by discussing the implications of asymmetries in the nodes' characteristics for EH (such as a battery capacity), and also we investigate the effect of having some information as private. One sensor updates its belief based only on the history of the game, while the other makes its decisions taking into consideration the information about the capacity and the energy state of the other player.

The ideal management of such a network would be to still exploit the nodes proportionally to their capabilities. However, since the management is distributed and the nodes do not have full awareness of the entire network, this principle may cease to be applicable. Thus, we use the model of the Bayesian game with asymmetric players as a

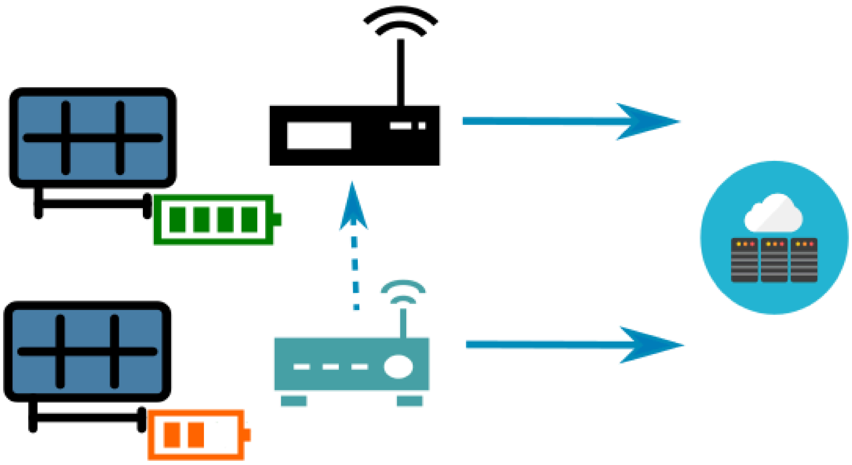

Figure 3.1: System model

way to quantify the resulting unfairness. We performed some simulations and showed that this situation does not lead to the ideal game performance proportion, but is still more balanced in comparison with the strategy, when all sensors are unaware of asymmetries.

Future research directions are identified to avoid these imbalances; for example, a proper belief update rule can be designed so that in the long run the nodes are able to acquire the knowledge they lack, or at least to estimate it.

3.2.2 System model

We consider a WSN virtually playing a repeated Bayesian two-player game with asymmetric players. Each game round represents the decision of each sensor about whether to pursue a given task. Players are denoted as j and k, respectively. Each task is also associated with the amount of energy for its transmission. We consider the transmission of data packets as the tasks that the sensors try to accomplish, in which case the amount of energy is a direct consequence of the packet size. However, the approach can be easily generalized to other kinds of tasks as well. The decision about whether to transmit the packet or not is also based on current and average energy level of the other sensor in the network [86]. The key point of this decision-making process is that, according to a Bayesian game setup, players may not have full knowledge about the scenario and therefore create themselves $beliefs$ to handle the situation. The decisions they make are actually based on expectations (averages) of their beliefs [85].

For our problem, we assume that node k is fully aware of the network operation, while node j represents an entire room full of LIFO policies. We use these notations:

e_l^i - level of energy of sensor $l \in \{j, k\}$ at round i

e_l^{max} - capacity of sensor l's battery, with $l \in \{j, k\}$

$\overline{e_l}$ - average energy level of sensor $l \in \{j, k\}$

e_q^i - amount of energy required to transmit data at round i

a_l^i - energy arrival at node $l \in \{j, k\}$, at round i.

In the repeated Bayesian game players care about the future consequences of their current behaviour. Every stage a sensor has to decide whether to spend energy or store it. In the former case, the level of energy in stage $i+1$ will be:

$$e_j^{i+1} = max(0, e_j^i - e_q^i + a_j^i) \tag{3.1}$$

If the sensor makes the decision to store energy, then the energy level of its battery will be corrected only by an amount of the arrival energy and will be:

$$e_j^{i+1} = min(e_j^i + a_j^i, e_j^{max}) \tag{3.2}$$

In a single-device system, sensor transmits only if the energy state of the battery is greater than a threshold, or in other words, sensor j transmits, only if $e_j^i \geq e_{th}$, where e_{th} is a given energy threshold [86]. If μ_j is a probability that the energy level of sensor j is greater than its threshold in the i round, or in other words, a probability, that the sensor has enough energy to transmit, then any $\widetilde{\mu}_j > \mu_j$ will allow the transmission:

$$\begin{cases} \mu_j = 1 & e_j \geq e_{th} \\ \mu_j = 0 & e_j < e_{th} \end{cases} \tag{3.3}$$

If we consider the situation with several sensors in the WSN, the performance analysis is to be distributed, and each sensor has to transmit less data in total, than in a single-device system. It can be proven that in this case the threshold is corrected by the probability that another sensor also transmits the data packet. Let μ_k be a probability that the energy level of sensor k is greater than its threshold in the i round, then:

$$\begin{cases} \mu_j = 1 & e_j \geq \frac{e_{th}}{1-\mu_k} \\ \mu_j = 0 & e_j < \frac{e_{th}}{1-\mu_k} \end{cases} \tag{3.4}$$

We now consider that information about the opponent's energy level and the capacity of the battery is not symmetric. We denote the information about the current energy level e_j^i and the capacity of the battery e_j^{max} of sensor j as a common knowledge.

The information about the energy levels of the sensor k (e_k^i, e_k^{max}) is private. Therefore, sensor k is able to make decisions guided by the rules of the rational behaviour, taking into consideration energy levels of both sensors. In particular, the probability that sensor k should increase its transmission rate if the energy level of sensor j may not be enough for transmitting an incoming data ($e_j \geq e_{th}$) packet, and monotonically increase if the value of the threshold increases over the energy level of sensor j in the $i-1$ round. In addition, the higher energy level of the sensor k, then the higher probability that sensor k will transmit the data packet in the next round only if the battery has enough resources or $\overline{e_q} > e_k^{i-1}$. Based on this, we bring the following

Proposition 1. The strategy of sensor k in the i stage is:

$$\mu_k^i = min([\overline{e_q} > e_j^{i-1}] \cdot \frac{\overline{e_q}}{e_j^{i-1}} + [\overline{e_q} > e_k^{i-1}] \cdot \frac{e_k^{i-1}}{e_k^{max}}, 1) \tag{3.5}$$

where threshold $\overline{e_q}$ is calculated by using the statistical information about the data packets sent in the $t = (0, ..., i-1)$.

In comparison with sensor k, sensor j operates based only on the information about its own energy level and the history of the game. Similarly with [89], we denote the history of sensor k' actions as $h_k^i = (a_k(t_0), ..., a_k(t_{i-1}))$, where $a_j(t_i) \in A_i = \{transmit, not\ transmit\}$ is an action of sensor j. We identify the system of belief updates for sensor j about the distribution probability of sensor k, i.e., sensor j updates its belief about the energy state is under or below its threshold of the sensor k by using Bayes rule from round i to $i+1$. Let $\mu_j(\theta_k|h^i)$ be belief of sensor j about the energy level of sensor k at round i, where $\theta_k = e_k^i \geq e_k^{th}$, then the posterior distribution will take form:

$$\mu_j^i(\theta_k|h_k^i) = \frac{\mu_k^i(\theta|h_k^i)P(a_k(t_i)|h_k^i)}{\sum \mu_k^i(\theta_k|h_k^i)P(a_k(t_i)|\theta_k|h_k^i)} \tag{3.6}$$

where $P(a_k(t_i)|e_k^i > e_k^{th}|a_j(t_i), h_k^i)$ is the probability that the action will be observed in the i round. From this equation we see that to update the belief, the whole history h_k^i of sensor k has to be taken into account to calculate the probability a given action $a_k(t_i)$ is played.

In our game, both sensors choose an action simultaneously at the beginning of each game. And sensor k make strategic decision expressed in equation 3.5, and sensor j every round updates beliefs using the Bayes' rule, as per equation 3.6. The performance of such a system will be presented in the next section.

Table 3.1: Simulation parameters

Parameters	**Values**
Capacity of S_j	0..20
Capacity of S_k	20
Energy consumption in i round e_q	1..5
Arrival amount of energy in i round a_j^i, a_k^i	1..4
Energy arrival rate α, β	0.6

3.2.3 Simulation and numerical results

We consider a two - sensor WSN, described by parameters previously outlined. Sensors have different battery capacities and the system has a single data queue that represents the source for tasks to be performed by nodes. Each round a data packet arrives to be transmitted with random energy consumption e_q^i.

We compare 2 scenarios of belief update and how they affect the fairness of the game. Firstly, *scenario 1*: when two sensors transmit randomly with probability $\mu_j = 0.5$ and $\mu_k = 0.5$ respectively, at each round i. We do not update beliefs about the energy level of the opponent player. In *scenario 2* we introduce the belief update rule about sensor k and the behaviour rule of sensor k with respect to the energy levels of both sensors, proposed in the previous section. We vary the value of e_j^{max} to reveal dependence between chosen strategy and fairness of the game. We expect that in the ideal situation the sensor with bigger capacity transmits more data amount, or by other words, to observe the directly proportional relationship between balance in throughput and capacity of a sensor's battery if the strategy is good enough.

Note that throughput depends on three components: amount of lost data, total energy consumption for data transmitted by sensor k and j. Fig.3.2 demonstrates three scenarios:

– ideal scenario, when no data loss is observed and each sensor transmits data according to its capacity of the battery, for example if $e_j^{max}/e_k^{max} = 0.5$, then k and j transmit 2/3 and 1/3 of total data amount respectively.

– *scenario 1*, in which each sensor transmits data randomly.

– *scenario 2*, in which one sensor transmits data according energy state and capacity information of the opponent sensor, obtaining each time slot, and the opponent sensor transmits data updating its belief about energy state of the first sensor by accumulating the history h_k^i of its transmission.

If sensors transmits data randomly with $\mu_k = \mu_j = 0.5$, when both sensors decide

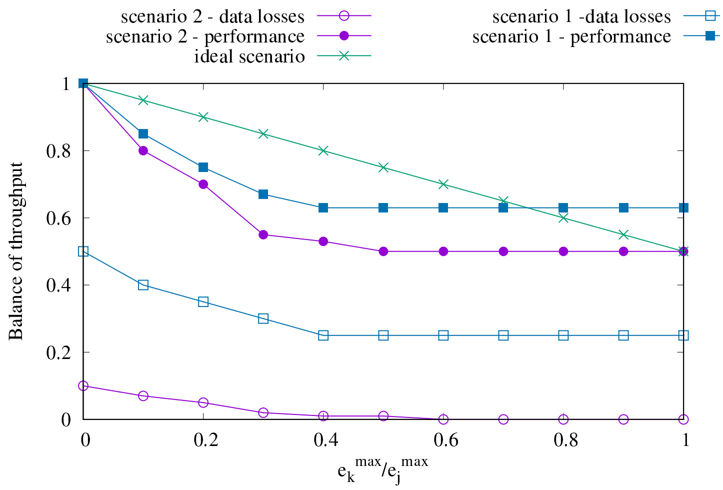

Figure 3.2: Numerical Results

to transmit the data packet or to drop it, we obtain an asymmetry reflected in the results (Fig. 3.2: data losses curves). Moreover, *scenario 2* demonstrates significantly smaller amount of data losses in comparison with the *scenario 1*.

Furthermore, from Fig. 3.2 we can notice, that in both scenarios if $e_k^{max}/e_j^{max} \geq 0.5$, performance and data losses of both sensors are equalized. Both scenarios do not provide the balanced performance, but *scenario 1* is slightly more rational, when $e_k^{max}/e_j^{max} < 0.5$, because sensor k takes into consideration in its strategy the capacity of sensor j. In particular, if $e_k^{max}/e_j^{max} = 0.1$, then in *scenario 1* 40 % of total data amount will be lost, 40 % is transmitted by the sensor with the higher capacity and 20% is transmitted by the sensor with the lower capacity. In *scenario 2*, 10 % of data will be lost, 80 % will be sent by a sensor with the battery with higher capacity and 10 % with the lower capacity. Note that in the ideal situation it should be equal to 0 %, 95 % and 5 % respectively. Thus, the results found prove that the knowledge about the asymmetric property of the system makes its performance more balanced and robust.

3.3 Energy cooperation

In this section, we investigate the possibility of integrating energy cooperation in IoT SC scenario. To do so, we design the optimal energy topology in a communication system, and analyse the effect of energy cooperation integration into the system with interconnected smart services.

The Section is organized as follows. In the Subsection 3.3.1 we discuss models proposed in the literature for energy cooperation features among communication nodes.

The concept of energy topology based on energy cooperation is studied in the Subsection 3.3.2. Finally, the case with interconnected cooperating GWs is considered in the Subsection 3.3.3.

3.3.1 Background on energy cooperation

Energy cooperation between wireless communication nodes was considered in [90], where energy sources and relay nodes have EH capabilities and exploit them in an attempt to maximize the end-to-end throughput. A few works have investigated energy cooperation among Base Station (BS)s. The authors of [91] propose an energy allocation scheme for EH-BSs. A convex formulation is posed and the obtained energy allocation policies are compared against an assignment problem solved through the Hungarian method. A similar scenario was considered in [92], where the set of BSs send out the harvested energy through a common aggregator and the solution for the optimal power allocation and energy transfer are obtained for a weighted-sum-rate maximization problem. A framework with two EH-BSs that have limited storage was studied in [93]. Two cases were considered: (i) the energy arrival profile is known in advance; or (ii) energy arrival statistics is not available. Online, offline, and hybrid algorithms were compared for both cases.

Lots of researches have been performed in investigating the energy cooperation capabilities in Smart Grids, in particular including: optimal scheduling among smart objects, optimizing both power expenditure and operation time [94]; optimal selection and sizing of a smart building system [95]; scheduling for optimal energy consumption to balance the load among residential subscribers [96]; analysis of the optimal power flow for distributed systems, in particular for the electrical network [97]; cooperative architecture for optimal voltage regulation [98]; optimal control of power exchange in a network of microgrid based on the energy consumption information [99].

These papers are aimed to study the Smart Grid without considering the communication topology and energy consumption of a system. Conversely, we consider the power consumption of a communication node to be also dependent on communication parameters, such as the distance from a sink node and the size of the transmitted data packets.

The efficient energy cooperation schemes that include both communication and energy cooperation usually are considered in wireless power transfer scenarios. In particular, in [100] authors introduced three techniques for multi-hop wireless energy transfer: store and forward, direct flow and hybrid technique. In [101], the authors consider a non-cooperative scheme, where information/energy are transported via direct links, then an optimization problem is formulated to minimize the transmitted power under outage probability and harvesting constraints.

In contrast with these outlined techniques, we focus on the energy links designing, which can be established not only with the near located nodes, but with any node of a network. It caused by possibilities to have cooperation between any IoT device that can belongs to different SC objects. Moreover, while in wireless power transfer scenarios the communication links and energy links are simultaneous, in our analysis, the energy and communication links are separated and not simultaneous.

3.3.2 Energy topologies in SCs

The definition of "energy topologies" based on energetic cooperation (exploitation and exchange) between interconnected objects is an important feature that can be implemented in SC. Based on the presence of EH devices, it is aimed at providing system-wide sustainability by allowing exchange of stored and supplied energy in a similar fashion to communication of data.

Our representation of a SC involves a network of nodes in which each element is capable of energy transmission to another node in need, meaning that each node has a possibility to manage the energy flows.

Designing the energy topology of connected IoT devices means establishment of energy links (edges) in an optimal way on top of the communication topology (Fig. 3.3). The system represents a biplex network, in which the two layer are the communication and energy networks. The number of optimal connected neighbouring nodes defines the energy topology of the system. The advantages of multiplex systems in SC, that includes the energy cooperation between objects was shown in [102]. Authors claim that considering a single type of static links is an oversimplification which can lead to inability to solve certain problems.

The power imbalance could be reduced when the effective interaction between the power supply and the demand is established. This was argued, for example, in [103], where an energy demand management solution was proposed to mitigate the imbalances between buildings. Authors proposed a scheme to analyse the energy potential of buildings and possibilities for cooperation, taking into account charging/discharging rate of buildings.

In this section, we investigate the possibility of integrating energy cooperation within the design of the energy topology, or, in other words, by establishing energy

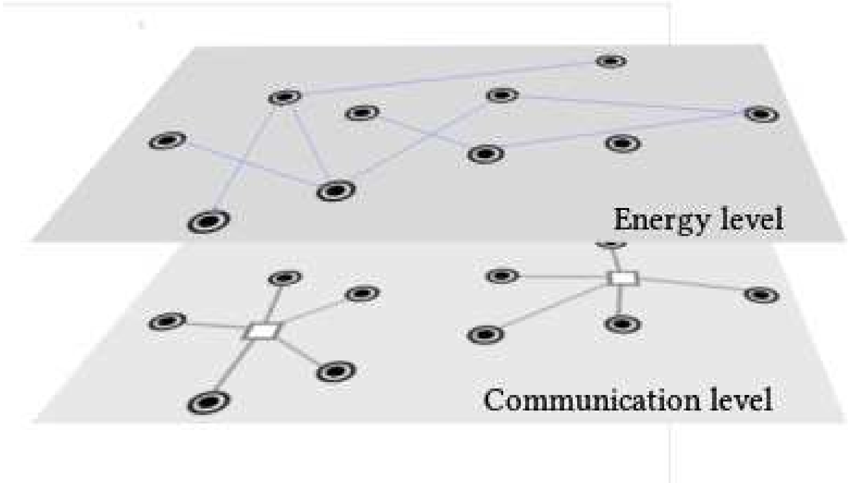

Figure 3.3: Topology scheme

links between objects, in particular wireless smart nodes powered by harvesting renewable energy sources. To do so, we construct an optimization model, where it is guaranteed that wireless nodes during operation will not be depleted and the optimal energy transfer does not exceed the energy demands of other communication nodes. We analyse how the system conditions can affect the energy topology, in particular, EH capabilities, energy levels, and energy thresholds. We also identify some theoretical limits for the system to guarantee complete sustainability, that is, nodes do not go out of charge. Also we demonstrated the effectiveness of the model comparing it with the system operation without applied optimization.

The rest of this section is organized as follows. In Subsection 3.3.2.1 we outline our proposed optimization model for a WSN scenario with a single sink node. The numerical results are discussed in Subsection 3.3.2.2 that shows the effectiveness of the proposed model and the behavior dependency from different parameters.

3.3.2.1 System model

We consider a system consisting of N communication nodes and a sink node, whose energy levels are denoted as $e_i, \quad i \in \{1...N\}$. V:=1,..,N is a vertex set of a complete graph $G = (V, A)$, where A is a set of edges (i, j) that represent the bidirectional energy link between communication nodes i and j. Node i can receive energy from other nodes as well as forward energy.

To provide a mathematical model to the problem, for each arc $a \in A$ we introduce a boolean variable:

$$l_a := \begin{cases} 1 & \text{if and only if the energy link between nodes} \quad i \text{ and } j \text{ is established,} \\ 0 & \text{otherwise} \end{cases} \tag{3.7}$$

The total number of possible bidirectional energy links varies in the following limits:

$$0 \leqslant L \leqslant \frac{(N-1)N}{2} \tag{3.8}$$

where $L = \sum_{i,j=1}^{N} l_{ij}$ is total number of links, $l_{ij} = \{0, 1\}$ is a link between nodes i and j, equals to 1 if the link is set.

Here is considered and applied the energy consumption of a communication node caused by communication exchanges between nodes. As done by [104], [105], we take into account that energy consumption of a connection between a transmitter and receiver depends on the distance between them. Increasing the distance from a sink node will cause a higher energy consumption E for communication, according to the following relationship:

$$E = a \cdot k + b \cdot k \cdot d^n \tag{3.9}$$

where k is the information unit size (packet) expressed in bits, and d is the distance between sink node and communication node. Parameters a and b are energy consumption parameters of the transmitter electronics and transmitter amplifier, respectively. In [106], the following parameters are suggested: $a = 50$, $b = 0.1$ and $n = 2$. We do not consider the energy consumption of a sink node, as the aim of this work to investigate the energy cooperation between communication nodes only.

The aim is to calculate the amount of energy links needed to provide sustainability taking into account the energy consumption, energy arrival profile and a current energy level of each object. In relevance with it, the optimization problem can be formulated as follows:

$$\sum_{i=1}^{N} \sum_{j=1}^{N} w_{ij} l_{ij} \rightarrow min \tag{3.10}$$

such that

$$l_{ii} = 0 \quad \text{for} \quad i = 1, .., N \tag{3.11}$$

$$l_{ij} = l_{ij} \quad \text{for} \quad i, j = 1, .., N \tag{3.12}$$

$$e_i - (a \cdot k + b \cdot k \cdot d_i^n) + f_i + \sum_{j=1}^{N} l_{ij} \cdot e_{tr}^{ij} > 0 \quad \text{for} \quad i, j = 1, .., N \tag{3.13}$$

$$e_i - (a \cdot k + b \cdot k \cdot d_i^) + f_i + \sum_{j=1}^{N} l_{ij} \cdot e_{tr}^{ij} \leqslant c \quad \text{for} \quad i, j = 1, .., N \tag{3.14}$$

$$\sum_{i=1}^{N} l_{i,j} \leqslant \alpha \leqslant N - 1 \quad \text{for} \quad j = 1, .., N \tag{3.15}$$

$$\sum_{j=1}^{N} l_{i,j} \leqslant \alpha \leqslant N - 1 \quad \text{for} \quad i = 1, .., N \tag{3.16}$$

where $w_i j$ is a weight of an energy link. A larger distance between energy arrival profiles and the communication consumptions results in a larger value w_{ij}. Value of w_{ij} is normalized:

$$w_{ij} = \left| \frac{e_n^{ij} + f_n^{ij} - (a \cdot k + b \cdot k \cdot d_{ij}^n)}{(e_n^{ij} + f_n^{ij} - (a \cdot k + b \cdot k \cdot d_{ij}^n))_{\max}} \right| \tag{3.17}$$

where f_n^{ij} and d_n^{ij} are differences in energy arrival profiles and distances to the sink node between communication nodes i and j:

$$e_n^{ij} = e_i - e_j \tag{3.18}$$

$$f_n^{ij} = f_i - f_j \tag{3.19}$$

$$d_n^{ij} = d_i - d_j \tag{3.20}$$

Constraints (3.11) and (3.12) are imposed to respect the requirements of the absence of energy links of a node with itself and symmetry of energy links: if energy can flow from object i to j, then automatically the energy can flow in opposite direction from j to i and the bidirectional link is established.

Constraints (3.13) and (3.14) provide the sustainability of a system after optimization, in particular, desirable energy levels range for each node. The first three terms represent the initial energy level of a node corrected by transmitting energy consumption and energy arrived to a node (f_i - energy arrival profile). The last term represents the energy transferred to the node i from all nodes j. The energy level has to be larger than 0 and do not exceed the battery capacity c, by this we guarantee that battery will not be out of charge and the transferring energy will not exceed demand of the node.

The transferred energy from node j to node i depend to conditions:

- the node j has enough energy to transmit;
- the node j has to have more energy than node i:
- the energy level of node j has to be higher than a threshold.

$$\begin{cases} e_{tr} = e_{th} - e_i \quad \text{if} \quad e_j > e_i \quad \text{and} \quad e_{th} < e_j \\ e_{tr} = 0 \quad \text{otherwise} \end{cases} \tag{3.21}$$

Objective function enforces to create energy links between nodes that have bigger energy potential differences. If nodes have similar energy arrival profile and consumption, then the cost of established energy link will not be justified as not much energy cooperation will be performed.

Another possible constraint arise if a node has to have a limited amount of energy links. In this case, the number of links are limited by constraints (3.15) and (3.16), where α is a maximum amount of allowed links, should not exceed $N-1$. Nevertheless, in this section we do not investigate the situation in which a communication object has such a limitation.

3.3.2.2 Numerical results

Numerical results were conducted with the aim to investigate the behaviour of an optimization model solution for different types of systems: different distance distribution, non-homogeneity in energy arrivals and in energy levels. As the second part of results we show the effectiveness of the optimization in comparison if no optimization is applied to the system.

Optimization is performed using the CPLEX solver ver. 12.6.1. We assume that all communication nodes have similar battery capacities.

As the first step, the matrices are defined: $(d_i) \in \mathbb{R}^{1xn}$, $(f_i) \in \mathbb{R}^{1xn}$, $(d_n^{ij}) \in \mathbb{R}^{nxn}$, $(f_n^{ij}) \in \mathbb{R}^{1xn}$, $(w_{ij}) \in \mathbb{R}^{nxn}$, $(e_{tr}^{ij}) \in \mathbb{R}^{nxn}$, $(e_i) \in \mathbb{R}^{1xn}$, $e_{th} = conts$, $c = conts$ and $k = conts$.

Matrices (d_i), (f_i) and (e_i) are random in ranges $(0, 15)$, $(0, 20)$ and $(0, 200)$ respectively, unless we vary their meanings in order to investigate these properties.

Table 3.2: Simulation parameters

Parameters	**Values**
Number of communication nodes (N)	50
Number of transmitted bits (k)	1
Communication parameter a	50
Communication parameter b	0.1
Communication parameter n	2
Battery capacity (c)	200

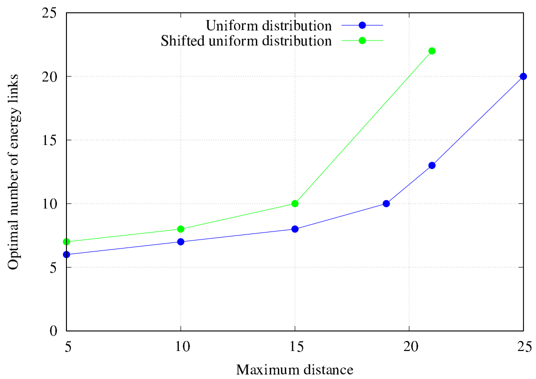

Figure 3.4: Distance distribution vs. optimal amount energy links

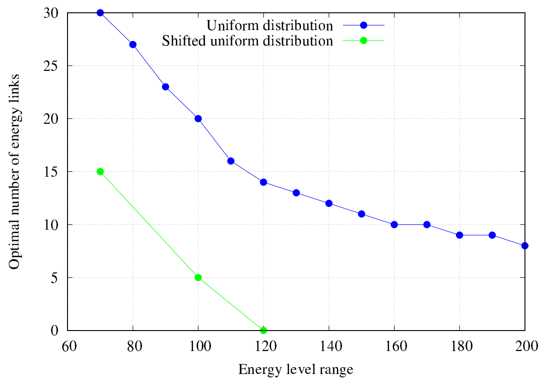

Figure 3.5: Optimal amount energy links vs. energy level distribution

Optimization parameters are presented in Table 3.2. Parameters a, b and n are chosen similarly with [106]. We consider the simple case transmission of 1 bit ($k = 1$).

In the first optimization setup, we check the dependence of optimal amount energy links and distance distribution (Figure 3.4). First, we set up an uniform distribution in the range from $(0, 5)$ till $(0, 20)$. In this case, the distance range increasing leads to increase of the energy consumption, therefore, a larger number of energy links is needed to provide sustainability of the system.

In the second experiment, we shifted the distance distribution from $(2, 5)$ to $(10, 20)$. By this, we guarantee that all communication nodes have a higher energy consumption, therefore the optimal amount of energy links is higher than in the first case. The optimal solution will not be obtained in case of distance increasing to $d_{ij} > 20$. Even with strengthen of the energy topology some communication nodes will be depleted. In particular, for range $[0, 21]$ the solution is 13 *links* obtained by feasible relaxed sum of infeasibilities.

Furthermore, we examine the dependency of the energy levels of the communication nodes and the optimal energy topology design (Figure 3.5). The energy level is varied

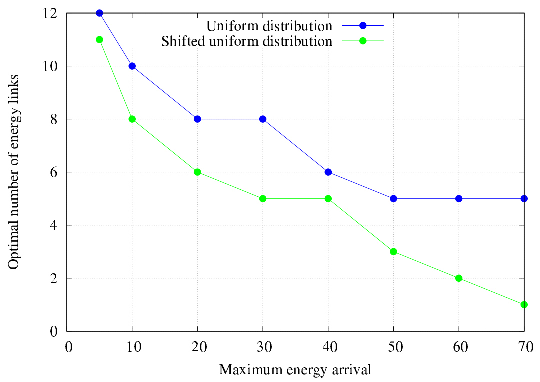

Figure 3.6: Optimal amount energy links vs. energy arrival profile

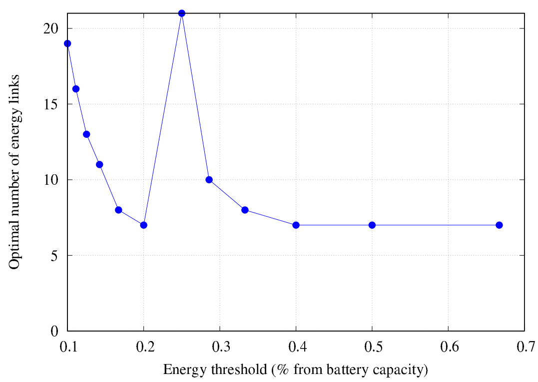

Figure 3.7: Optimal amount energy links vs. energy threshold

in range from $(0, 70)$ till $(0, 200)$, where the highest value is the maximum capacity of the battery. The increase in the energy levels of the communication nodes tends to decrease the demand of energy links. If the energy level range is less than an energy threshold, then no optimization is performed as no energy transmission is done, according to equation (3.21).

Then the energy distribution was shifted from $(35, 70)$ to $(100, 200)$. This provides on average a higher initial charge of the system and higher energy independence of communication nodes. Due to it, in comparison with the first case, the optimal amount of required energy links is halved; for $e_i > 120$ no energy topology is required.

Energy harvesting capabilities of communication nodes in the model are defined by an energy arrival profile. It is an important feature of a communication node that defines the sustainability of a node. To examine this feature, we vary the energy profile of each node in range from $(0, 5)$ till $(0, 70)$, as is shown in Figure 3.6. Notably, increasing the average EH capability of a system will decrease the need for providing additional energy topology links. In case $f_i \geqslant 70$, a near-optimal solution is obtained, in which the transmitted energy from one communication node to another is higher than a real demand of a node, i.e., the capacity constraints (3.14) are violated.

Shifted distribution from $(2, 5)$ till $(35, 70)$ provides a higher energy capabilities of a system in general and lower optimal amount of energy links. In both cases, for $f_i = 70$ the solution is near-optimal in the plot.

Finally, the dependency of optimal energy topology and energy threshold was studied. Here, a simple case is considered in which all batteries have similar capacity and, therefore, similar energy threshold, defined as a ratio from the battery capacity. For threshold in range from $e_{th} = c/10$ till $e_{th} = c/5$, the increase of ratio leads in decreasing

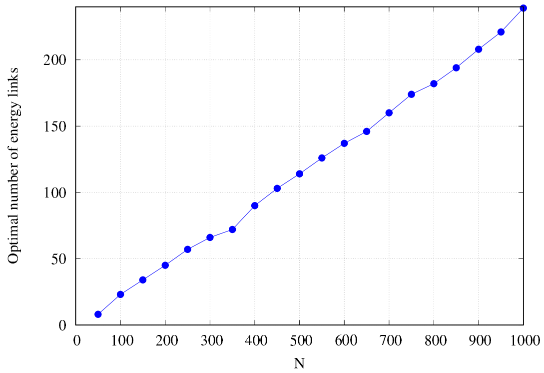

Figure 3.8: Optimal amount energy links vs. amount of communication nodes in WSN

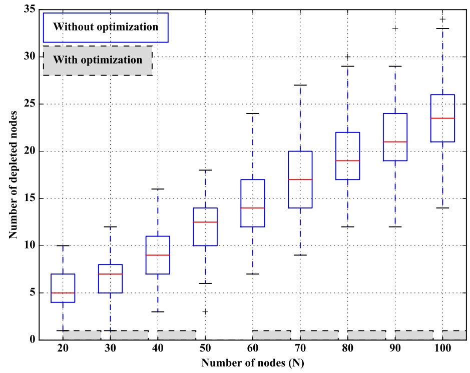

Figure 3.9: Amount of depleted communication nodes with/without optimization

the optimal amount of energy links. However, the solution is always near optimal, low values of energy threshold are accompanied by violation of outage constraints (3.13).

The same tendency is observed for $e_{th} > c/10$, but in this case the optimal solution is obtained and after optimization no communication nodes is completely depleted.

The optimization model was tested on systems of different size, i.e., the number of communication nodes was changed ($N \leqslant 1000$). From Figure 3.8 we can see that the optimal amount of energy links and the system size has a linear behaviour. In case of big size systems with high value of N, a clustering algorithm would need to be applied, to obtain a nearly-optimal solution restricted to a cluster with tractable size.

Simulations were conducted without any optimization on top as comparison terms, in order to analyse the effectiveness of proposed model. For each amount of communication nodes we simulate 100 instances, in which distances are in range $(0, 15)$, initial energy level is in range $(0, 200)$ and energy arrival profile is in range $(0, 20)$. The distribution of depleted communication nodes are shown in Fig. 3.9. With increase of system size the amount of depleted objects and variance is increasing. For $N = 100$ the amount of depleted nodes is around $10-30\%$ of total object's amount.

The optimization model was applied to the same simulated instances. In this case, the number of depleted nodes did not increase of more than 1 node per instance. In particular, for $N = 20, 30, 40, 100$ only in one instance out of 100 one node was depleted. For $N = 60, 70, 90$ in two instances one communication node was depleted. For $N = 80$ in three instances one communication node was out of charge; here, due to the absence of an optimal solution, the near-optimal one was proposed. Applying optimization framework to the system significantly increase the sustainability of the system.

3.3.3 Energy cooperation for sustainable IoT services within SCs

In this subsection, we consider smart services to be interconnected among each other, exploring an energy cooperation scheme to increase the energy sustainability and therefore reliability of IoT scenarios. Specifically, smart services are represented as GWs that collect and process data from IoT sensors and objects. GWs are sink nodes that can be thought of as routers in residential scenarios. Examples may be smartphones that collect and aggregate data from wearable biomedical sensors, SC GWs collecting pollution, traffic, or parking data from cameras or road-side sensing units [107]. Therefore, the power sources for IoT GWs are diverse and depend on the GW's type and/or the considered application. The GW energy consumption is related to its data collection task and the transmission of the aggregated data to the base station via, e.g., Time Division Multiple Access (TDMA) scheduling [108]. Hence, the overall GW energy consumption depends on the amount of served IoT devices and their throughput. Typically, GWs are connected to the electrical grid and equipped with a backup battery to provide resilience to power network outages. In this work, we additionally consider that GWs have EH capabilities. EH allows increasing the energy sustainability of a system, but, at the same time it is a volatile energy supply due to its intermittent nature. For instance, solar energy arrival is not homogeneous over a day and depends on the solar panel size, deployment site, and orientation. Other works have also studied this feature; for example, the solar GW *CerfCube* for habitant monitoring presented in [109], consumes about 2.5 W and is equipped with a solar panel that provides 60-100 W but only during sunny days; thus, also a rechargeable battery is added. The authors of [110] propose an aquatic environmental monitoring framework where GWs and sensors are powered by solar panels. The proposed design was successfully integrated at Moreton Bay, Brisbane (Australia) to monitor a segment of the Australian Coral Reef.

The main contribution of this subsection is the integration of these aforementioned topics and technologies in a single optimization framework to come up with a SC scenario that intelligently provides services, but at the same time is aware of its carbon footprint and tries to reduce it as much as possible.

The combination of energy cooperation with EH and IoT systems is the scenario that is considered in this work, and is sketched in Fig. 3.10. IoT smart services are represented by GWs. Some of them are only powered by solar panels (for instance, applications in rural areas), termed *offgrid*. Others are also connected to the electrical grid, i.e., *ongrid* (for example, GWs located in buildings). The energy arrival profile for the solar energy is derived from [57]. Moreover, GWs are equipped with a backup battery that allows energy storage and prevents the system from sudden operation stops due to power grid outages.

All the GWs are connected to a central node called the *energy router*, which determines the energy allocation among GWs and implement the needed energy transfers. This nomenclature is taken from [91]. Through the interconnected grid, energy is exchanged from high battery level GWs to the almost depleted ones. The IoT GW load is generated randomly in a range that includes different available communication technologies that are suitable for IoT applications. Hence, an energy allocation optimization problem is formulated, with the objective of prolonging the life-time and the energy sustainability of the system.

Numerical results are provided to demonstrate the effectiveness of the proposed energy cooperation policy. In particular, we investigate the impact of key parameters on the system sustainability, including the number of GWs that are connected to the energy router, the amount of data traffic generated by the field sensor nodes, and the fraction of GWs connected to the power grid. We compare the energy cooperation scenario with the case where no energy cooperation scheme is used, and compare the average battery level for both scenarios.

This section is organized as follows. In Subsection 3.3.3.1, we outline our proposed system model. The formulation of the energy allocation problem is presented in Subsection 3.3.3.2. Numerical results are discussed in Subsection 3.3.3.3 that shows the effectiveness of the energy cooperation scheme and the behavior dependency from different parameters.

3.3.3.1 System Model

We consider a system of N GWs (set $\mathcal{N}$) with EH capabilities serving n associated IoT devices. GWs are divided into two sets: connected to the power grid (set $\mathcal{N}_{\text{ongrid}}$) and only depending upon harvested solar energy (set $\mathcal{N}_{\text{offgrid}}$). Time t is slotted, i.e., $t = 1, 2, \dots,$ with the slot duration implicitly assumed to be equal to one hour. The GW energy consumption is modeled following [111]. The model takes into account the

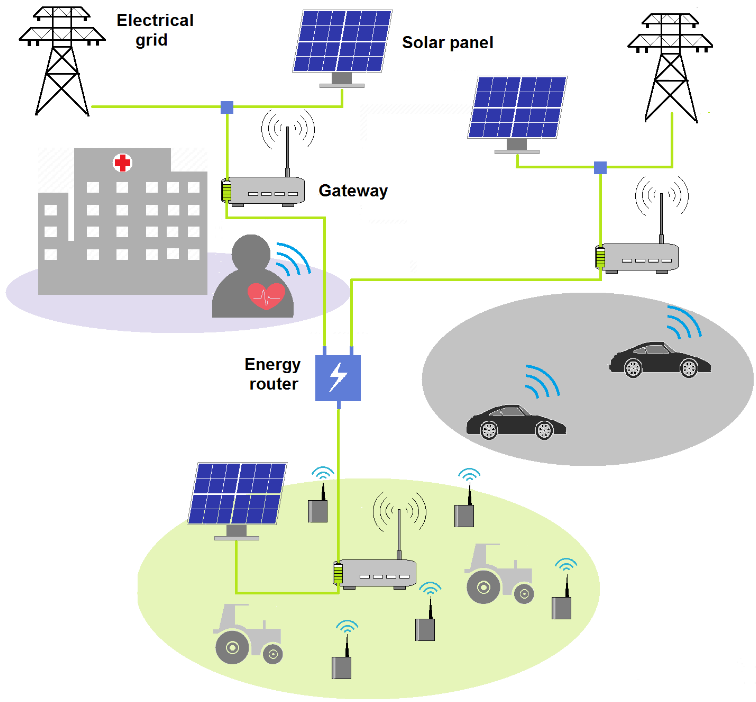

Figure 3.10: Energy framework for interconnected smart services.

energy consumption for receiving k bits of data and aggregating m messages:

$$E_{\mathrm{RX}}(k) = E_{\mathrm{elec}} \cdot k \,, \tag{3.22}$$

$$E_m(m,k) = m \cdot k \cdot E_{\mathrm{DA}} \,, \tag{3.23}$$

where E_{elec} and E_{DA} are the energy for the activation of the data receiving circuit board and the energy required for the aggregation of a single message of unit length, respectively. Hence, the total power consumption of a GW $i \in \mathcal{N}$, E_i^{con}, amounts to the sum of communication and aggregation terms, that is,

$$E_i^{\mathrm{con}} = n \cdot E_{\mathrm{RX}}(k) + E_m(m,k) \,, \tag{3.24}$$

where the energy consumption is eventually connected to the number of sensing nodes n that are associated to the GW, and the individual data rate of each sensor node.

The energy transfer among GWs is performed following the same technique used in [91]. Energy losses are considered and depend on the distance ℓ between source and destination GWs, the resistivity of the wire connecting them (denoted as ρ, measured in Ω mm^2/m) and its cross sectional area (A, mm^2) [112]:

$$R = \frac{\rho l}{A} \,. \tag{3.25}$$

In the considered scenario, the connection among GWs is established via the energy router through a star topology. Different topologies shall be explored in future work. For the numerical results, the distances between the energy router and GWs are uniformly distributed at random, on a square area. Therefore, energy links between GWs have also random length.

Solar EH is accomplished with a reference model inspired by a real-world device, i.e., Panasonic N235B PV technology, in which each solar module has a size of $0.44\,\mathrm{m}^2$ and is equipped with 25 solar cells. The SolarStat tool was used to obtain the energy arrival profile $p(t)$ across an entire day considering the city of Los Angeles as the deployment site [57]. This energy profile is reshaped for each GW, taking into account different installation environmental conditions for the solar panels, in particular attenuations that may occur due to nearby buildings or trees. This variability in the EH model is taken into account as follows. $A_i^h(t)$ is the amount of harvested energy in time slot t for GW i [91]: it depends on the energy profile $p(t)$ (equal for all GWs) and $r(0,s)$, which is sampled from a uniform probability distribution function in the open interval $(0,s)$, where s represents the correlation among the harvested energy profiles across GWs:

$$A_i^h(t) = r(0,s)p(t)\,. \tag{3.26}$$

The energy level of a GW battery changes at each time slot t due to energy arrivals (EH process), the energy obtained from the power grid, the GW energy consumption (reception and aggregation of data) and the amount of transferred energy among GWs. Specifically, the battery level of GW $i \in \mathcal{N}$ evolves according to the following update equation:

$$E_i(t+1) = E_i(t) - E_i^{\mathrm{con}}(t) + E_i^{\mathrm{tr}}(t) + A_i^h(t) + A_i^g(t) \tag{3.27}$$

where $E_i(t)$ is the amount of energy at time slot t, $E_i^{\mathrm{con}}(t)$ is the energy consumption calculated according to equation (3.24) in that time slot, $E_i^{\mathrm{tr}}(t)$ is the amount of energy to be transferred or received to/from other GWs (if a GW is an energy *provider*, then $E_i^{tr}(t) < 0$, otherwise, the GW is an energy *consumer* and $E_i^{tr}(t) > 0$). Values $A_i^h(t)$ and $A_i^g(t)$ represent the amount of energy harvested and obtained from the power grid, respectively. For GWs $i \in \mathcal{N}_{\mathrm{offgrid}}$, which are not connected to the power grid, we have $A_i^g(t) = 0$, if $i \in \mathcal{N}_{\mathrm{ongrid}}$ then $A_i^g(t) \geqslant 0$. The battery has a finite capacity $C_{\max}$ and two predefined thresholds: upper and lower, denoted by $C_{\mathrm{th}}^{\mathrm{up}}$ and $C_{\mathrm{th}}^{\mathrm{low}}$, respectively. These thresholds are used to define the behaviour of a GW in terms of the amount of energy that it is allowed to transfer or receive. Specifically, in each time slot t, GWs can precisely define their roles in the energy cooperation scheme depending on the energy battery level and these energy thresholds. Hence, the behaviour of GW $i \in \mathcal{N}$ is set in the following way [91]:

$$\begin{cases} E_i(t) \geq C_{\text{th}}^{\text{up}} & \text{GW } i \text{ is an } \textit{energy provider} \\ E_i(t) < C_{\text{th}}^{\text{low}} & \text{GW } i \text{ is an } \textit{energy consumer}. \end{cases} \tag{3.28}$$

If a GW $i \in \mathcal{N}_{\text{ongrid}}$ is an energy provider, the amount of energy that it can transfer in time slot t is calculated as the difference between its current battery level and the upper threshold, i.e., $E_i(t) - E_{\text{th}}^{\text{up}}$. Instead, if a GW $j \in \mathcal{N}_{\text{offgrid}}$ is identified as an energy consumer, then the amount of demanded energy is obtained as the difference between the lower threshold and its current battery level: $E_{\text{th}}^{\text{low}} - E_i(t)$.

3.3.3.2 Optimization Problem

To increase the sustainability of the system under study, we formulate an optimization problem, whose solution consists of an energy allocation policy that transfers energy from energy providers to energy consumers. The sets of energy providers and consumers are denoted here as $\mathcal{N}_{\text{prov}} = \{1, .., P\}$ and $\mathcal{N}_{\text{cons}} = \{1, .., C\}$, respectively. The available energy to transfer from providers to consumers is captured by matrix $\boldsymbol{B} = [b_{ij}]$, where element b_{ij} represents the amount of energy available from provider i to consumer j. If i is an energy provider, element b_{ij} accounts for the energy that this node can transfer, namely, $E_i(t) - C_{\text{th}}^{\text{up}}$, which is corrected by a coefficient k_{ij} depending on the distance between i and j, which takes into account energy losses. Vector $\boldsymbol{d} = [d_j]$ represents the energy demand of energy consumers.

We now write an objective function that aims at reducing the imbalance between energy demand and supply, so that energy is allocated (and used) as efficiently as possible across the whole system. As we shall see shortly, a well balanced energy allocation also reduces the overall energy that is purchased from the power grid. The optimization problem is formulated as follows:

$$\min_{\boldsymbol{X}} \quad \sum_{j=1}^{C} \left(\sum_{i=1}^{P} x_{ij} b_{ij} - d_j \right)^2 \tag{3.29a}$$

$$\text{subject to:} \quad 0 \leq x_{ij} \leq 1, \qquad \forall i \in \mathcal{N}_{\text{prov}}, \forall j \in \mathcal{N}_{\text{cons}}, \tag{3.29b}$$

$$\sum_{j=1}^{C} x_{ij} \leq 1, \qquad \forall i \in \mathcal{N}_{\text{prov}}, \tag{3.29c}$$

where $x_{ij} \in [0, 1]$ are the decision variables, which represent the fraction of the available energy b_{ij} that is allocated from provider $i \in \mathcal{N}_{\text{prov}}$ to consumer $j \in \mathcal{N}_{\text{cons}}$, in matrix notation $\boldsymbol{X} = [x_{ij}]$. The first constraint represents the fact that x_{ij} is a fraction of the available energy b_{ij}, and the second one means that the total amount of energy that a certain provider i transfers to consumers j cannot exceed the total amount of available energy at this provider.

The optimal solution of the problem $\boldsymbol{X}^* = [x^*_{ij}]$ returns the optimal energy allocation between providers and consumers, meaning that any provider i can transfer energy to more than one consumer j at a time, and any consumer j can receive energy from multiple providers i. Due to the convex nature of the formulation, the problem can be solved using standard methods, the Matlab toolbox `CVX` [113] has been used to this purpose.

3.3.3.3 Numerical results

In this section, we numerically evaluate the proposed energy trading model. Simulations are performed as follows: every time slot t, GWs energy battery levels are updated following equation (3.27); then, every GW decides upon its energy role using equation (3.28) and, after that, matrices $\boldsymbol{B}$ and $\boldsymbol{D}$ are calculated. Finally, the solution $\boldsymbol{X}^*$ of the optimization problem in equation (3.29) is found and the energy transfer among GWs is performed thanks to the energy router, see Fig. 3.10. The numerical results that follow show a performance comparison between two scenarios: system *with* and *without* energy cooperation.

For the simulations, the sensor node data rate is picked randomly in the range $[1\,\text{kb/s} - 1\,\text{Mb/s}]$. This rather wide range of data rates is selected to mimic the diversity of technologies that are expected to coexist in future smart cities. A few technologies that may be amenable for the provisioning of smart services are: SigFox ($<$ 0.1 kb/s) [114], LoRa - 0.3 – 50 kb/s [115], Z-Wave - 9.6/40/100 kb/s [116], NFC - $106, 212, 424$ kb/s [117], ZigBee - 250 kb/s [118], Bluetooth - 1 Mb/s [119]. GWs are randomly distributed within an area of $1\,\text{km} \times 1\,\text{km}$ and each GW is equipped with a Li-Ion battery with capacity in the range [24.4 – 57.7]Wh. The remaining simulation parameters are listed in Table 3.3.

To quantify the effectiveness of our energy cooperation model, we define the *sustainability ratio* metric, representing the number of depleted GWs over the total number of GWs in the system; the goal is to minimize this metric, reducing as much as possible the number of GWs that run out of energy. The results in Fig. 3.11 are obtained using $|\mathcal{N}_{\text{ongrid}}| = 10$, a random number of sensor nodes per GW in the range [1000 – 10000] (see Table 3.3) and a data rate in the range $[1\,\text{kb/s} - 1\,\text{Mb/s}]$. The figure plots the

Table 3.3: Simulation parameters

Parameters	**Values**
Number of deployed GWs N	20
Number of sensor nodes per GW	$[1000, 10000]$
Energy per received bit E_{elec}	$5\,\text{nJ/bit}$
Energy to aggregate m messages E_{DA}	$5\,\text{pJ/bit}$
Number of aggregated messages m	10
Cable resistivity ρ	$0.023\,\Omega\text{mm}^2/\text{m}$
Cable cross-section A	$10\,\text{mm}^2$
EH correlation coefficient s	2
Energy battery capacity $C_{\max}$	[24.4-57.7]Wh
Upper threshold C_{th}^{up}	70%
Lower threshold C_{th}^{low}	30%

dynamical changes of the sustainability ratio values for the system over a day with and without energy cooperation. When no energy cooperation is accounted for (termed "Without EC" in the figure) the sustainability ratio is relatively high (i.e., up to 50% of the GWs run out of battery). When our optimization is used ("With EC"), no GW runs out of energy across the entire day and this is due to two reasons: 1) energy rich GWs transfer some of their excess energy to energy poor ones and 2) ongrid GWs assist those that are offgrid, by transferring energy towards them whenever the energy that can be harvested from the environment is insufficient.

The same simulation settings are used in Fig. 3.12, where the average GW battery level is plotted across a full day for the two cases: with and without energy cooperation. Without energy cooperation, the average battery level is higher from 6:00 pm to 9:00 am. In fact, during such hours the harvested energy from the sun is negligible and the application of energy transfer among GWs reduces the battery level of all of them. This does not happen without EC, where ongrid GWs maintain a high battery level that on average is better than using EC during this time period.

The next figures show the role of some of the system parameters. First, we explore the impact of the number of GWs that are connected to the energy router. The

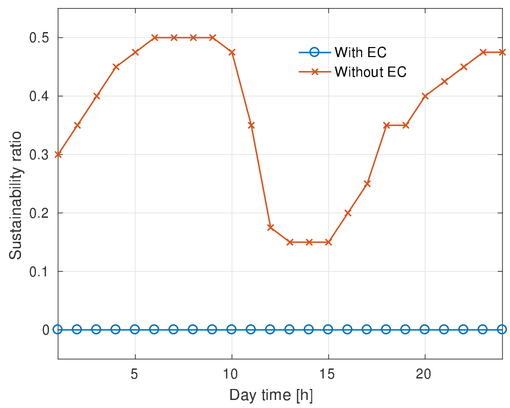

Figure 3.11: Sustainability ratio across an entire day.

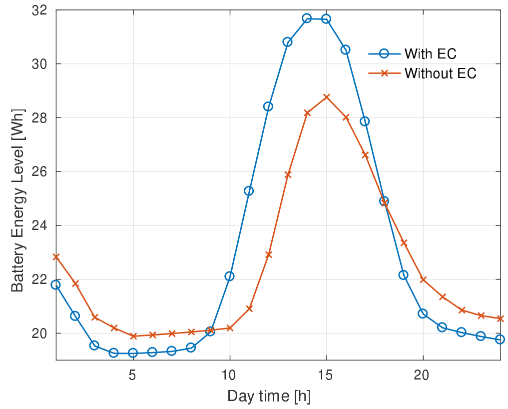

Figure 3.12: Average GW battery level across an entire day.

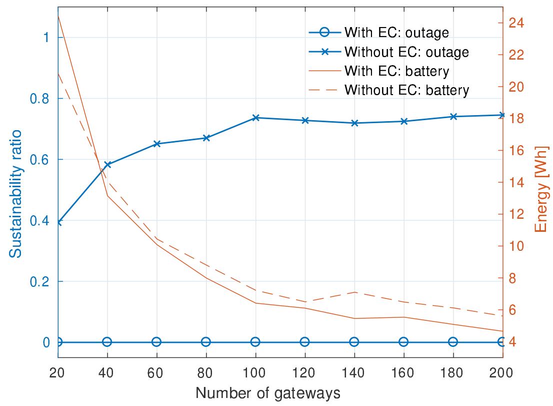

Figure 3.13: Sustainability ratio performance varying the number of GWs N.

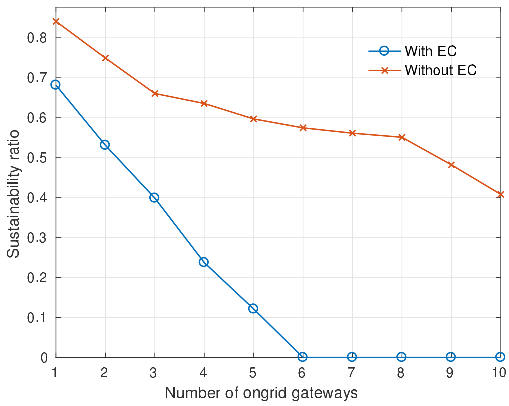

Figure 3.14: Sustainability ratio evaluation increasing the number of ongrid GWs.

results in Fig. 3.13 are obtained using $|\mathcal{N}_{\text{ongrid}}| = 10$, a random number of sensor nodes per GW in the range $[1000 - 10000]$, and a throughput in the range $[1\,\text{kb/s} - 1\,\text{Mb/s}]$. As expected, an increase in the number N of GWs deployed in the system, without a corresponding increase in the number of ongrid ones, when EC is not applied leads to a worse performance, i.e., the number of depleted GWs gets higher and the sustainability ratio correspondingly increases. Nevertheless, the system becomes fully energy sustainable applying EC even when N is equal to 200. The average battery energy level in the system with EC is however smaller than without EC, due to the energy losses in the energy transfer process.

In Fig. 3.14, we plot the sustainability ratio as a function of the number of GWs that are connected to the grid. Results are obtained using the same settings as for Fig. 3.12. As expected, increasing the number of ongrid GWs provides a gradual decrease of the

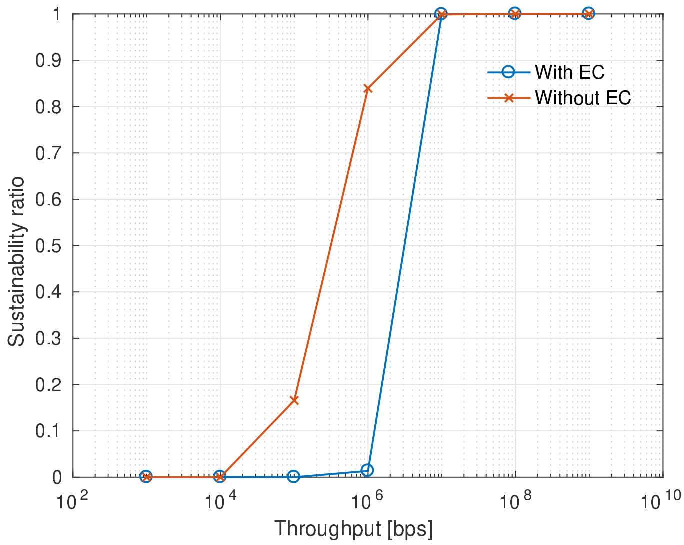

Figure 3.15: Sustainability ratio varying sensor nodes throughput.

sustainability ratio when there is no EC. But increasing the ongrid GWs is especially beneficial when EC is applied. In that case, as the number of ongrid GWs gets larger than five, no energy GWs run out of energy any longer.

Finally, we study how the number of depleted GWs depends on the sensor nodes data rate, which is spanning over the [0.1 kb/s – 10 Gb/s]. In this case, we also explore considerably higher data rate values as our aim is to identify the full extent of the benefits provided by EC. The remaining parameters are $N = 20$, $|\mathcal{N}_{\text{ongrid}}| = 10$ and a random number of sensor nodes per GW in the range [1000 – 10000] is considered. The results are presented in Fig. 3.15 and show that for the case without EC and a data rate smaller than 10 kb/s the sustainability ratio is zero, therefore no energy cooperation is needed for these values. However, in the range [10 kb/s – 10 Mb/s], EC performs better providing a gain of about 25%. If the data rate is higher than 10 Mb/s, then the system cannot be energy sustainable, and all GWs will be depleted, no matter whether EC is used.

3.4 Conclusions

We consider a wireless sensor network consisting of two asymmetric sensors, powered by batteries with different capacities. We investigate the role of asymmetries by means of game theory. We focus on an unbalanced scenario, where, for example, one sensor knows the asymmetric property of the system by knowing the energy state and the capacity of the second sensor, whereas the other one does not know. We assume that the ideal scenario for such a system is transmitting data by each sensor proportionally to their battery capacities.

We study the interaction between sensors as an instance of a Bayesian game, iteratively updated to better estimate the prior. We obtained that if both sensors do not take into account the asymmetric property of the system at all, then the system is less balanced. The same happens if one sensor knows about the asymmetry and exploits it in its strategy. In addition, we demonstrated that these strategies are not effective and ignore the asymmetric property of EH-WSN if the relation between sensor's capacities is more than 0.5.

Further, we propose the energy cooperation scheme in SCs, in which the energy flows from nodes with higher energy level, less energy consumption and with more EH capabilities to the nodes that have lower energy arrival profile, more distant from a sink node and more exploited. For this purpose, an energy topology is designed, in which energy links are established among communication nodes. The priority is given to nodes with higher energy potential differences. As every link establishment is associated with costs, the energy topology has to be optimized such that no communication node is depleted, and energy transmission does not exceed the demand of the interacting node.

Based on the proposed optimization model, we analyse the dependency of optimal energy topology of a system from such factors as distance distribution of communication nodes, EH capabilities of the nodes, and distribution of energy arrival profiles of each node, selected energy threshold and energy level distributions. All these factors define the optimal amount of energy links. We demonstrated that in the generated scenarios, the system will have up to 30% of depleted nodes and embedded optimization scenario helps to decrease the amount to almost 0.

Also, the energy arrival profile was formed for each communication node randomly, with independent and identical distribution for all the nodes. The realistic energy arrival profiles have to be integrated based on the chosen source of renewable energy, possibly including some correlation. Another possibility is to consider alternative energy exchange models, based not only on the energy thresholds but on more diverse parameters of each communication nodes. In relevance with energy consumption model, more diverse data size has to be considered and other energy consumption models should be applied and compared.

As an extension, we consider a SC scenario represented as a set of interconnected IoT GWs that offer smart services by collecting and aggregating data from IoT sensing devices. GWs are endowed with EH capabilities, which in this study means that they are equipped with a solar panel and an energy storage (rechargeable battery). Energy cooperation is accounted for providing energy sustainability to the system through the transfer of energy from GWs with a high battery level to those whose battery is about to deplete. For this scenario, an optimal energy allocation was found, solving a convex problem with the goal to reduce the imbalance between available energy in GW batteries and energy demand in the system. We analyse the effectiveness of the proposed energy allocation strategy, comparing it against the case where energy cooperation is not allowed, and also checking the impact of several system parameters, such as number of GWs that are connected to the energy router, the number of ongrid GWs and the data rate of sensor nodes. Numerical results show that, with energy cooperation, the system is fully energy sustainable for many system configurations, showing a substantial improvement against a scenario where cooperation is not allowed.

Chapter 4
Energy management for EH IoT-systems deployed for critical operations

In this chapter, we consider a special case, where the main performance metric of an energy-harvesting IoT-system is AoI. AoI is a crucial parameter for the critical operation systems (automation, intelligent transportation and smart cities). We investigate the optimal policy of an energy-harvesting IoT monitoring system, that with the given energy budget minimizes the average AoI of a system with a backup information source. We also extend this work to the case with multiple heterogeneous information sources.

4.1 Introduction

IoT is increasingly being deployed for critical operations such as factory and process automation, intelligent transportation and smart cities [120]. Differently from other networks that are generally characterized in terms of throughput and delay, a key performance indicator for such applications is the AoI, which quantifies the freshness of the destination's knowledge about the status of the system being monitored [121, 122]. For instance, in a smart driving systems, timely collecting of a traffic information and other indicators by sensors mounted in a vehicle, is essential regarding the safety of all road users. Another example can be a factory automation, where the real-time control of some production parameters also requires timely delivery of status updates [123].

In this chapter, we focus on the EH communication systems. On one hand, the strategy employed in such systems has to provide the timely delivery of status updates, and on another hand, to balance the erratic energy arrivals from ambient sources of energy. We consider instead an IoT system that can exploit *multiple* sources of information, each providing a different energy-age trade-off. For example, an IoT device may exploit multiple sensors with different reliabilities and costs. Alternatively, we may think of a terminal that can update the system status through either a cellular technology, which guarantees reliability and high coverage, but is very expensive in terms of energy, or a low-range energy-aware technology.

One might guess, that increasing the number of information sources, that monitors the same underlying process of interest might be a solution to increase the robustness of EH systems regardless the prompt deliveries of status updates. In this chapter, we argue this statement by analysing the additional gain in reduction of average AoI by adding more information sources in the system as well as how the quality of these sources affects the system performance.

The chapter is organized as follows. The background in AoI is given in Section 4.2. The case with two information sources is studied in Section 4.3, and with multiple sources in Section 4.4. The chapter is concluded in Section 4.5, where possible further developments are also outlined.

4.2 Background in age-of-information

A growing number of papers investigate the evolution and control of AoI in energy-harvesting systems [124–128]. The scenario of reference involves a device making optimal decisions about acquiring status updates depending on the energy cost and the available battery level.

Multiple papers study the average AoI minimization with a single Energy Harvesting Source [125, 127, 129–138]. Very few papers are focused on average AoI with multiple information sources. In [139, 140], authors considered a system, where independent sources send status updates through a shared first come first serve M/M/1 queue to a monitor, and found the region of feasible average status ages for two and multiple sources. Similarly, in [141] a system with n sources was considered to provide status updates to multiple servers via a common queue. The authors formulated an AoI minimization problem and proposed online scheduling policies. Another system was considered in [142], where a single source node transmits status updates of two-type to multiple receivers. Authors determined the optimal stopping thresholds to individually and jointly optimize the average age of two types updates at the receiver nodes. Authors in [143] proposed a multi-objective formulation for scheduling transitions in a system with multiple information sources that monitor different processes. The objective is to balance the AoI of these different processes. Similarly, in [144] the AoI minimization problem was also formulated for a system with multiple information sources that monitor different processes, and a monitoring node that communicates with the information sources through orthogonal channels. The authors proposed the policy that converts the scheduling problem into a bipartite matching problem between the set of channels and set of sensors.

In this work, we consider another types of multi-source systems, where the status updates are generated by request of an energy-harvesting *monitoring node* from multiple heterogeneous information *sources*, that monitor the same underlying process. Each source provides different energy-cost trade-off, which can provide status updates through various technologies with different quality (freshness and/or reliability) and energy cost. Monitoring node optimizes the resulting AoI over time within a constrained energy budget, based on the assumption about the reliability of information sources. One of the possible framework for such a system is crowdsensing in which AoI can play an important role in choosing a source to be updated from. In the crowdsensing system, a crowdsource and smartphone users, that are exploited to provide sensing services, are connected via cloud [145]. In this framework, a crowdsourcer sends the sensing task description to the group of smartphone users, and receives from them sensing plans, based on which the crowdsourcer performs a user selection.

We analyse different sets of heterogeneous information sources, and how the different combinations of costs and reliabilities affect the resulting average AoI. Also, we analyse if the increase in size of the information source set affects the overall performance regarding the average AoI.

4.3 Average age-of-information with a backup information source

We investigate policies to minimize the average AoI in a monitoring system that collects data from two sources of information denoted as *primary* and *backup* sources, respectively (Fig. 4.1). We assume that each source offers a different trade-off between the AoI and the energy cost. The monitoring node is equipped with a finite size battery and harvests ambient energy. For this setup, we formulate the scheduling of status updates from the two sources as a Markov Decision Process (MDP), and obtain a policy

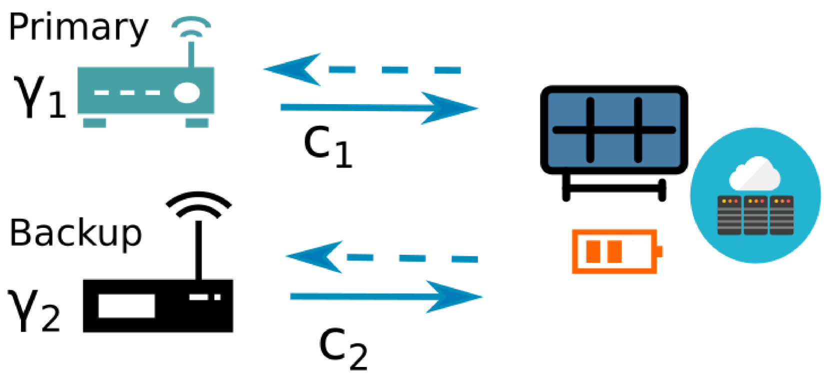

Figure 4.1: System model

that decides on the optimal action to take (i.e., which source to query or remain idle) depending on the current energy level and AoI. The performance of the obtained policy is compared with an aggressive policy for different system parameters. We identify few types of optimal solution structures and discuss the benefits of having a backup source of information in the system.

The rest of this section is organized as follows. In Subsection 4.3.1, the system model description, problem formulation and solution approaches are introduced. Numerical results are presented in Subsection 4.3.2, providing a performance comparison between the proposed solution and a reference approach, namely, the aggressive policy.

4.3.1 System overview

For the purpose of the analysis we refer to the following model. We consider two *sources* providing information with different costs and qualities (freshness and/or reliability) to a *monitoring node* that tries to optimize the resulting AoI over time within a constrained energy budget. The information source with higher cost and quality is called the *primary* source of information, while the other is referred to as the *backup* source. These sources provide the monitoring node with the most fresh status update in their buffer. Therefore, the monitoring node does not know with certainty the AoI of the packet that will be delivered from a source node. The only assumption the monitoring node can make is the reliability of a source, i.e., the probability of receiving a fresh data packet from that source.

We consider a system consisting of a single energy-harvesting monitoring node and two sources of information, where each source takes measurements of the same underlying process that is of interest to the monitoring node. Time is discretized into time slots with a unit slot length of arbitrary duration. At each time slot, the monitoring node can receive a status update from only one of the sources. The status update from the chosen source becomes available to the monitoring node at the beginning of the time slot.

The monitoring node consumes different amounts of energy to receive a status update from the two sources. We assume that the status updates provided by the two sensors are of age either α or β, referred to as *fresh* and *stale*, respectively, with $\alpha<\beta$. For the sake simplicity, we consider only two possible age values α and β, which can model, for example, useful and useless data packets. We assume that source i can provide a fresh status update at each time slot with probability γ_i, $i = 1, 2$, and a stale packet with probability $1 - \gamma_i$, such that $\gamma_1>\gamma_2$ for *primary* and *backup* sources, respectively. The AoI at the monitoring node increases by 1 if no new update is received.

The energy costs of requesting a status update from source i is denoted by c_i, $i = 1, 2$, where we assume $c_1>c_2$. Here $c_1, c_2 \in \mathbb{Z}^+$ correspond to integer multiples of a unit of energy.

Battery level $b(t)$ is updated at each time slot depending on the energy harvested in the previous time slot and the energy cost of receiving a data packet from one of the sources:

$$b(t) = \min\{b(t-1) - \sum_{i=1}^{2} c_i \cdot \mathbb{1}(a(t) = a_i) + e(t), B\}, \tag{4.1}$$

where $e(t) \in \{0, \bar{e}\}$ denotes the harvested energy available to be used in time slot t, B is the battery capacity, and $\mathbb{1}(x)$ is an indicator function: $\mathbb{1}(x) = 1$ when x holds, and $\mathbb{1}(x) = 0$ otherwise. We assume $\{e(t)\}_{t=1}^{\infty}$ is an independent and identically distributed (i.i.d.) binary random process with $P(e(t) = \bar{e}) = \lambda$.

The monitoring node makes a decision at the beginning of each time slot whether to request a new status update or not, and if so, which source to request it from. We seek the policy that minimizes the average AoI at the monitoring node by optimally choosing the action to take at each time slot, accounting for the battery level and the current age of information. We first formulate the problem as an MDP.

4.3.1.1 System model and problem formulation

An MDP consists of a tuple $<S, A, P, R>$ of state space S, action space A, probability transition function P, and a reward or cost function R. In our problem, finite space of actions A includes requesting an update from either of the two sources (primary/backup) and remaining idle. We set $A = \{a_0, a_1, a_2\}$, where a_0 corresponds to remaining idle, a_1 updating from the primary source, and a_2 updating from the backup source.

Action a_i is not allowed if $b(t){<}c_i$. This can be incorporated into the framework with the same action space by imposing very high energy costs for action a_i when $b(t) < c_i$, $i = 1, 2$.

Let $\delta(t) \in \{1, 2, ..., \delta_{max}\}$ denote the AoI at the monitoring node at time slot t, where δ_{max} is the maximum age in the system. Equivalently, we assume that having a status information of age δ_{max}, or any $\delta > \delta_{max}$ have the same utility. Depending on action $a(t)$, $\delta(t)$ can take one of the following values $\{\delta(t-1)+1, \alpha, \beta\}$. The system state is described by the pair of variables $s(t) = (b(t), \delta(t))$. Note that we have a finite state space of dimension $(\delta_{max} + 1)(B + 1)$. We set β as the maximum AoI, i.e., $\beta = \delta_{max}$, beyond which increase in age becomes irrelevant. Accordingly, receiving a stale status update is equivalent to not receiving a useful update.

P denotes the transition probabilities of the MDP, where $P(s'|s, a) = Pr(s(t+1) = s'|s(t) = s, a(t) = a)$; that is, the probability that taking action a at state s will lead to a transition to state s' in the following time slot. The transition probabilities for our problem are given as follows for $a_i \in \{a_1, a_2\}$:

$$\begin{cases} P((\min\{b{+}\bar{e}{-}c_i, B\}, \min\{\alpha, \delta{+}1\})|(b, \delta), a_i) = \lambda\gamma_i \\ P((\min\{b{+}\bar{e}{-}c_i, B\}, \min\{\beta, \delta{+}1\})|(b, \delta), a_i) = \lambda(1{-}\gamma_i) \\ P((b{-}c_i, \min\{\alpha, \delta{+}1\})|(b, \delta), a_i) = (1{-}\lambda)\gamma_i \\ P((b{-}c_i, \min\{\beta, \delta{+}1\})|(b, \delta), a_i) = (1{-}\lambda)(1{-}\gamma_i) \end{cases} \tag{4.2}$$

Note that, if the received status update is older than the currently available one, then the monitoring node drops the new packet and keeps the previous status update. We can conclude that if $\delta_t{<}\alpha$, then the optimal action is to remain idle, i.e., $a_t = a_0$.

When the node remains idle, i.e., $a_t = a_0$, the transition probabilities are given as follows:

$$\begin{cases} P((b, \delta + 1)|(b, \delta), a_0) = 1 - \lambda & b{<}B \\ P((\min\{b + \bar{e}, B\}, \delta + 1)|(b, \delta), a_0) = \lambda & b{<}B \\ P((B, \delta + 1)|(B, \delta), a_0) = 1 \end{cases} \tag{4.3}$$

The policy π defines an action $a(t)$ at each time slot depending on the current state.

The infinite-horizon time average AoI, when policy π is employed, starting from initial state s_0, is defined as [146]:

$$V^{\pi}(s_0) = \lim\sup_{T\to\infty} \frac{1}{T}\mathbb{E}\left[\sum_{t=0}^{T} \delta^{\pi}(t)|s(0) = s_0\right]. \tag{4.4}$$

A policy is optimal if it minimizes the average AoI - $V^{\pi}(s_0)$. The optimal infinite-horizon average AoI for a starting state s_0 is found by solving:

$$V(s_0) = \min_{\pi} V^{\pi}(s_0). \tag{4.5}$$

To solve this optimization problem, we can use the offline dynamic programming approach adopting the Relative Value Iteration (RVI) algorithm described in [147]. In the offline approach we model the state transition function based on the statistical prior knowledge of the information sources' reliability and environmental characteristics. The RVI differs from Value Iteration (VI) by the value function of some state $V(s^*)$ in each update. In this case, the Bellman equation is defined as:

$$V^n(s) = \min_{a\in A}\left(\delta(s,a) - V^{n-1}(s^*) + \sum_{s'\in S} P(s'|s,a)V^{n-1}(s')\right), \tag{4.6}$$

where V^n is the value function, and s^* is a fixed state chosen arbitrarily.

The optimal stationary deterministic policy, obtained by Algorithm 2, specifies the decision rule that maps the current energy level and AoI to actions taken with probability one. In Algorithm 2, $sp(V^n - V^{n-1}) < \epsilon$ stands for the stopping criteria, where $sp(V) = \max_{s\in S} V(s) - \min_{s\in S} V(s)$. We run the RVI algorithm until the stopping criteria holds. At that moment the policy π achieves an average-cost AoI that is within $\epsilon \cdot 100\%$ of optimal.

4.3.2 Numerical results

In this section, we analyse the optimal policies for different settings, in particular, we consider the cost ratios between the primary and backup information sources, reliability of the sources, and the parameters of the EH process (λ, $\bar{e}$). We study the structure of the optimal policy, and try to identify the added value in average AoI from employing an extra information source in the system.

Algorithm 2 Relative Value Iteration Algorithm

set $v^0(s) = 0$, $\forall s \in S$

set n $=$ 1, ϵ>0

repeat

$n \leftarrow n + 1$

for all $s \in S$ **do**

$$v^n(s) = \min_{a \in A} \sum_{s' \in S} P(s'|s,a)\Big[\delta(s'|s,a) + V^{n-1}(s')\Big]$$

$$V^n(s) = v^n(s) - v^n(s_0)$$

where s_0 is a fixed state chosen arbitrary

end for

until $sp(V^n - V^{n-1})$<ϵ

return $arg \min V(s)$

Table 4.1: Default parameters.

Parameters	**Values**
Battery capacity, B	20
Maximum age in the system, δ_{max}	30
AoI states, $[\alpha, \beta]$	$[1, 20]$
Amount of harvested energy per time slot, $\{0, \bar{e}\}$	$\{0, 3\}$
Reliability of the primary source, γ_1	0.9

4.3.2.1 Simulation parameters

System parameters that remain constant for all the numerical simulations are presented in Table 4.1. The efficiency of the optimal policy is verified via simulations run over $T = 5000$ time slots, and compared with a so-called *aggressive policy* [148]. The aggressive policy (Algorithm 3) tries to always receive a status update whenever it has sufficient energy in its battery, and goes for the expensive source whenever it can afford it.

Denoting by $\bar{\delta}_T^m$ the time-average AoI over T time slots at the m-th run of the simulations, we consider the mean AoI $\bar{\delta}_T = \frac{1}{M}\sum_{m=1}^{M}\bar{\delta}_T^m$ and its standard deviation:

$$st \triangleq \sqrt{\frac{\sum_{m=1}^{M}(\bar{\delta}_T^m - \bar{\delta}_T)^2}{M-1}}, \tag{4.7}$$

over $M = 1000$ runs of the simulations for each settings.

Algorithm 3 Aggressive Policy

set $b(0) = 0$, $\delta(0) = 0$
for $t = 1 : T$ **do**
  if $b(t)\geq c_1$ **then**
    $b(t) = \min\{b(t-1) + e(t) - c_1, B\}$
    if $p\leq\gamma_1$ **then**
      $\delta(t)=\alpha$
    else
      $\delta(t)=\{\beta{:}\delta(t{-}1)\geq\beta;\delta(t{-}1){+}1{:}\delta(t{-}1)<\beta\}$
    end if
  else if $c_2 \leq b(t)<c_1$ **then**
    $b(t) = \min\{b(t-1) + e(t) - c_2, B\}$
    if $p\leq\gamma_2$ **then**
      $\delta(t)=\alpha$
    else
      $\delta(t)=\{\beta{:}\delta(t{-}1)\geq\beta;\delta(t{-}1){+}1{:}\delta(t{-}1)<\beta\}$
    end if
  else
    $\delta(t) = \delta(t{-}1){+}1,$
    $b(t) = \min\{b(t{-}1){+}e(t), B\}$
  end if
end for

4.3.2.2 Cost Ratio

The relative value of an information source can be measured by the portion of the states, in which the monitoring node chooses to exploit this source. To demonstrate this, we vary the cost ratio among the sources, c_2/c_1, and study the optimal policy obtained through RVI. We see in Fig. 4.2 that, when the cost ratio increases, the number of states at which the backup source is utilized shrinks, and the monitoring node opts to remain idle in most of the states. The disappearance of the backup source from the optimal action set is more rapid, if it is characterized by low reliability, γ_2 (see Figs. 4.2(a) - 4.2(c), 4.2(g) - 4.2(i)).

The relation between the average AoI and cost ratio is shown in Figs. 4.3 - 4.4. Predictably, the optimal average AoI grows when the cost ratio increases, but it saturates at a certain value, beyond which the backup source is not utilized at all. On

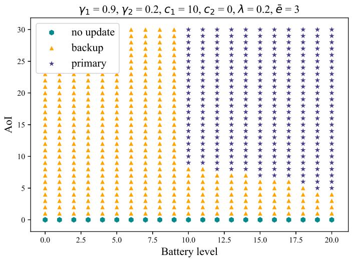

(a) Cost ratio = 0.0, $\lambda = 0.2$, $\gamma_2 = 0.2$

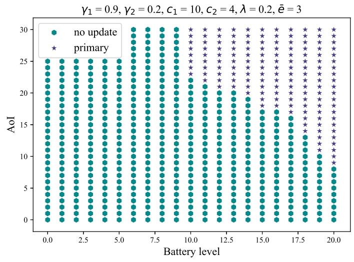

(b) Cost ratio = 0.4, $\lambda = 0.2$, $\gamma_2 = 0.2$

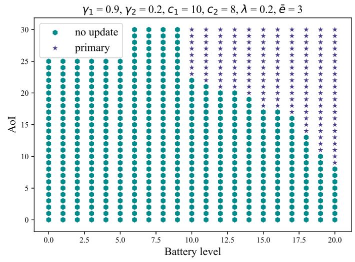

(c) Cost ratio = 0.8, $\lambda = 0.2$, $\gamma_2 = 0.2$

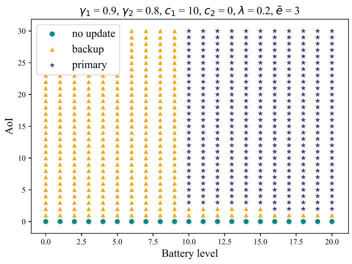

(d) Cost ratio = 0.0, $\lambda = 0.2$, $\gamma_2 = 0.8$

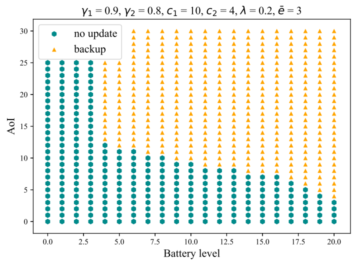

(e) Cost ratio = 0.4, $\lambda = 0.2$, $\gamma_2 = 0.8$

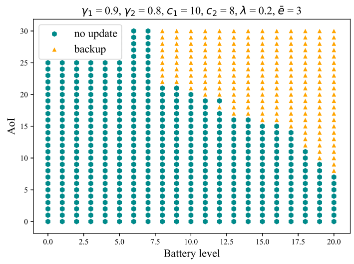

(f) Cost ratio = 0.8, $\lambda = 0.2$, $\gamma_2 = 0.8$

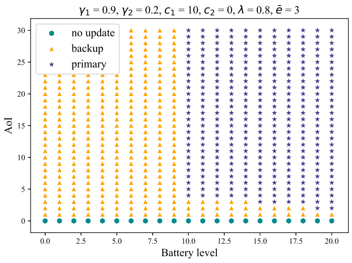

(g) Cost ratio = 0.0, $\lambda = 0.8$, $\gamma_2 = 0.2$

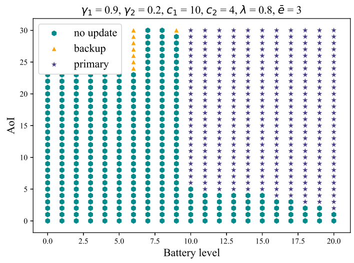

(h) Cost ratio = 0.4, $\lambda = 0.8$, $\gamma_2 = 0.2$

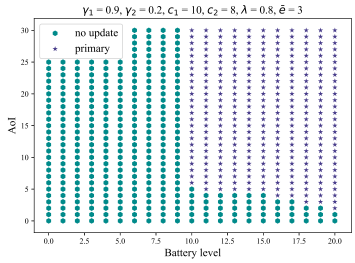

(i) Cost ratio = 0.8, $\lambda = 0.8$, $\gamma_2 = 0.2$

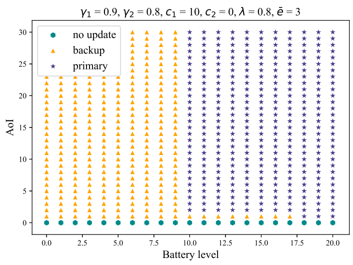

(j) Cost ratio = 0.0, $\lambda = 0.8$, $\gamma_2 = 0.8$

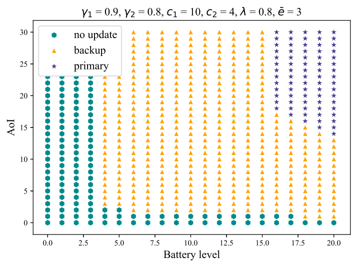

(k) Cost ratio = 0.4, $\lambda = 0.8$, $\gamma_2 = 0.8$

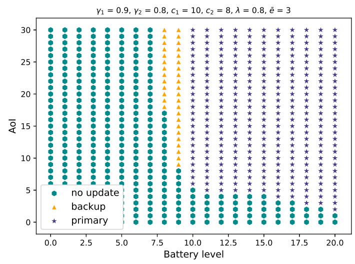

(l) Cost ratio = 0.8, $\lambda = 0.8$, $\gamma_2 = 0.8$

Figure 4.2: Illustration of the optimal policy for different energy cost ratios c_2/c_1.

the other hand, the average AoI increases quite rapidly at low values of the cost ratio. Moreover, for low values of λ, i.e., low energy generation rate, the saturation of the

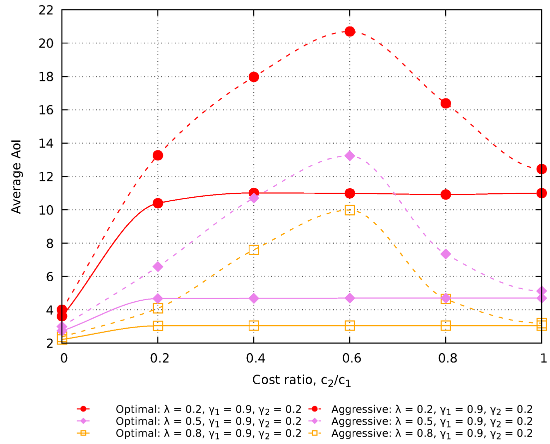

Figure 4.3: Dependency of average AoI and energy cost ratio for $\gamma_2 = 0.2$.

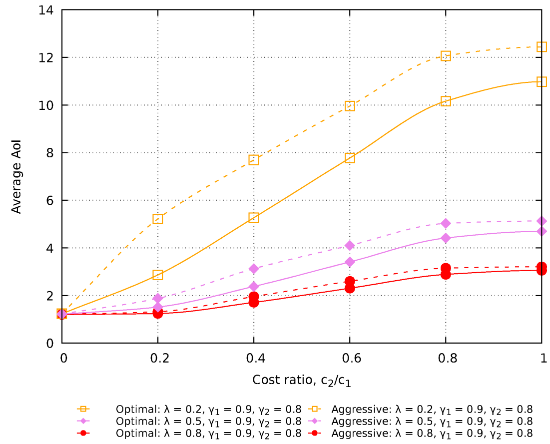

Figure 4.4: Dependency of average AoI and energy cost ratio for $\gamma_2 = 0.8$.

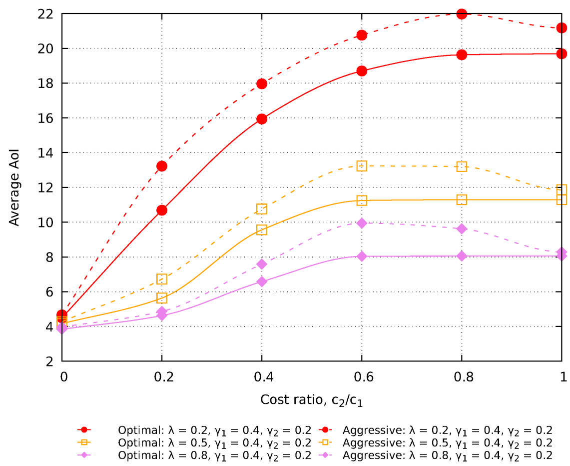

Figure 4.5: Dependency of average AoI and energy cost ratio for $\gamma_1 = 0.4$.

optimal average AoI happens at lower values of the cost ratio (see Fig. 4.3). At lower values of source reliability, γ_2, the average AoI achieved by the aggressive policy does not have an intuitive behaviour (see Fig. 4.3). Up to a certain point (when $c_1 - c_2 > \bar{e}$), increasing usage of the backup source causes the average AoI to grow. After some point (when $c_1 - c_2 \leq \bar{e}$), the system starts to be more energy conserving, i.e., starts to reserve energy for getting updates from the more reliable primary source, and the average AoI starts decreasing. If we set $\gamma_1 = 0.4$, a similar behaviour in average AoI is observed; however, the average AoI saturates at higher values of the cost ratio compared to the case when $\gamma_1 = 0.9$ (Fig. 4.3).

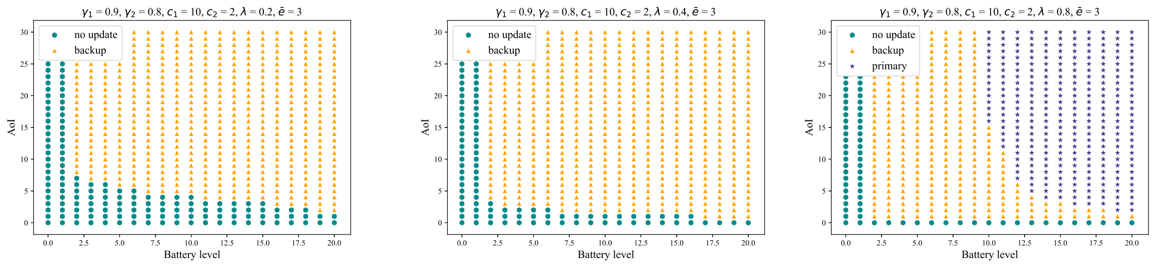

(a) $\lambda = 0.2$, cost ratio $= 0.8$, $\gamma_2 = 0.2$

(b) $\lambda = 0.4$, cost ratio $= 0.8$, $\gamma_2 = 0.2$

(c) $\lambda = 0.8$, cost ratio $= 0.8$, $\gamma_2 = 0.2$

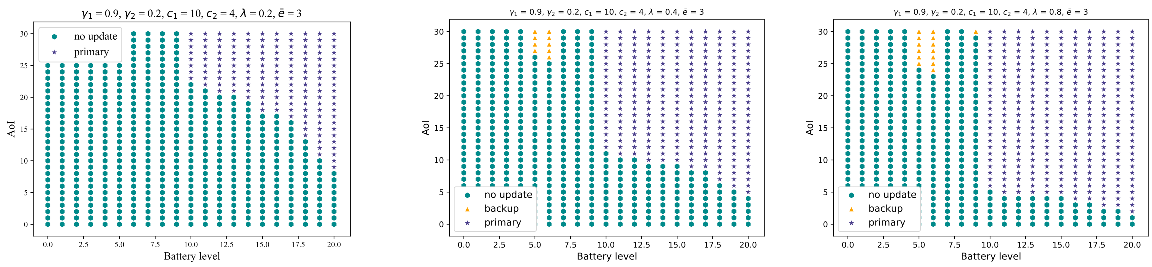

(d) $\lambda = 0.2$, cost ratio $= 0.4$, $\gamma_2 = 0.2$

(e) $\lambda = 0.4$, cost ratio $= 0.4$, $\gamma_2 = 0.2$

(f) $\lambda = 0.8$, cost ratio $= 0.4$, $\gamma_2 = 0.2$

Figure 4.6: Illustration of the optimal policy for different EH rates λ.

4.3.2.3 Energy harvesting

Another important parameter that impacts the optimal solution is the EH rate, λ. With increasing λ the monitoring node has tendency to request an update rather than staying idle (see Fig. 4.6). Furthermore, increasing EH capabilities enables the monitoring node to request updates more often from the primary information source, and reduces the utility of the backup source, which gradually disappears from the optimal solution.

Some system configurations are characterized by having a 'pocket' region, e.g., see Fig. 4.6(e) and 4.6(f). This situation is observed when the reliability of the backup source is quite low and the EH rate is sufficiently high. In this case, the energy buffer can recover in a short amount of time, which enables the monitoring node to request an update from a primary source, instead of an extremely unreliable backup source.

The dependence of the average AoI on λ is demonstrated in Fig. 4.7. As expected, the increase in the EH rate leads to a decrease in the achievable AoI.

4.3.2.4 Reliability of information sources

In Fig. 4.2 we can also observe the evolution of the optimal solution as the reliability of the backup source, γ_2, increases. The increase in γ_2 leads to an increase in the number of states in which the backup source is queried. In other words, the utility of the backup source also increases.

The dependence of average AoI on γ_2 is shown in Fig. 4.8. As expected, the increase in the EH rate decreases the achievable average AoI. However, if c_2/c_1 is high, then the increase in γ_2 does not severely affect the average AoI. As the backup source has a high cost, then the primary source prevails in the optimal solution, and the reliability of the backup source does not affect the average AoI significantly. If both the cost ratio and the EH rate are low, then the backup source becomes more preferable as its reliability increases. Therefore, in this case we observe a significant drop in average AoI (see Fig. 4.8).

4.3.2.5 Efficiency evaluation

Finally, in Fig. 4.9 we compare the performance of the optimal and aggressive policies in terms of the average AoI. The convergence time for both policies are similar, and does not exceed 200 time slots.

We observe that the gap between the average AoI achieved by the aggressive and optimal policies gets higher as the EH rate increases (Fig. 4.7), i.e., if the energy arrivals to the system are relatively stable, then the aggressive policy can be as effective as the optimal one. Similarly, there is no gain in average AoI if $c_2/c_1 = 0$. c_2/c_1 does not significantly influence the relative performance of the optimal policy over the aggressive one, since the gap remains relatively constant as a function of c_2/c_1 (Fig. 4.3 - 4.4). Generally speaking, since the backup source is less expensive but also less reliable than the primary one, the optimal policy tends to preserve energy when convenient in order to use the primary source, while the aggressive policy would always use the backup source whenever possible. Thus, the gap between the two policies shrinks as the backup source improves its reliability. However, if c_2/c_1 increases, the gap remains larger.

4.3.2.6 Discussion

We observe that the structure of the optimal solution varies depending on the characteristics of the environment and system parameters. In particular, we consider the EH rate as an environmental characteristic; the reliability of the information sources and

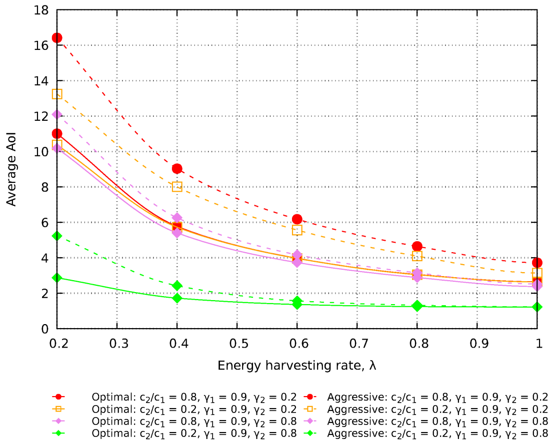

Figure 4.7: Average AoI as a function of the EH rate, λ.

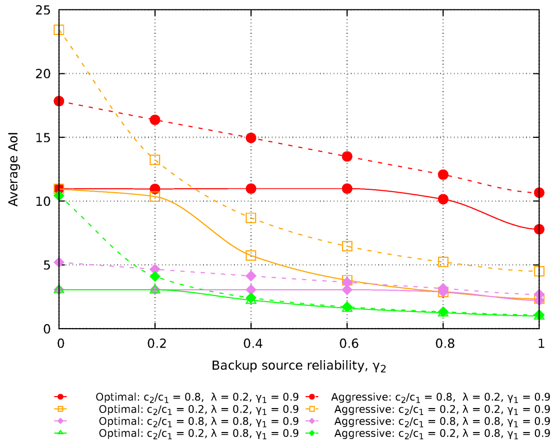

Figure 4.8: Average AoI as a function of the backup source reliability, γ_2.

the associated costs as system parameters. Two types of solution structure (behaviour) can be distinguished: *pocket region*, or appearance of the buffer (or accumulating) region in the optimal action set, where the monitoring node chooses to stay idle in order to gain extra energy, and *monotonic disappearance* of a source from the optimal action set.

Results reported above answer the question when employing a backup source is beneficial in reducing average AoI. Low values of cost ratio, as well as high reliability of the backup source are key requirements to be met in order to integrate a backup source to the system. Improving environmental characteristics can reduce the need for the backup source, but also the benefits from employing the optimal policy. Sometimes improving the environmental characteristics (for instance, device relocation) can be a solution, instead of increasing the complexity of the system by adding extra backup devices.

4.4 Average age-of-information with multiple heterogeneous information sources

For the purpose of analysis, the system with an EH monitoring node that is equipped with a finite size battery and collects status updates from multiple heterogeneous information sources is considered. We investigate the policies that minimize the average AoI, and answer the question, what is sufficient amount of monitoring devices in the system. To do so, we formulate the problem as an MDP. The optimal policy represents

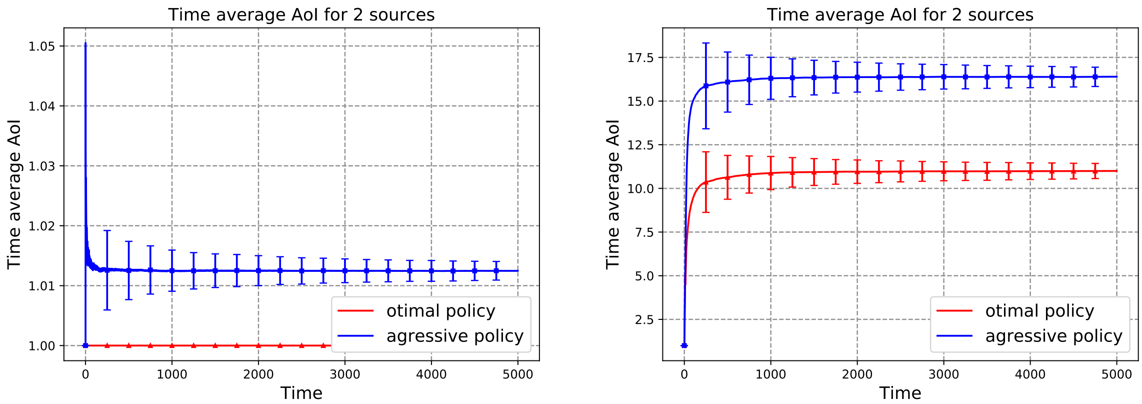

(a) $\lambda = 1.0$, cost ratio $= 0.2$, $\gamma_2 = 1.0$ (b) $\lambda = 0.2$, cost ratio $= 0.8$, $\gamma_2 = 0.2$

Figure 4.9: Average AoI vs. time for the aggressive and optimal policies.

the scheduling of actions to be taken (update from one of the sources or remain idle) at a time slot based on current energy level and AoI of an available packet at the monitoring node. We analyse the structure of the optimal solution for different cost/reliability combinations, and compared the performance of the optimal policy with the aggressive strategy.

The rest of this section is organized as follows. In Subsection 4.4.1, the system model description, problem formulation and solution approaches are introduced. Numerical results are presented in Subsection 4.4.2, providing a performance comparison between the proposed solution and the aggressive policy.

4.4.1 System model and problem formulation

In this subsection, we focus on a communication system formed by a single energy-harvesting monitoring node and n heterogeneous information sources, where each source can take samples of the current status of the process of interest (Fig. 4.10). The monitoring node can query these information sources to receive updates on the status of the underlying process. These information sources may, for example, model sensors with different technologies measuring the same process. Time is divided into time slots of equal length, and we consider a finite session of T time slots. We assume that the monitoring node can request a status update from only one of the sources in each time slot. A received status update becomes available at the beginning of the next time slot. We highlight two important dynamics at the monitoring node: energy fluctuations and the AoI about the process of interest. The objective is to minimize

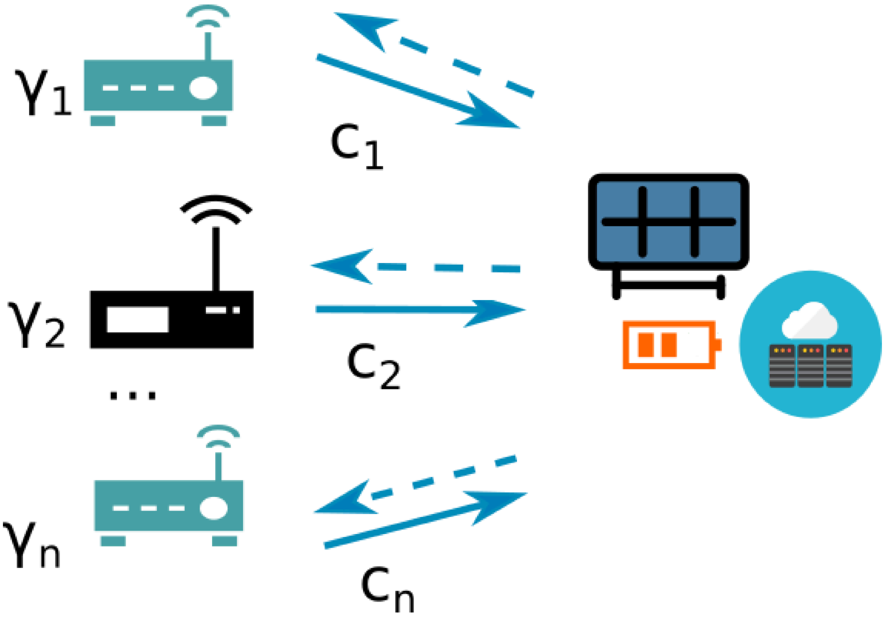

Figure 4.10: System model

the average AoI at the monitoring node, taking into account the time-varying energy budget.

4.4.1.1 Energy fluctuations

We assume that the monitoring node is equipped with the battery of finite capacity B, and can harvest energy from ambient sources. Fluctuations in the battery of the monitoring node are defined by two processes: harvested energy in each time slot and the energy consumption caused by the queries for a status update. Energy harvested over time is represented as an independent and identically distributed (i.i.d.) binary random process $\{e(t)\}_{t=1}^{\infty}$. At each time slot t the monitoring node receives $e(t) \in \{0, \bar{e}\}$ energy units, such that $P(e(t) = \bar{e}) = \lambda$.

The energy cost of requesting a status update from a source i, $i = 1, 2, ..., n$ is denoted by c_i. For the sake of simplicity, we consider $c_i \in \mathbb{Z}^+$ corresponding to integer multiples of a unit of energy that takes values between c_{min} and c_{max}. In order to analyse the effect of different possible cost combinations, we consider three cases, depicted in Fig. 4.12, that are:

1. Sublinear, $c_i \approx i^2$

2. Linear, $c_i \approx i$

3. Superlinear, $c_i \approx \lceil \log_2 i \rceil$

The aforementioned dependencies do not carry any "physical meaning", and were chosen in order to investigate the impact of cost values on the average AoI. We expect, that the fluctuations in cost values in the same range will not impact the results.

4.4.1.2 Age-of-information

The status updates provided by the information sources need not be *fresh*, i.e., with zero age. Due to various factors, such as the sensing technology or the processing of the measurements, we assume that the status updates provided by the sources may have different ages when they arrive at the monitoring node. To reflect it, we assume that the source nodes provide the status update to the monitoring node having ages in the interval $[\alpha, \beta]$ $(\alpha<\beta)$, where α is the most *fresh* status update while β is the most *stale* one.

The probability to receive a status update of age j from a source i, where $j \in [\alpha, \beta]$ and $i = 1, 2, ..., n$, is denoted by $\gamma_{i,j}$. The probabilities to receive a status update in the considered age interval $[\alpha, \beta]$ correspond to a geometric distribution as in Fig. 4.11. The distribution depends to the value of the parameter p. The geometric distribution provides the probability that the first success requires k independent trials, each trial is with success probability p. In this case, the probability that the kth trial is the first success is:

$$Pr(X = k) = (1 - p)^k p, k = 1, 2, 3, ... \tag{4.8}$$

The distribution parameter differs for all information sources, and, therefore, denoted as p_i, $i = 1, 2, ..., n$. In the introduced problem setup, the parameter p_i reflects the success probability to receive a fresh status update of age α from a source i: $p_i = \gamma_{i,j}$, where $j = \alpha$. We assume that sources with a higher value of success probability to deliver a fresh status update have a higher energy cost. We consider following values of $p_i \in [p_i^{min}, p_i^{max}]$ (Fig. 4.11):

1. Sublinear $p_i \approx c_i^2$
2. Linear $p_i \approx c_i$
3. Superlinear $p_i \approx \log_2 c_i$

Sublinear, linear and superlinear cases correspond to low, medium and high average sources reliability in the system, respectively. The introduced cases investigate the

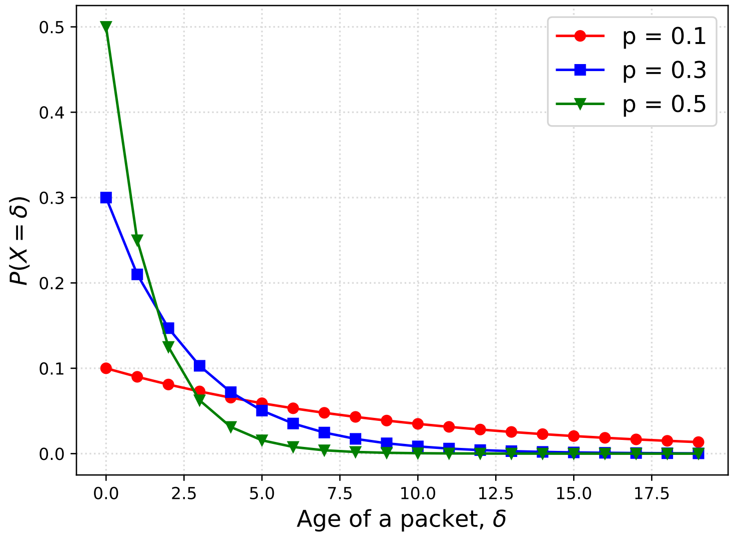

Figure 4.11: Geometric distribution of status updates' ages, with $p = \gamma_i$

impact of values of reliabilities on the average AoI, and serve to justify the obtained results for various combinations of average values of costs and reliabilities.

4.4.1.3 MDP formulation

We aim to determine the policy that minimizes the average AoI at the monitoring node. To achieve this, the monitoring node optimally chooses the action to take at each time slot, that includes either to request an update from one of the information sources at the beginning of each time slot, or to stay idle. This choice is made taking into account the battery level and the age of the most recent status update available at the monitoring node. We will show that this problem can be formulated as an MDP, consisting of a tuple $<S, A, P, R>$.

The action taken by the monitoring node at time t is denoted by $a(t)$, which takes values from the finite action space $A = \{a_0, a_1, a_2, ..., a_n\}$, where a_i corresponds to querying source i for a status update, $i = 1, ..., n$, and a_0 to remain idle.

The system state is described by the pair of variables $s(t) = (b(t), \delta(t))$. Let $\delta(t) \in \{1, 2, ..., \delta_{max}\}$ denote the AoI at the monitoring node at time slot t, where δ_{max} is the maximum age in the system. Equivalently, we assume that having a status information of age δ_{max} or any $\delta > \delta_{max}$ have the same utility. Depending on the decision $a(t)$, $\delta(t)$ is updated as $\{\delta(t-1)+1, j\}$, $j \in \{\alpha, \alpha+1, ..., \beta\}$. The energy level in the battery $e(t)$ evolves according to Eq. (4.1).

The transition probabilities for our problem are given as in Eq. (4.9) for $a_i \in$

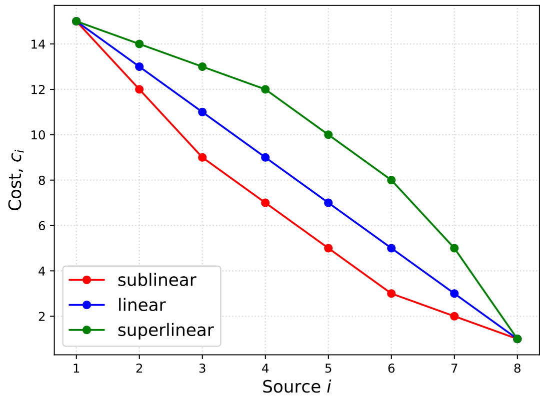

(a) Sources's rank vs. cost

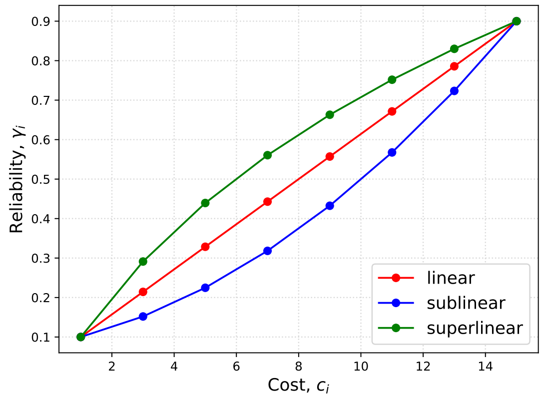

(b) Linar cost vs. reliability

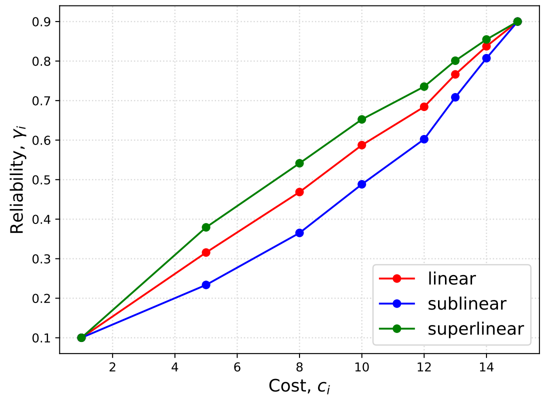

(c) Sublinar cost vs. reliability

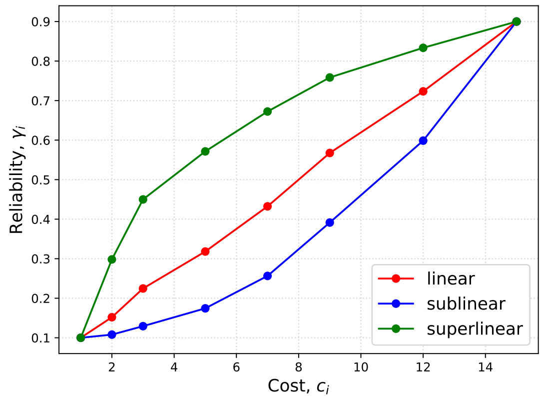

(d) Superlinar cost vs. reliability

Figure 4.12: Dependency of a source's cost and reliability

$\{a_1, a_2, ..., a_n\}$, $j \in \{\alpha, \alpha+1, ..., \beta\}$.

$$\begin{cases} P\big[s(t+1) = (\min\{b{+}\bar{e}{-}c_i, B\}, \min\{j, \delta{+}1, \delta_{max}\})|s(t) = (b,\delta), a(t) = a_i\big] = \lambda(\gamma_{i,j} + \sum_{j=\alpha}^{\beta} \gamma_{i,j}[j == \delta+1]) \\ P\big[s(t+1) = (b{-}c_i, \min\{j, \delta{+}1, \delta_{max}\}\})|s(t) = (b,\delta), a(t) = a_i\big] = (1{-}\lambda)(\gamma_{i,j} + \sum_{j=\alpha}^{\beta} \gamma_{i,j}[j == \delta+1]) \end{cases} \tag{4.9}$$

Note that, if the received status update is older than the currently available one, then the monitoring node drops the new update and keeps the fresher one.

When the node remains idle, i.e., $a(t) = a_0$, the transition probabilities takes the form as in Eq. (4.10):

$$\begin{cases} P\big[s(t+1) = (b, \min\{\delta+1, \delta_{max}\})|s(t) = (b,\delta), a(t) = a_0\big] = 1-\lambda & b{<}B \\ P\big[s(t+1) = (\min\{b+\bar{e}, B\}, \min\{\delta+1, \delta_{max}\})|s(t) = (b,\delta), a(t) = a_0\big] = \lambda & b{<}B \\ P\big[s(t+1) = (B, \min\{\delta+1, \delta_{max}\})|s(t) = (B,\delta), a(t) = a_0\big] = 1 \end{cases} \tag{4.10}$$

The values of the reward function depend on the action chosen at the monitoring node, and the age of a packet arrived to the monitoring node:

$$R(s(t+1)|s(t), a(t) = a_i) = \begin{cases} j, j \in \{\alpha, \alpha+1, ..., \beta\}, & a_i : i \neq 0 \wedge j < \delta + 1 \\ \delta + 1, & a_i : i = 0 \vee i \neq 0 \wedge j \geq \delta + 1 \end{cases} \tag{4.11}$$

The problem is framed as a first-order Markovian dynamics (history independence), where the next state only depends on current state $s(t)$ and current action $a(t)$:

$$Pr(s(t+1)|a(t), s(t), a(t-1), s(t-1), .., s(0)) = Pr(S(t+1)|a(t), s(t)) \tag{4.12}$$

Similarly, the first-order Markovian reward process is applied, such that the reward is specified by a deterministic function $R(s)$:

$$Pr(R(t) = R(s(t))|a(t), s(t)) = 1 \tag{4.13}$$

We find the optimal policy is *optimal* that minimizes the infinite-horizon average AoI - $V^{\pi}(s)$. To solve this optimization problem, we use the offline dynamic programming approach adopting the value iteration (VI) algorithm described in Section 4.3. The optimal stationary deterministic policy, obtained by Algorithm 2, specifies the decision rules that maps the current energy level and AoI to actions taken with probability one.

4.4.2 Numerical results

In this section, we analyse the optimal policies for different settings, in particular, we consider the cost distribution of information sources, the source reliability distribution, and the parameters of the EH processes (λ, $\bar{e}$). We study the added value in average AoI of employing on extra information source in the system.

4.4.2.1 Simulation parameters

System parameters that remain constant for all the setups are presented in Table 4.1. The efficiency of the optimal policy is verified via simulations run over $T = 5000$ time slots, and compared with a so-called aggressive policy. The aggressive policy (Algorithm 4) tries to always receive a status update wherever it has sufficient energy in its battery, and goes for the expensive source wherever it can afford it.

Simulated results for the optimal and aggressive policies are averaged over $M = 1000$ simulations. To demonstrate the results we plot the mean AoI at time slot t ($\bar{\delta_t}$). Default parameters for presented results are obtained for parameters as in Table 4.2.

Algorithm 4 Aggressive Policy

set $b(0) = 0$, $\delta(0) = 0$
for $t = 1 : T$ **do**
  for $i \in A \backslash \{a_0\}$ **do**
    if $b(t) \geq c_i$ **then** ▷ check for the availability of energy for updating from a source i
      $b(t) = \min\{b(t-1) + e(t) - c_i, B\}$
      $j = \alpha$ ▷ counter for range of possible AoI values, $j \in [\alpha, \beta]$
      while $j < \beta$ **do**
        if $p \in [\gamma_i^j, \gamma_i^{j+1}]$ **then** ▷ see Fig. 4.11
          if $\delta(t-1) < j$ **then** ▷ comparing of AoI of available packet at the destination node and nearly received packet
            $\delta(t) = \delta(t-1) + 1$
          else
            $\delta(t) = j$
          end if
        end if
        break
        $j+ = 1$
      end while
    end if
  end for
  if $b(t) < \min(C \backslash \{c_0\})$ **then**
    $b(t) = \min\{b(t-1) + e(t), B\}$
    $\delta(t) = \delta(t-1) + 1$
  end if
end for

4.4.2.2 Markov model solution

The optimal solutions for different values of EH rate and cost/reliability combinations a re presented in Fig. 4.13 - 4.15. If $\lambda = 0.2$, then the destination node requests a status update only from the cheapest sources, denoted in Fig. 4.13 as sources *6-8*. If the reliability is sublinear, then the destination node only exploits the cheapest source 8 for all cost combinations. The most desirable combination is when the cost is sublinear (meaning that the average cost level of all sources is lower than for other

Table 4.2: Default parameters

Parameters	**Values**
Battery capacity, B	20
AoI states, $[\alpha, \beta]$	$[1, 20]$
Amount of harvested energy per a time slot, $\{0, \bar{e}\}$	$\{0, 3\}$
Amount of devices in the system, n	8
Cost range, $[c_{min}, c_{max}]$	$[1, 16]$
Reliability range, $[\gamma_i^{min}, \gamma_i^{max}]$	$[0.1, 0.9]$

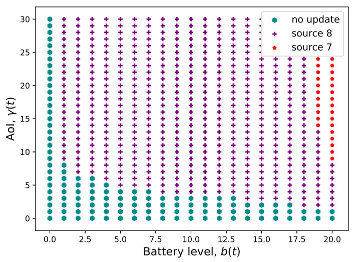

(a) Cost: superlinear; reliability: superlinear

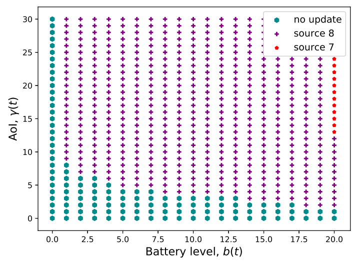

(b) Cost: superlinear; reliability: linear

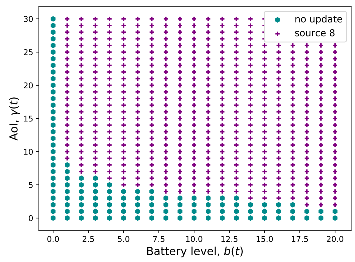

(c) Cost: superlinear; reliability: sublinear

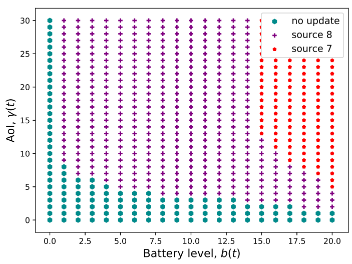

(d) Cost: linear; reliability: superlinear

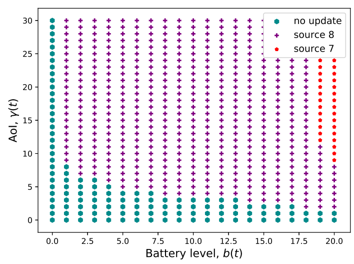

(e) Cost: linear; reliability: linear

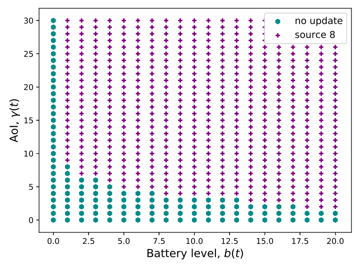

(f) Cost: linear; reliability: sublinear

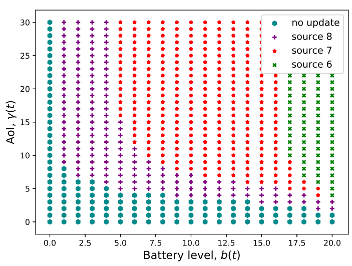

(g) Cost: sublinear; reliability: superlinear

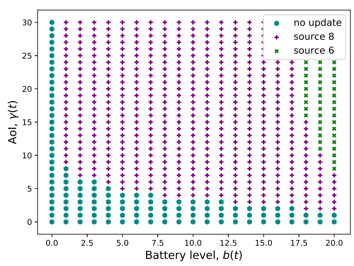

(h) Cost: sublinear; reliability: linear

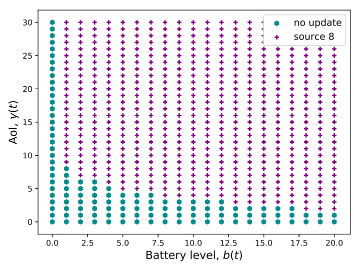

(i) Cost: sublinear; reliability: sublinear

Figure 4.13: Illustration of the optimal policy for different energy cost/ reliability combinations for $\lambda = 0.2$.

combinations), and the reliability is superlinear (when the average reliability level is higher in the system comparing with other combinations). In this case the device more widely exploits other sources that are following the cheapest one (Fig. 4.13(g)). We also would like to compare the solutions for two combinations, when the average cost is higher (bad case) or superlinear and average reliability is higher or superlinear (good case) (Fig 4.13(a)) and vice versa (Fig 4.13(i)). In the former case, the destination node requests two cheapest information sources $7, 8$ for an update, while in the latter case, the destination node goes for the cheapest source 8. Therefore, the structure changing of the optimal solution is more sensitive to the change of the average level of reliability.

With the increase of EH rate, more sources are composed in the optimal solution. For instance, in Fig. 4.14(a) there are three sources in the optimal solution, while in Fig. 4.15(a) - four sources. With the decrease of average cost level and/or the increase in average level of reliability, the same sources are requested for an update at lower battery levels and exploiting more resources in the solution. Similar results are observed for various values of $\bar{e}$.

The dependency of average AoI and EH rate for different cost/reliability combinations is demonstrated in Figs. 4.16(a) - 4.16(c). In addition, the comparison with the aggressive strategy is presented. For all three combinations of cost, the optimal average AoI does not significantly differs, as well as for different average values of reliability. This statement does not hold itself for average AoI obtained by adopting the aggressive strategy in the destination node. With the decrease of average cost level, the gaps between optimal solutions for different reliability combinations will increase. In other words, with the decrease average cost of the information sources, values of the optimal average AoI become more sensitive to source reliability values. With the increase of EH rate, the performance of optimal and aggressive strategies almost equalizes. For all cost combinations the reliability dependency is superlinear. But with the decrease of average level of the sources' reliabilities, the gap in performance between optimal and aggressive strategies always increases for high values of EH rate. In other words, if the reliability of sources is high enough, same as the EH characteristics, then the aggressive strategy performs as well as the optimal one for any costs combinations.

4.4.2.3 Size of a network

Further, we analyse how the size of the system affects the performance regarding to the average AoI for different values of EH rate, λ and energy arrival units $\bar{e}$. The analysis is

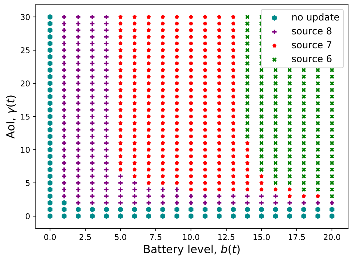

(a) Cost: superlinear; reliability: superlinear

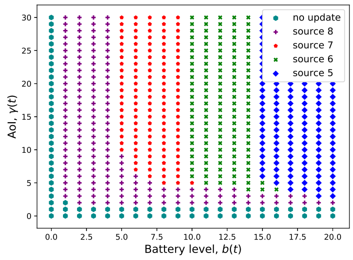

(b) Cost: superlinear; reliability: linear

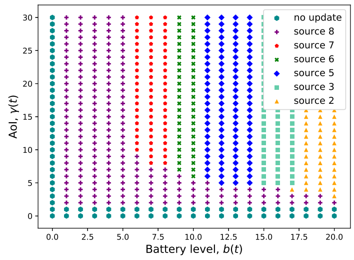

(c) Cost: superlinear; reliability: sublinear

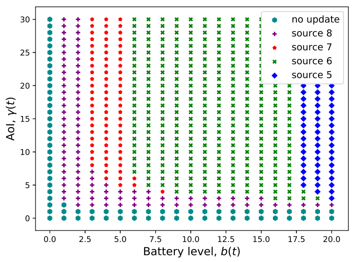

(d) Cost: linear; reliability: superlinear

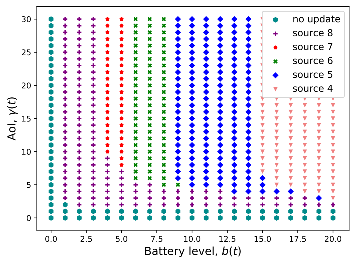

(e) Cost: linear; reliability: linear

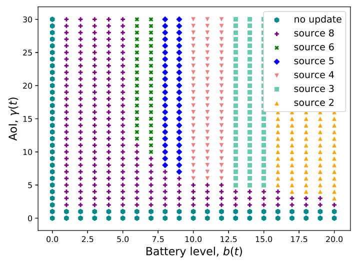

(f) Cost: linear; reliability: sublinear

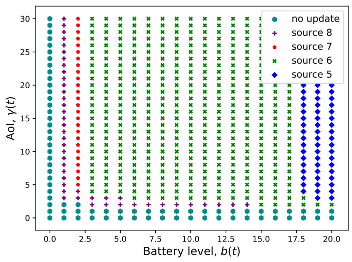

(g) Cost: sublinear; reliability: superlinear

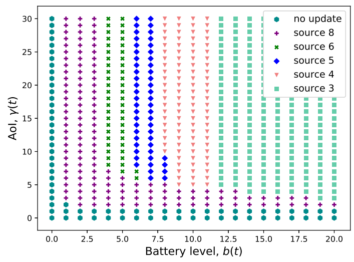

(h) Cost: sublinear; reliability: linear

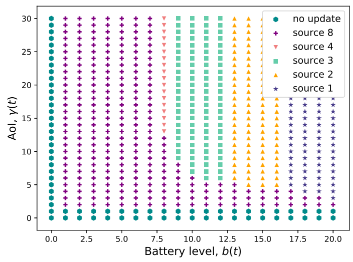

(i) Cost: sublinear; reliability: sublinear

Figure 4.14: Illustration of the optimal policy for different energy cost/ reliability combinations for $\lambda = 0.6$.

performed for the linear dependency between number of devices and its costs same as the linear dependency between receiving cost and sources' highest possible reliabilities.

With the increase of the number of information sources, the optimal average AoI has a tendency to decrease, the curves saturates, when number of sources $n = 8$, but the biggest gain in performance is obtained when the system is of size $n = 4$. If the EH rate is low ($\lambda = 0.2$ in the Fig. 4.17), then the increase in number of devices does not provide any gain for the system performance, but with the increase of EH rate, the gain increases with the increase of system size from $n = 2$ to $n = 4$. Similar statement

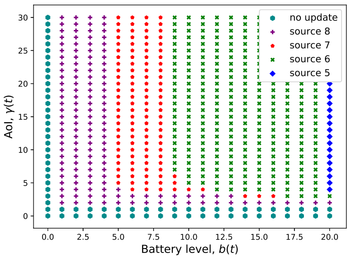

(a) Cost: superlinear; reliability: superlinear

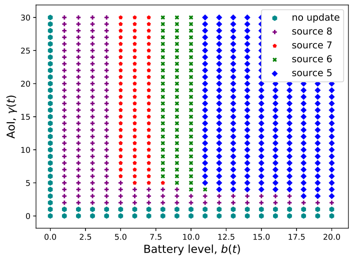

(b) Cost: superlinear; reliability: linear

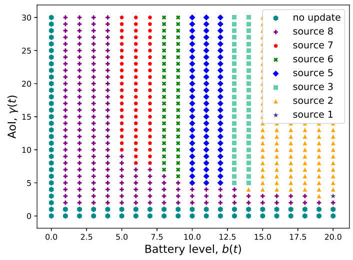

(c) Cost: superlinear; reliability: sublinear

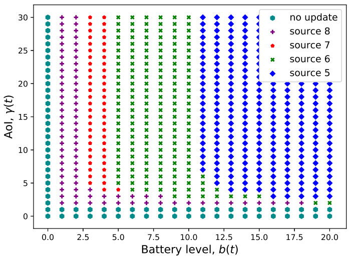

(d) Cost: linear; reliability: superlinear

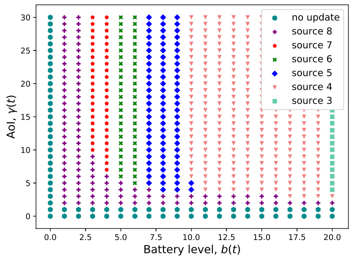

(e) Cost: linear; reliability: linear

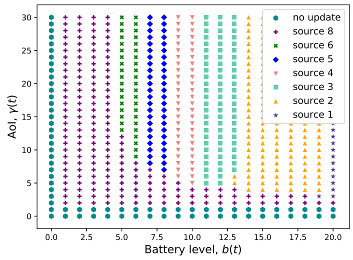

(f) Cost: linear; reliability: sublinear

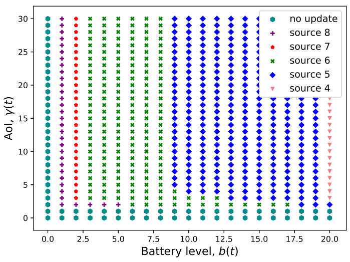

(g) Cost: sublinear; reliability: superlinear

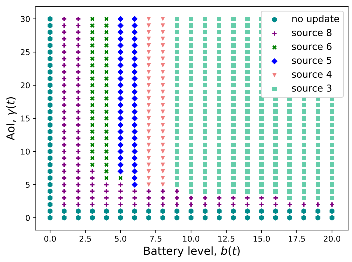

(h) Cost: sublinear; reliability: linear

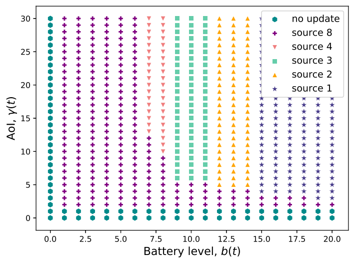

(i) Cost: sublinear; reliability: sublinear

Figure 4.15: Illustration of the optimal policy for different energy cost/ reliability combinations for $\lambda = 0.8$.

holds when we vary the values of energy arrivals, $\bar{e}$.

If the destination node exploits the aggressive strategy, then we observe the controversial behaviour: with increase of the system size, the performance is worsening, or, by other words, the average AoI at the destination node grows. Moreover, lower is the EH rate, higher the growth of the average AoI, or more inefficient is the aggressive policy with growth of the system size. Similarly, for various values of energy arrival units $\bar{e}$, with the system's increase, the aggressive policy becomes more inefficient and average AoI grows. If the EH rate is low, then the optimal policy requests a status update

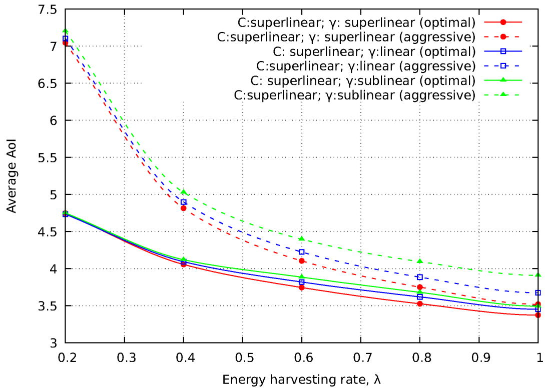

(a) Superlinear

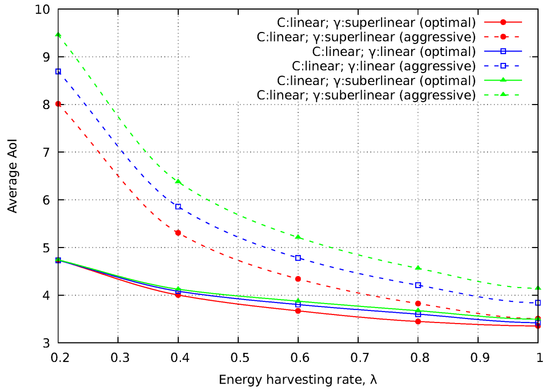

(b) Linear

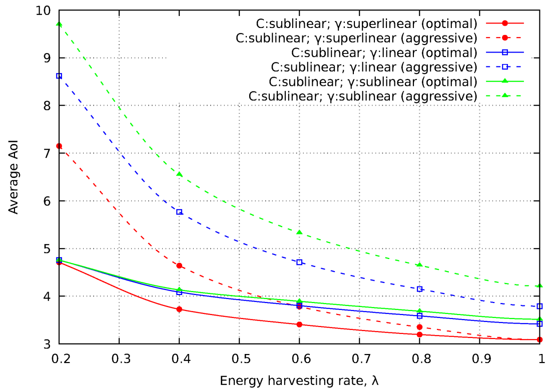

(c) Sublinear

Figure 4.16: Dependency of average AoI and EH rate for different devices/cost dependencies

from the cheapest sources, while the aggressive policy requests the status update for the most expensive source that is available, that causes the difference in the achieved average AoI.

For both policies, the increase of system size is not beneficial. For the optimal policy, the increase of size will not provide any gain performance and will only increase the computational complexity. If the adopted policy is aggressive, then without increase of the computational complexity, the system performance will become even worse.

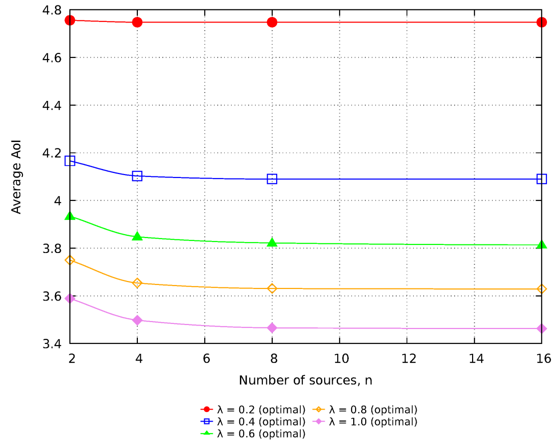

Figure 4.17: Number of information sources vs. optimal average AoI for different values of EH rates, λ.

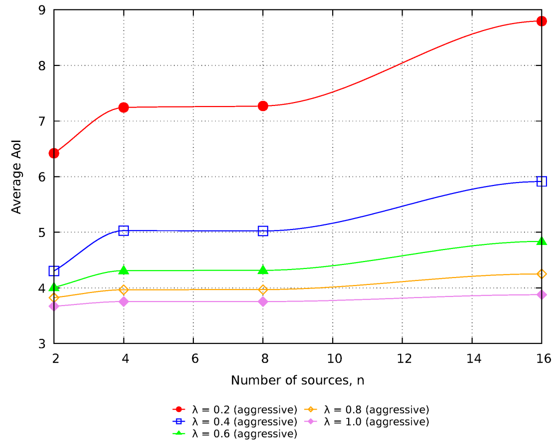

Figure 4.18: Number of information sources vs. average AoI if destination node adopts aggressive strategy for different values of EH rates, λ.

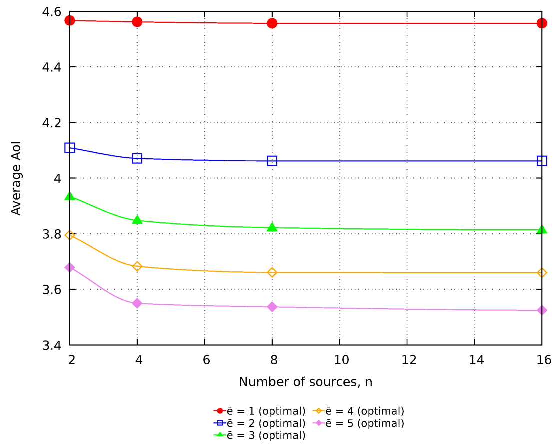

Figure 4.19: Number of information sources vs. optimal average AoI for different values of energy arrival units, $\bar{e}$.

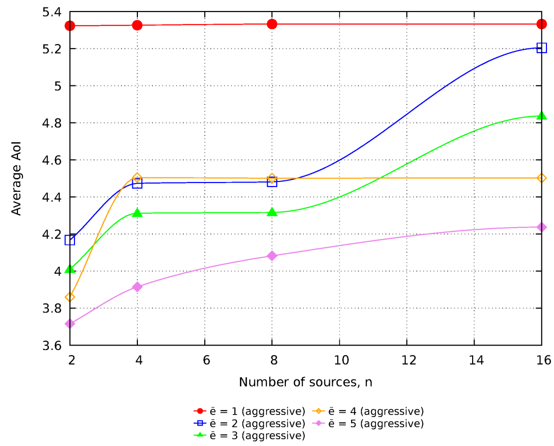

Figure 4.20: Number of information sources vs. average AoI if destination node adopts aggressive strategy for different values of energy arrival units, $\bar{e}$.

4.5 Conclusions

We have investigated a monitoring node that can query two or more distinct sources of information, to receive status updates of an underlying process of interest. We formulated this problem as an MDP, and derived the optimal policy that minimizes the average AoI. We compared the performance of the optimal policy with that of the aggressive policy, which tries to query the most expensive source it can afford, and demonstrated that the gain from the optimal policy increases as the EH rate decreases or the backup source characteristics become worse (i.e., decreasing reliability or increasing cost).

We have shown that employing an alternative source of information is justified when the energy cost of requesting from the backup source is relatively low and its reliability is high.

Most importantly, we demonstrated, that the further increase of system size does not improve system performance, and optimal average AoI saturates in some point ($n = 8$) for all values of EH rates and energy arrival units. Increase of system size in case of adoption of aggressive strategy leads to increase of average AoI and also not beneficial.

Chapter 5
Summary and Future Directions

The limited life span of rechargeable batteries for IoT devices is one of the major limitations to be confronted. Nowadays, the only feasible solution for prolonging battery life a network of interconnected IoT devices is to harvest energy from surroundings ambient sources. Incorporating energy-harvesting in IoT deliver many challenges and aspects to be considered, such as:

- availability of ambient sources, that depends on the physical placement and mobility of IoT devices
- design aspects such as determining the suitable energy source for the given application, harvester type and energy storage.
- energy management, to handle the erratic energy arrivals as well as optimizing the device performance so as to manage the trade-offs between performance characteristics (throughput, AoI, coverage, etc.) and energy.

This thesis focused on the development of sustainable energy management for energy-harvesting communication systems, mainly considering the IoT scenarios. The obtained results demonstrated the capability of smart management to deal with ambient sources of energy that are characterized of unstable energy arrivals randomly distributed over time.

Chapter 2 studied non-ideal batteries, in particular charge recovery effect, and how these aspects affect the battery outage probabilities. To do so, we constructed a Makrov model of non-ideal battery with bi-dimensional energy levels. We discovered that charge recovery severely affects the performance, as the apparent outage probability can be significantly larger than that of real outage. We developed a simplified self-control management for non-ideal battery, that decreases the number of apparent outage and data losses events.

For future work, it is possible to consider the situation where some information is unknown or hidden (imperfect state of charge knowledge). Another possibility for the future work is to generalize the regulation of the μ parameter of Self-turning Control Systems (STC). STC systems are based on the derivation of the parameters to adapt and achieve an optimal state of a change of parameters in situation of unsteady external conditions, which is possible to realize by parameter value estimation based on recorded statistical information. These considerations may shed new light on the possibility to design a fully autonomic sensor device that is not only capable of energy harvesting, but also to exploit it at its fullest to reach a true energy independence, which would be key to guarantee successful and durable IoT applications.

Finally, within this chapter, we explored the implementation of different sampling strategies for the practical EH data-logger, that prevents packet delivery failures and simple enough to be implemented on the low complexity hardware. The proposed strategies balances the unstable energy arrivals, and improves the performance of state-of-the-art DDASA.

Chapter 3 is focused on multi-device scenarios. We studied the system with non-homogeneous (asymmetric) sensors in terms of energy harvesting capabilities and size of energy buffers. We examined the system performance for the three scenarios: random transmissions; transmissions that are proportional to energetic capabilities (benchmark); transmissions based on the knowledge of one node about asymmetric property of the system, framed as a Bayesian game with incomplete information. We found out, that the latter scenario is the most energy balanced, and the performance in this scenario is close to the benchmark performance.

For the future work, it is useful to consider asymmetries not only in the battery capacity, but also in energy arrival rates, leakage rate and other parameters. Another possibility is to develop appropriate rules of interaction between asymmetric sensors in EH-WSNs with the proportion of performance close to the ideal scenario, meaning that each sensor transmits data proportionally with its battery capacity.

Further, we considered the energy cooperation as a way to overpass system energy asymmetries. In particular, we proposed to design an energy topology, that connects the communication nodes with energy links. The optimization problem is formulated in a way such that no communication node is depleted. Integration of energy topology with embedded energy cooperation significantly decreases the amount of depleted node in a system from 30% of depleted nodes to almost 0%. Similar result were obtained for the SC scenario, where the interconnected smart services represented by GWs are interconnected via Smart Grid.

To extend the present results to more general cases, we remark that we focused on a single cluster case, with just one cluster head/sink. As future work, clustering schemes could be considered with embedded energy cooperation capabilities of EH multi-hop wireless networks. The assumption about homogeneity of a system has to be relaxed, therefore in the clustering scheme batteries capacities and energy thresholds have to be individual for each node.

Chapter 4 instead is focused on the systems, where the main performance metric is AoI. We considered a system with an EH monitoring node that can request status updates from two or more heterogeneous information sources. The objective is minimization of average AoI. The problem was formulated as an MDP. We analyzed the optimal solution depending on values of reliabilities of information sources, energy costs of requests and EH rate. The main conclusion is that an increase of the system size does not improve the performance in terms of decreasing of average AoI. For the future work, we propose to design learning algorithms, where the environmental parameters and information sources characteristics are considered as unknown parameters to be learned through automated procedures.

List of Publications

This thesis summarizes the work developed over three years where the main outcomes are the following articles.

List of journal papers:

[J1] E. Gindullina, L. Badia and X. Vilajosana "Adaptive sampling algorithms for energy harvesting sensing nodes with sampling rate limitations", *Wiley Transactions on Emerging Telecommunications Technologies (ETT) (accepted)*, 2019.

[J2] E. Gindullina, L. Badia and D. Gunduz "Average Age-of-information with multiple heterogeneous information sources" *(to be submitted)*, 2019

List of publications on conference proceedings:

[C1] A.F. Gambin, **E. Gindullina**, L. Badia, and M. Rossi "Energy cooperation for sustainable IoT services within smart cities" in Proc. *IEEE Wireless Communications and Networking Conference (WCNC)*, 2018

[C2] E. Gindullina, and L. Badia "An optimization framework for energy topologies in smart cities" in Proc. *IEEE Wireless Communications and Networking Conference (WCNC)*, 2018

[C3] E. Gindullina, and L. Badia "Towards self-control of service rate for battery management in energy harvesting devices" in Proc. *IEEE International Conference on Communications Workshops (ICC Workshops)*, 2017

[C4] L. Badia, E. Feltre, and **E. Gindullina** "A Markov Model Accounting for

Charge Recovery in Energy Harvesting Devices" in Proc. *IEEE Wireless Communications and Networking Conference Workshops (WCNCW)*, 2017

[C5] E. Gindullina, and L. Badia "Asymmetry in energy-harvesting wireless sensor network operation modeled via Bayesian games", in Proc. *IEEE 18th International Symposium on A World of Wireless, Mobile and Multimedia Networks (WoWMoM)*, 2017

[C6] E. Gindullina, L. Badia and D.Gunduz "Average Age-of-Information with a Backup Information Source", in Proc. *IEEE International Symposium on Personal, Indoor and Mobile Radio Communications (PIMRC)*, 2019

[C7] E. Gindullina, and L. Badia "Distributed sensing from energy harvesring wireless devices", in Proc. *IEEE International Conference on Software, Telecommunications and Computer Networks (SoftCOM)*, 2019

Aknowledgements

Firstly, I would like to express my sincere gratitude to my advisor Prof. Leonardo Badia for the continuous support during the course of my studies, for his patience, motivation, and immense knowledge. His guidance helped me in all the time of research.

I would also like to thank my family and loved ones for all their help, understanding and moral support.

Last but not the least, this work has received funding from the European Union's Horizon 2020 research and innovation programme under the Marie Sklodowska-Curie grant agreement No. 675891

References

[1] M. A. Green, Y. Hishikawa, W. Warta, E. D. Dunlop, D. H. Levi, J. Hohl-Ebinger, and A. W. Ho-Baillie, “Solar cell efficiency tables (version 50),” *Progress in Photovoltaics: Research and Applications*, vol. 25, no. 7, pp. 668–676, 2017.

[2] T. Shu, M. Xia, J. Chen, and C. de Silva, “An energy efficient adaptive sampling algorithm in a sensor network for automated water quality monitoring,” *Sensors*, vol. 17, no. 11, p. 2551, 2017.

[3] M. P. Mills, “The cloud begins with coal,” *Digital Power Group*, 2013.

[4] I. Humar, X. Ge, L. Xiang, M. Jo, M. Chen, and J. Zhang, “Rethinking energy efficiency models of cellular networks with embodied energy,” *IEEE Network*, vol. 25, no. 2, pp. 40–49, 2011.

[5] L. Da Xu, W. He, and S. Li, “Internet of Things in industries: A survey,” *IEEE Transactions on industrial informatics*, vol. 10, no. 4, pp. 2233–2243, 2014.

[6] L. Atzori, A. Iera, and G. Morabito, “The Internet of Things: A survey,” *Computer networks*, vol. 54, no. 15, pp. 2787–2805, 2010.

[7] B. Alhadidi, N. A. Rumman *et al.*, “Scalability and tracking issues in wireless distributed sensor network,” in *IEEE International Conference on Future Computer and Communication*, 2009, pp. 385–389.

[8] N. Michelusi, L. Badia, and M. Zorzi, “Optimal transmission policies for energy harvesting devices with limited state-of-charge knowledge,” *IEEE Transactions on Communications*, vol. 62, no. 11, pp. 3969–3982, 2014.

[9] J. A. Paradiso and T. Starner, “Energy scavenging for mobile and wireless electronics,” *IEEE Pervasive computing*, no. 1, pp. 18–27, 2005.

[10] S. Basagni, M. Y. Naderi, C. Petrioli, and D. Spenza, "Wireless sensor networks with energy harvesting," *Mobile Ad Hoc Networking: Cutting Edge Directions*, pp. 701–736, 2013.

[11] M. Gatzianas, L. Georgiadis, and L. Tassiulas, "Control of wireless networks with rechargeable batteries," *IEEE Trans. Wireless Commun*, vol. 9, no. 2, pp. 581–593, 2010.

[12] D. Gunduz, K. Stamatiou, N. Michelusi, and M. Zorzi, "Designing intelligent energy harvesting communication systems," *IEEE Communications Magazine*, vol. 52, no. 1, pp. 210–216, 2014.

[13] J. Ventura and K. Chowdhury, "Markov modeling of energy harvesting body sensor networks," in *IEEE 22nd International Symposium on Personal, Indoor and Mobile Radio Communications*, 2011, pp. 2168–2172.

[14] J. Yang and S. Ulukus, "Optimal packet scheduling in an energy harvesting communication system," *IEEE Transactions on Communications*, vol. 60, no. 1, pp. 220–230, 2011.

[15] J. Kurose and K. Ross, "Computer networks: A top down approach featuring the internet," *Peorsoim Addison Wesley*, 2010.

[16] M. Fouladlou and A. Khademzadeh, "An energy efficient clustering algorithm for wireless sensor devices in Internet of Things," in *IEEE Artificial Intelligence and Robotics (IRANOPEN)*, 2017, pp. 39–44.

[17] C. Krishna, "Managing battery and supercapacitor resources for real-time sporadic workloads," *IEEE Embedded Systems Letters*, vol. 3, no. 1, pp. 32–36, 2010.

[18] A. Baumgardt, F. Bachheibl, and D. Gerling, "Utilization of the battery recovery effect in hybrid and electric vehicle applications," in *IEEE 17th International Conference on Electrical Machines and Systems (ICEMS)*, 2014, pp. 254–260.

[19] K. Wei, W. Zhang, and Y. Yang, "Prolonging battery usage time in smart phones," in *2013 IEEE International Conference on Communications (ICC)*, 2013, pp. 2360–2364.

[20] P. M. Gomadam, J. W. Weidner, R. A. Dougal, and R. E. White, "Mathematical modeling of lithium-ion and nickel battery systems," *Journal of power sources*, vol. 110, no. 2, pp. 267–284, 2002.

[21] R. Rao, S. Vrudhula, and D. N. Rakhmatov, "Battery modeling for energy aware system design," *IEEE Computer*, vol. 36, no. 12, pp. 77–87, 2003.

[22] N. Michelusi, L. Badia, R. Carli, L. Corradini, and M. Zorzi, "Energy management policies for harvesting-based wireless sensor devices with battery degradation," *IEEE Transactions on Communications*, vol. 61, no. 12, pp. 4934–4947, 2013.

[23] K. Tutuncuoglu, A. Yener, and S. Ulukus, "Optimum policies for an energy harvesting transmitter under energy storage losses," *IEEE Journal on Selected Areas in Communications*, vol. 33, no. 3, pp. 467–481, 2015.

[24] B. Devillers and D. Gündüz, "A general framework for the optimization of energy harvesting communication systems with battery imperfections," *IEEE Journal of Communications and Networks*, vol. 14, no. 2, pp. 130–139, 2012.

[25] C.-F. Chiasserini and R. R. Rao, "Energy efficient battery management," *IEEE journal on selected areas in communications*, vol. 19, no. 7, pp. 1235–1245, 2001.

[26] L. Badia and M. Zorzi, "On the construction of broadcast and multicast trees in wireless networks-global vs. local energy efficiency," in *IEEE Global Telecommunications Conference (GLOBECOM)*, vol. 1, 2002, pp. 122–127.

[27] L. Badia, "On the impact of correlated arrivals and errors on ARQ delay terms," *IEEE Transactions on communications*, vol. 57, no. 2, pp. 334–338, 2009.

[28] I. Kaj and V. Konané, "Modeling battery cells under discharge using kinetic and stochastic battery models," *Applied Mathematical Modelling*, vol. 40, no. 17-18, pp. 7901–7915, 2016.

[29] M. D. Levi and D. Aurbach, "Diffusion coefficients of lithium ions during intercalation into graphite derived from the simultaneous measurements and modeling of electrochemical impedance and potentiostatic intermittent titration characteristics of thin graphite electrodes," *The Journal of Physical Chemistry B*, vol. 101, no. 23, pp. 4641–4647, 1997.

[30] R. Valentini, M. Levorato, and F. Santucci, "Aging aware random channel access for battery-powered wireless networks," *IEEE Wireless Communications Letters*, vol. 5, no. 2, pp. 176–179, 2016.

[31] A. Biason and M. Zorzi, "Energy harvesting communication system with SOC-dependent energy storage losses," in *IEEE International Symposium on Wireless Communication Systems (ISWCS)*, 2015, pp. 406–410.

[32] N. Michelusi, K. Stamatiou, L. Badia, and M. Zorzi, "Operation policies for energy harvesting devices with imperfect state-of-charge knowledge," in *IEEE International Conference on Communications (ICC)*, 2012, pp. 5782–5787.

[33] N. Michelusi, L. Badia, R. Carli, K. Stamatiou, and M. Zorzi, "Correlated energy generation and imperfect state-of-charge knowledge in energy harvesting devices," in *IEEE 8th International Wireless Communications and Mobile Computing Conference (IWCMC)*, 2012, pp. 401–406.

[34] R.-S. Liu, P. Sinha, and C. E. Koksal, "Joint energy management and resource allocation in rechargeable sensor networks," in *IEEE Proceedings IEEE INFOCOM*, 2010, pp. 1–9.

[35] N. Michelusi, L. Badia, R. Carli, L. Corradini, and M. Zorzi, "Impact of battery degradation on optimal management policies of harvesting-based wireless sensor devices," in *2013 Proceedings IEEE INFOCOM*, 2013, pp. 590–594.

[36] F. Martel, S. Kelouwani, Y. Dubé, and K. Agbossou, "Optimal economy-based battery degradation management dynamics for fuel-cell plug-in hybrid electric vehicles," *Journal of Power Sources*, vol. 274, pp. 367–381, 2015.

[37] A. Biason and M. Zorzi, "On the effects of battery imperfections in an energy harvesting device," in *IEEE International Conference on Computing, Networking and Communications (ICNC)*, 2016, pp. 1–7.

[38] F. Yuan, Q. Zhang, S. Jin, and H. Zhu, "Optimal harvest-use-store strategy for energy harvesting wireless systems," *IEEE transactions on wireless communications*, vol. 14, no. 2, pp. 698–710, 2014.

[39] L. Badia, E. Feltre, and E. Gindullina, "A markov model accounting for charge recovery in energy harvesting devices," in *2017 IEEE Wireless Communications and Networking Conference Workshops (WCNCW)*, 2017, pp. 1–6.

[40] "Worldsensing | Loadsensing | Mining and Construction Monitoring." [Online]. Available: https://www.worldsensing.com/product/loadsensing/

[41] J. A. Khan, H. K. Qureshi, and A. Iqbal, "Energy management in wireless sensor networks: A survey," *Computers & Electrical Engineering*, vol. 41, pp. 159–176, 2015.

[42] A. Kansal, J. Hsu, S. Zahedi, and M. B. Srivastava, "Power management in energy harvesting sensor networks," *ACM Transactions on Embedded Computing Systems (TECS)*, vol. 6, no. 4, p. 32, 2007.

[43] J. Polastre, R. Szewczyk, and D. Culler, "Telos: enabling ultra-low power wireless research," in *IEEE Proceedings of the 4th international symposium on Information processing in sensor networks*, 2005, p. 48.

[44] P. Juang, H. Oki, Y. Wang, M. Martonosi, L. S. Peh, and D. Rubenstein, "Energy-efficient computing for wildlife tracking: Design tradeoffs and early experiences with ZebraNet," *ACM SIGARCH Computer Architecture News*, vol. 30, no. 5, pp. 96–107, 2002.

[45] C. Alippi, G. Anastasi, M. Di Francesco, and M. Roveri, "Energy management in wireless sensor networks with energy-hungry sensors," *IEEE Instrumentation & Measurement Magazine*, vol. 12, no. 2, 2009.

[46] ——, "An adaptive sampling algorithm for effective energy management in wireless sensor networks with energy-hungry sensors," *IEEE Transactions on Instrumentation and Measurement*, vol. 59, no. 2, pp. 335–344, 2010.

[47] B. Srbinovski, M. Magno, F. Edwards-Murphy, V. Pakrashi, and E. Popovici, "An energy aware adaptive sampling algorithm for energy harvesting WSN with energy hungry sensors," *Sensors*, vol. 16, no. 4, p. 448, 2016.

[48] C. Lee and J. Lee, "Harvesting and energy aware adaptive sampling algorithm for guaranteeing self-sustainability in wireless sensor networks," in *IEEE International Conference on Information Networking (ICOIN)*, 2017, pp. 57–62.

[49] J. Yang, X. Wu, and J. Wu, "Adaptive sensing scheduling for energy harvesting sensors with finite battery," in *IEEE International Conference on Communications (ICC)*, 2015, pp. 98–103.

[50] L. V. Nguyen, S. Kodagoda, R. Ranasinghe, and G. Dissanayake, "Information-driven adaptive sampling strategy for mobile robotic wireless sensor network,"

IEEE Transactions on Control Systems Technology, vol. 24, no. 1, pp. 372–379, 2016.

[51] Y. Xu, J. Choi, S. Dass, and T. Maiti, "Sequential Bayesian prediction and adaptive sampling algorithms for mobile sensor networks," *IEEE Transactions on Automatic Control*, vol. 57, no. 8, pp. 2078–2084, 2012.

[52] R. Rieger and J. T. Taylor, "An adaptive sampling system for sensor nodes in body area networks," *IEEE Transactions on Neural Systems and Rehabilitation Engineering*, vol. 17, no. 2, pp. 183–189, 2009.

[53] Y. Sun, Y. Yuan, X. Li, Q. Xu, and X. Guan, "An adaptive sampling algorithm for target tracking in underwater wireless sensor networks," *IEEE Access*, vol. 6, pp. 68 324–68 336, 2018.

[54] X. Yin, J. Goudriaan, E. A. Lantinga, J. Vos, and H. J. Spiertz, "A flexible sigmoid function of determinate growth," *Annals of botany*, vol. 91, no. 3, pp. 361–371, 2003.

[55] J. Hofierka, M. Suri *et al.*, "The solar radiation model for Open source GIS: implementation and applications," in *Proceedings of the Open source GIS-GRASS users conference*, vol. 2002, 2002, pp. 51–70.

[56] T. Khatib, A. Mohamed, and K. Sopian, "A review of solar energy modeling techniques," *Renewable and Sustainable Energy Reviews*, vol. 16, no. 5, pp. 2864–2869, 2012.

[57] M. Miozzo, D. Zordan, P. Dini, and M. Rossi, "SolarStat: Modeling photovoltaic sources through stochastic Markov processes," in *IEEE International Energy Conference (ENERGYCON)*, 2014, pp. 688–695.

[58] C. Tao, D. Shanxu, and C. Changsong, "Forecasting power output for grid-connected photovoltaic power system without using solar radiation measurement," in *2nd IEEE International Symposium on Power Electronics for Distributed Generation Systems (PEDG)*, 2010, pp. 773–777.

[59] "SoDA: Solar radiation data," http://www.soda-pro.com/, [Online; accessed 09-May-2018].

[60] W. Chong, M. Naghavi, S. Poh, T. Mahlia, and K. Pan, "Techno-economic analysis of a wind–solar hybrid renewable energy system with rainwater collection feature for urban high-rise application," *Applied Energy*, vol. 88, no. 11, pp. 4067–4077, 2011.

[61] U. Akram, M. Khalid, and S. Shafiq, "An innovative hybrid wind-solar and battery-supercapacitor microgrid system—development and optimization," *IEEE Access*, vol. 5, pp. 25 897–25 912, 2017.

[62] G.-A. Migan, "Study the operating temperature of a PV module," *Project Report*, 2013.

[63] M. R. Maghami, H. Hizam, C. Gomes, M. A. Radzi, M. I. Rezadad, and S. Hajighorbani, "Power loss due to soiling on solar panel: A review," *Renewable and Sustainable Energy Reviews*, vol. 59, pp. 1307–1316, 2016.

[64] M. Murnane and A. Ghazel, "A closer look at state of charge (SOC) and state of health (SOH) estimation techniques for batteries," *Analog Devices Technical Article*, 2017.

[65] M. A. Hannan, M. Lipu, A. Hussain, and A. Mohamed, "A review of lithium-ion battery state of charge estimation and management system in electric vehicle applications: Challenges and recommendations," *Renewable and Sustainable Energy Reviews*, vol. 78, pp. 834–854, 2017.

[66] W.-Y. Chang, "The state of charge estimating methods for battery: A review," *ISRN Applied Mathematics*, 2013.

[67] B. Homan, G. J. Smit, R. P. van Leeuwen, V. Marnix, and B. Ten, "A comprehensive model for battery state of charge prediction," in *IEEE Manchester PowerTech*, 2017, pp. 1–6.

[68] "City Rail Link." [Online]. Available: https://www.cityraillink.co.nz/

[69] A. Millner, "Modeling lithium ion battery degradation in electric vehicles," in *IEEE Conference on Innovative Technologies for an Efficient and Reliable Electricity Supply*, 2010, pp. 349–356.

[70] R. R. Harmon, E. G. Castro-Leon, and S. Bhide, "Smart cities and the Internet of Things," in *IEEE Portland International Conference on Management of Engineering and Technology (PICMET)*. IEEE, 2015, pp. 485–494.

[71] R. P. Dameri, “Searching for smart city definition: a comprehensive proposal,” *International Journal of Computers & Technology*, vol. 11, no. 5, pp. 2544–2551, 2013.

[72] J. Lee and H. Lee, “Developing and validating a citizen-centric typology for smart city services,” *Government Information Quarterly*, vol. 31, pp. S93–S105, June 2014.

[73] P. Fraga-Lamas, T. M. Fernández-Caramés, M. Suárez-Albela, L. Castedo, and M. González-López, “A review on Internet of Things for defense and public safety,” *Sensors*, vol. 16, no. 10, p. 1644, 2016.

[74] J. Gubbi, R. Buyya, S. Marusic, and M. Palaniswami, “Internet of Things (IoT): A vision, architectural elements, and future directions,” *Future generation computer systems*, vol. 29, no. 7, pp. 1645–1660, Sep 2013.

[75] C. Pielli, C. Stefanovic, P. Popovski, and M. Zorzi, “Minimizing data distortion of periodically reporting iot devices with energy harvesting,” in *Proc. IEEE SECON*, 2017.

[76] G. Tsoumanis, K. Oikonomou, S. Aïssa, and I. Stavrakakis, “Recharging vehicle distance minimization in wireless sensor networks,” in *Proc. BalkanCom*, 2017.

[77] B. Da Lio, A. V. Guglielmi, and L. Badia, “Markov models for electric vehicles: the role of battery parameters and charging point frequency,” in *IEEE 20th International Workshop on Computer Aided Modelling and Design of Communication Links and Networks (CAMAD)*, 2015, pp. 207–210.

[78] S. Leng and A. Yener, “Resource allocation in body area networks for energy harvesting healthcare monitoring,” pp. 553–587, 2017.

[79] R. Tripathi, S. Vignesh, V. Tamarapalli, A. T. Chronopoulos, and H. Siar, “Non-cooperative power and latency aware load balancing in distributed data centers,” *J. Paral. Distrib. Comput.*, vol. 107, pp. 76–86, 2017.

[80] Z. Fadlullah, F. Tang, B. Mao, N. Kato, O. Akashi, T. Inoue, and K. Mizutani, “State-of-the-art deep learning: Evolving machine intelligence toward tomorrow’s intelligent network traffic control systems,” *IEEE Commun. Surv.&Tut.*, 2017 (to appear).

[81] M. Simonov, M. Mussetta, A. Pirisi, F. Grimaccia, D. Caputo, and R. E. Zich, "Real time energy management in smart cities by future internet." in *Future Internet Assembly*, 2010, pp. 173–182.

[82] M. Rossi, L. Badia, P. Giacon, and M. Zorzi, "Energy and connectivity performance of routing groups in multi-radio multi-hop networks," *Wirel. Commun. Mob. Comput.*, vol. 8, no. 3, pp. 327–342, 2008.

[83] I. Ahmed, M. M. Butt, C. Psomas, A. Mohamed, I. Krikidis, and M. Guizani, "Survey on energy harvesting wireless communications: Challenges and opportunities for radio resource allocation," *Computer Networks*, vol. 88, pp. 234–248, 2015.

[84] S. Ulukus, A. Yener, E. Erkip, O. Simeone, M. Zorzi, P. Grover, and K. Huang, "Energy harvesting wireless communications: A review of recent advances," *IEEE Journal on Selected Areas in Communications*, vol. 33, no. 3, pp. 360–381, 2015.

[85] H.-Y. Shi, W.-L. Wang, N.-M. Kwok, and S.-Y. Chen, "Game theory for wireless sensor networks: a survey," *Sensors*, vol. 12, no. 7, pp. 9055–9097, 2012.

[86] F.-Y. Tsuo, H.-P. Tan, Y. H. Chew, and H.-Y. Wei, "Energy-aware transmission control for wireless sensor networks powered by ambient energy harvesting: A game-theoretic approach," in *IEEE International Conference on Communications (ICC)*, 2011, pp. 1–5.

[87] J. Zheng, H. Zhang, Y. Cai, R. Li, and A. Anpalagan, "Game-theoretic multi-channel multi-access in energy harvesting wireless sensor networks," *IEEE Sensors Journal*, vol. 16, no. 11, pp. 4587–4594, 2016.

[88] T. Zou, S. Lin, Q. Feng, and Y. Chen, "Energy-efficient control with harvesting predictions for solar-powered wireless sensor networks," *Sensors*, vol. 16, no. 1, p. 53, 2016.

[89] A. V. Guglielmi and L. Badia, "Bayesian game analysis of a queueing system with multiple candidate servers," in *IEEE 20th International Workshop on Computer Aided Modelling and Design of Communication Links and Networks (CAMAD)*, 2015, pp. 85–90.

[90] B. Gurakan, O. Ozel, J. Yang, and S. Ulukus, "Energy cooperation in energy harvesting wireless communications," in *IEEE International Symposium on Information Theory Proceedings (ISIT)*, 2012, pp. 965–969.

[91] A. Fernandez Gambin and M. Rossi, "Energy cooperation for sustainable base station deployments: principles and algorithms," in *IEEE Global Communications Conference (GLOBECOM)*, 2017.

[92] J. Xu and R. Zhang, "CoMP meets smart grid: A new communication and energy cooperation paradigm," *IEEE Transactions on Vehicular Technology*, vol. 64, no. 6, pp. 2476–2488, Aug 2015.

[93] Y.-K. Chia, S. Sun, and R. Zhang, "Energy cooperation in cellular networks with renewable powered base stations," *IEEE Transactions on Wireless Communications*, vol. 13, no. 12, pp. 6996–7010, 2014.

[94] Z. Zhu, J. Tang, S. Lambotharan, W. H. Chin, and Z. Fan, "An integer linear programming based optimization for home demand-side management in smart grid," in *IEEE PES Innovative Smart Grid Technologies (ISGT)*, 2012, pp. 1–5.

[95] A. Ashouri, S. S. Fux, M. J. Benz, and L. Guzzella, "Optimal design and operation of building services using mixed-integer linear programming techniques," *Energy*, vol. 59, pp. 365–376, 2013.

[96] A.-H. Mohsenian-Rad, V. W. Wong, J. Jatskevich, and R. Schober, "Optimal and autonomous incentive-based energy consumption scheduling algorithm for smart grid," in *IEEE Innovative Smart Grid Technologies (ISGT)*, 2010, pp. 1–6.

[97] R. S. Ferreira, C. L. Borges, and M. V. Pereira, "A flexible mixed-integer linear programming approach to the AC optimal power flow in distribution systems," *IEEE Transactions on Power Systems*, vol. 29, no. 5, pp. 2447–2459, 2014.

[98] A. Vaccaro, G. Velotto, and A. F. Zobaa, "A decentralized and cooperative architecture for optimal voltage regulation in smart grids," *IEEE Transactions on Industrial Electronics*, vol. 58, no. 10, pp. 4593–4602, 2011.

[99] R. Minciardi and R. Sacile, "Optimal control in a cooperative network of smart power grids," *IEEE Systems Journal*, vol. 6, no. 1, pp. 126–133, 2012.

[100] M. K. Watfa, H. AlHassanieh, and S. Selman, "Multi-hop wireless energy transfer in WSNs," *IEEE Communications Letters*, vol. 15, no. 12, pp. 1275–1277, 2011.

[101] I. Krikidis, "Simultaneous information and energy transfer in large-scale networks with/without relaying," *IEEE Transactions on Communications*, vol. 62, no. 3, pp. 900–912, 2014.

[102] L. Badia, M. Levorato, F. Librino, and M. Zorzi, "Cooperation techniques for wireless systems from a networking perspective," *IEEE Wireless Communications*, vol. 17, no. 2, pp. 89–96, 2010.

[103] X. Xue, S. Wang, Y. Sun, and F. Xiao, "An interactive building power demand management strategy for facilitating smart grid optimization," *Applied Energy*, vol. 116, pp. 297–310, 2014.

[104] J. Tang, Z. Zhou, J. Niu, and Q. Wang, "An energy efficient hierarchical clustering index tree for facilitating time-correlated region queries in the Internet of Things," *Journal of Network and Computer Applications*, vol. 40, pp. 1–11, 2014.

[105] H. O. Tan, I. Korpeoglu, and I. Stojmenovi, "Computing localized power-efficient data aggregation trees for sensor networks," *IEEE Transactions on Parallel and Distributed Systems*, vol. 22, no. 3, pp. 489–500, 2011.

[106] W. R. Heinzelman, A. Chandrakasan, and H. Balakrishnan, "Energy-efficient communication protocol for wireless microsensor networks," in *IEEE Proceedings of the 33rd annual Hawaii international conference on System sciences*, 2000, pp. 10–pp.

[107] L. Costantino, N. Buonaccorsi, C. Cicconetti, and R. Mambrini, "Performance analysis of an LTE gateway for the IoT," in *IEEE International Symposium on a World of Wireless, Mobile and Multimedia Networks (WoWMoM)*, San Francisco, CA, USA, June 2012, pp. 1–6.

[108] A. Awamry, D. Maga, and T. Nahdi, "Energy Consumption of Wireless Sensor Network," in *Proceedings of the 17th International Conference on Research in Telecommunication Technologies*, Chengdu, China, Oct 2015.

[109] A. Mainwaring, D. Culler, J. Polastre, R. Szewczyk, and J. Anderson, "Wireless sensor networks for habitat monitoring," in *Proceedings of the 1st ACM international workshop on Wireless sensor networks and applications.* Atlanta, GA, USA: Acm, Sep 2002, pp. 88–97.

[110] C. Alippi, R. Camplani, C. Galperti, and M. Roveri, "A robust, adaptive, solar-powered WSN framework for aquatic environmental monitoring," *IEEE Sensors Journal*, vol. 11, no. 1, pp. 45–55, 2011.

[111] R. Sharma and D. K. Lobiyal, "Multi-Gateway-Based Energy Holes Avoidance Routing Protocol for WSN," in *Informatics*, vol. 3, no. 2. Multidisciplinary Digital Publishing Institute, April 2016, p. 5.

[112] A. Von Meier, *Electric power systems: a conceptual introduction.* John Wiley & Sons, 2006.

[113] M. Grant, S. Boyd, and Y. Ye. (2008) CVX: Matlab software for disciplined convex programming. [Online]. Available: http://cvxr.com/cvx/

[114] M. Centenaro, L. Vangelista, A. Zanella, and M. Zorzi, "Long-range communications in unlicensed bands: The rising stars in the IoT and smart city scenarios," *IEEE Wireless Communications*, vol. 23, no. 5, pp. 60–67, 2016.

[115] F. Adelantado, X. Vilajosana, P. Tuset-Peiro, B. Martinez, J. Melia-Segui, and T. Watteyne, "Understanding the limits of LoRaWAN," *IEEE Communications Magazine*, vol. 55, no. 9, pp. 34–40, 2017.

[116] *Short range narrow-band digital radiocommunication transceivers - PHY, MAC, SAR and LLC layer specifications*, ITU-T, 01 2015.

[117] C. Bajaj, "Near Field Communication," *International Journal of Advanced Research in Computer Science and Software Engineering, Department of Computer Science & Engineering, Ambedkar Institute of Advanced Communication Technologies and Research, Delhi, India*, vol. 4, no. 8, 2014.

[118] *ZigBee Specification*, ZigBee Alliance, 09 2012.

[119] J. Nieminen, C. Gomez, M. Isomaki, T. Savolainen, B. Patil, Z. Shelby, M. Xi, and J. Oller, "Networking solutions for connecting bluetooth low energy enabled machines to the Internet of Things," *IEEE network*, vol. 28, no. 6, pp. 83–90, Nov 2014.

[120] P. Schulz, M. Matthe, H. Klessig, M. Simsek, G. Fettweis, J. Ansari, S. A. Ashraf, B. Almeroth, J. Voigt, I. Riedel *et al.*, "Latency critical IoT applications in 5G: Perspective on the design of radio interface and network architecture," *IEEE Communications Magazine*, vol. 55, no. 2, pp. 70–78, 2017.

[121] S. Kaul, R. Yates, and M. Gruteser, "Real-time status: How often should one update?" in *Proc. IEEE INFOCOM*, 2012, pp. 2731–2735.

[122] S. Kaul, M. Gruteser, V. Rai, and J. Kenney, "Minimizing age of information in vehicular networks," in *IEEE Conf. on Sensor, Mesh and Ad Hoc Comm. and Nets. (SECON)*, 2011, pp. 350–358.

[123] Q. Zhang and F. H. Fitzek, "Mission critical IoT communication in 5G," in *Future Access Enablers of Ubiquitous and Intelligent Infrastructures*. Springer, 2015, pp. 35–41.

[124] B. T. Bacinoglu and E. Uysal-Biyikoglu, "Scheduling status updates to minimize age of information with an energy harvesting sensor," in *IEEE Int'l Symp. on Inf. Theory (ISIT)*, 2017, pp. 1122–1126.

[125] A. Arafa, J. Yang, S. Ulukus, and H. V. Poor, "Age-minimal online policies for energy harvesting sensors with incremental battery recharges," *arXiv preprint arXiv:1802.02129*, 2018.

[126] ——, "Age-minimal transmission for energy harvesting sensors with finite batteries: Online policies," *arXiv preprint arXiv:1806.07271*, 2018.

[127] S. Feng and J. Yang, "Age of information minimization for an energy harvesting source with updating erasures: With and without feedback," *arXiv preprint arXiv:1808.05141*, 2018.

[128] E. T. Ceran, D. Gündüz, and A. György, "Reinforcement learning to minimize age of information with an energy harvesting sensor with HARQ and sensing cost," *IEEE INFOCOM*, 2019.

[129] X. Wu, J. Yang, and J. Wu, "Optimal status update for age of information minimization with an energy harvesting source," *IEEE Transactions on Green Communications and Networking*, vol. 2, no. 1, pp. 193–204, 2017.

[130] A. Arafa and S. Ulukus, "Age minimization in energy harvesting communications: Energy-controlled delays," in *51st Asilomar Conference on Signals, Systems, and Computers*, 2017, pp. 1801–1805.

[131] S. Feng and J. Yang, "Minimizing age of information for an energy harvesting source with updating failures," in *IEEE International Symposium on Information Theory (ISIT)*, 2018, pp. 2431–2435.

[132] B. T. Bacinoglu, Y. Sun, E. Uysal, and V. Mutlu, "Optimal status updating with a finite-battery energy harvesting source," *arXiv preprint arXiv:1905.06679*, 2019.

[133] M. Dabiri and M. J. Emadi, "Average age of information minimization in an energy harvesting wireless sensor node," in *IEEE 9th International Symposium on Telecommunications (IST)*, 2018, pp. 123–126.

[134] B. T. Bacinoglu, Y. Sun, E. Uysal-Bivikoglu, and V. Mutlu, "Achieving the age-energy tradeoff with a finite-battery energy harvesting source," in *IEEE International Symposium on Information Theory (ISIT)*, 2018, pp. 876–880.

[135] S. Leng and A. Yener, "Age of information minimization for an energy harvesting cognitive radio," *IEEE Transactions on Cognitive Communications and Networking*, 2019.

[136] S. Farazi, A. G. Klein, and D. R. Brown, "Average age of information for status update systems with an energy harvesting server," in *IEEE Conference on Computer Communications Workshops (INFOCOM WKSHPS)*, 2018, pp. 112–117.

[137] ——, "Age of information in energy harvesting status update systems: When to preempt in service?" in *IEEE International Symposium on Information Theory (ISIT)*, 2018, pp. 2436–2440.

[138] A. Arafa, J. Yang, S. Ulukus, and H. V. Poor, "Online timely status updates with erasures for energy harvesting sensors," in *IEEE 56th Annual Allerton Conference on Communication, Control, and Computing (Allerton)*, 2018, pp. 966–972.

[139] R. D. Yates and S. K. Kaul, "The age of information: Real-time status updating by multiple sources," *IEEE Trans. on Inf. Theory*, vol. 65, no. 3, pp. 1807–1827, 2019.

[140] R. D. Yates and S. Kaul, "Real-time status updating: Multiple sources," in *IEEE International Symposium on Information Theory Proceedings*, 2012, pp. 2666–2670.

[141] Y. Sun, E. Uysal-Biyikoglu, and S. Kompella, "Age-optimal updates of multiple information flows," in *IEEE INFOCOM 2018-IEEE Conference on Computer Communications Workshops (INFOCOM WKSHPS)*. IEEE, 2018, pp. 136–141.

[142] B. Buyukates, A. Soysal, and S. Ulukus, "Age of information in multicast networks with multiple update streams," *arXiv preprint arXiv:1904.11481*, 2019.

[143] N. Pappas, J. Gunnarsson, L. Kratz, M. Kountouris, and V. Angelakis, "Age of information of multiple sources with queue management," in *IEEE Int'l Conf. on Comms. (ICC)*, 2015, pp. 5935–5940.

[144] V. Tripathi and S. Moharir, "Age of information in multi-source systems," in *IEEE GLOBECOM*, 2017, pp. 1–6.

[145] D. Yang, G. Xue, X. Fang, and J. Tang, "Incentive mechanisms for crowdsensing: Crowdsourcing with smartphones," *IEEE/ACM Transactions on Networking (TON)*, vol. 24, no. 3, pp. 1732–1744, 2016.

[146] E. T. Ceran, D. Gündüz, and A. György, "Average age of information with hybrid ARQ under a resource constraint," *IEEE Trans. on Wireless Comms.*, vol. 18, no. 3, pp. 1900–1913, 2019.

[147] D. P. Bertsekas, *Dynamic Programming and Optimal Control*. Athena scientific Belmont, MA, 1995.

[148] L. Badia and G. Mansutti, "Evaluation of operation policies for energy harvesting sensor nodes with variable data traffic," in *Proceedings of European Wireless 2015; 21th European Wireless Conference*. VDE, 2015, pp. 1–6.